Circuit and Discharge Models for Excimer Lasers

CIRCUIT AND DISCHARGE MODELS

FOR EXCIMER LASERS

A thesis presented by David I. Wheatley B.A.
to the University of St. Andrews
in application for the degree of
Master of Science

December 1981

I hereby declare that this thesis is composed by myself, that it is a record of work carried out by myself and that it has not previously been presented for a higher degree. The work was carried out in the Physical Laboratories of St. Andrews University under the supervision of Dr. A. Maitland.

I certify that David Ian Wheatley B.A. has spent four terms as a research student in the Physical Laboratories of the United College of St. Salvator and St. Leonard in the University of St. Andrews, that he has fulfilled the conditions of Ordinance 51 of the University Court of St. Andrews and that he is qualified to submit the accompanying thesis in application for the Degree of Master of Science.

(Supervisor)

CURRICULUM VITAE

From October 1976 the author studied physics at St. John's College, Cambridge, graduating in June 1979 with 2ii honours. Between October 1979 and June 1981 he was engaged in excimer laser research at the University of St. Andrews under the sponsorship of Ferranti (Dundee) Ltd. Since June 1981 he has been researching into aspects of supported metal catalysts at the New Cavendish Laboratories under a S.E.R.C. CASE studentship in collaboration with I.C.I. Ltd.

ACKNOWLEDGEMENTS

I acknowledge with gratitude the considerable help and encouragement given to me by my supervisor Dr. A. Maitland and by my colleagues A.B. Duval, T.G. Frank, T. Govindanunny and R. B. Millington. A special mention is due to C.A. Pirrie for the question which started this work.

I wish to thank Mr. & Mrs. G.G. Stevenson of G.G. Stevenson (Printers) Ltd. and Fiona Stevenson for their great kindness during my stay in St. Andrews and for much valued advice, encouragement and the extensive use of equipment during the preparation, typing and binding of this thesis. I am indebted to Fiona for her patience and hard work in its typing and organization.

I wish wholeheartedly to thank my parents, Alan and Maureen Wheatley, Susan Wheatley and Des Walsh for their faith, enthusiasm and support in all aspects of my career.

This work was sponsored by Ferranti (Dundee) Ltd. whose help I most gratefully acknowledge.

TABLE OF CONTENTS

CHAPTER 1

Gaseous Discharges and Time-Dependent Resistance

Gaseous Discharges and Time-Dependent Resistance

1.1 Introduction

The excimer laser transition is characterized by a short wavelength and wide gain profile. In order to achieve the threshold gain in such an active medium a concentration of excited molecules typically of the order of 10^{14}-$10^{15}cm^{-3}$ is required and this value is attained by the deposition of a high energy density in a short amount of time of the order of 10 to 100nsecs. Two main schemes have been used to achieve this fast energy deposition; an intense beam of fast electrons injected into a high density gas or a fast electric discharge through a high density gas. The latter forms the subject of this dissertation.

When the voltage across a charged capacitor is applied suddenly across a gaseous laser medium the rapid rise of the voltage pulse can lead to a substantial overvoltage beyond the static breakdown point. The breakdown of the gas in a properly designed system will include a uniform glow before the discharge is terminated by arcing. The resistance of the gas will be a rapidly decreasing function of time, reaching a fraction of an ohm in some tens of nanoseconds. The fast high energy deposition requirement will be best served if the energy is deposited during the region of high resistance before the resistance collapses with the onset of arcing.

1.2 The Development of the Discharge

In an early paper on the subject of pulsed discharge development, R.C. Fletcher made measurements of the impulse

breakdown of air using then new micro-oscillographic techniques. He was particularly interested in the formative period of the discharge preceding the resistive phase and rapid current rise, and measured this period in the range 0·5 to 50nsec. A typical trace of breakdown voltage from his paper is shown in figure (1.1). His results indicated that the formative time was dependent upon applied field only (decreasing for higher fields) and was independent of gap width or applied voltage separately. This rule failed, however, below a certain critical value of field when the time would increase for a smaller gap in the same field.

Following a suggestion by Raether, Fletcher proposed a model for the discharge which could be used to predict the formative time. This model was based upon the streamer mechanism of breakdown and assumed a single initiating electron. In this model the influence of the electric field causes an avalanche with electron gain $e^{\alpha x}$ where x is the distance travelled by the head of the avalanche and α is Townsend's first ionization coefficient. The separation of positive ions and negative electrons leads to space charges which significantly enhance the applied field. Secondary avalanches, initiated by photon absorption before and behind the head of the initial avalanche then form two streamers in this enhanced field, moving towards the anode and cathode at greatly increased speeds.

The formative time was seen as the time taken for a single electron avalanche to grow to a magnitude where the field due to the space charge separation was comparable to the applied field. Very shortly afterwards the complete

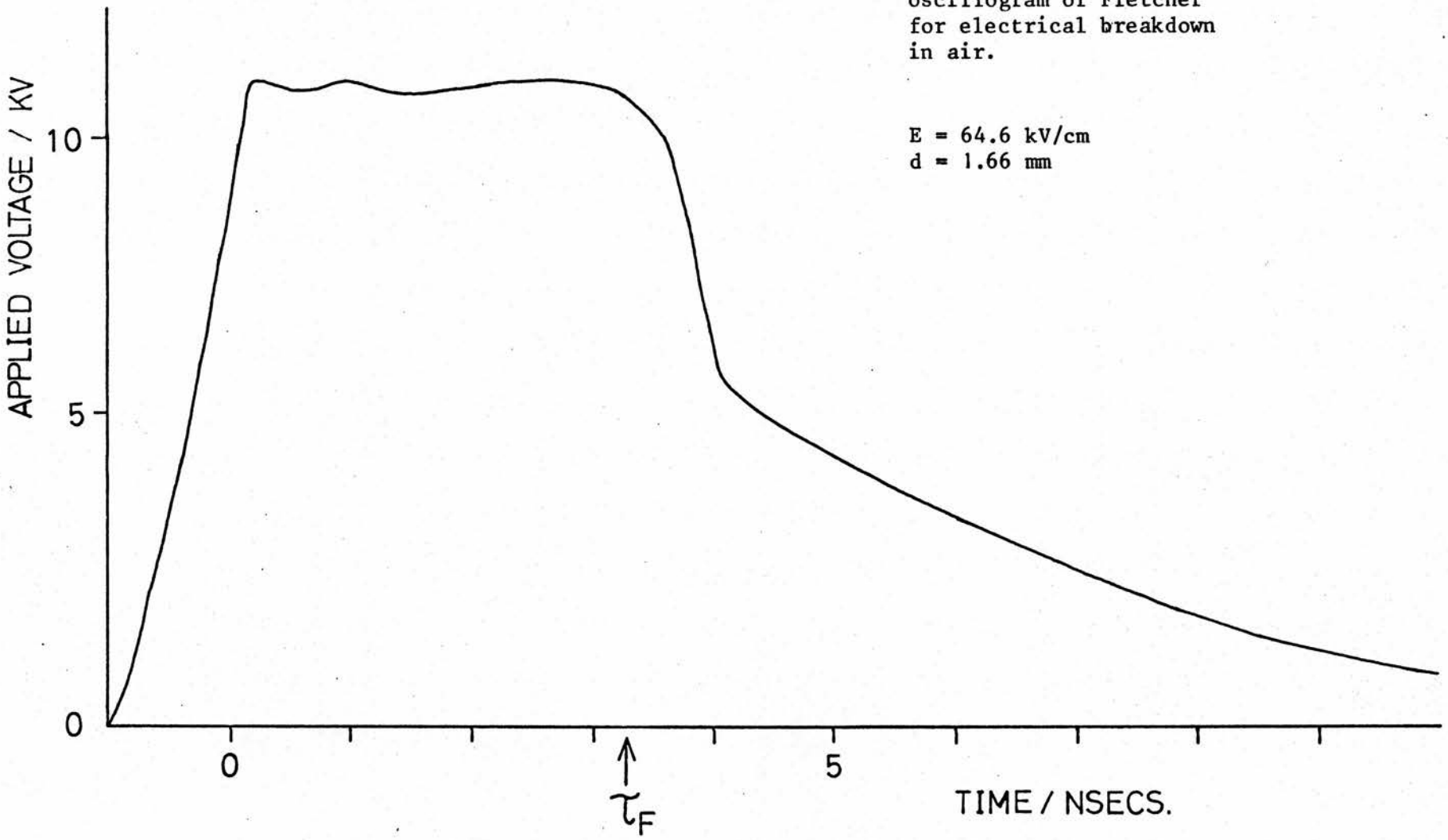

Figure 1.1 A typical oscillogram of Fletcher for electrical breakdown in air.

E = 64.6 kV/cm
d = 1.66 mm

discharge channel would be formed.

The Gaussian electron distribution predicted for an electron avalanche is modified by space charge effects, and Fletcher assumed in his calculations that this becomes important after a time when the diffusion velocity and drift velocity due to the space charge are equal. After this time, the electrons and the ions can be modelled as spherical distributions with the avalanche radius dependent upon drift velocity due to the space charge.

With a drift velocity v in the applied field and a calculated critical size of avalanche N_c, the formative time T_F was modelled as

$$T_F = \frac{\log_e N_c}{\alpha v} . \qquad -(1.1)$$

Fletcher pointed out that the dependence on N_c was weak and that only order of magnitude predictions could be implied. A constant value of $N_c = 10^8$ could serve equally well. Then the prediction would be roughly

$$T_F \sim \frac{20}{\alpha v} . \qquad -(1.2)$$

The experimental and theoretical values of formative lag were found by Fletcher to be in good agreement. The dependence of T_F on field alone was seen as a dependence of αv on field alone. The existence of a critical field below which the dependence failed was attributed to the equality at the critical field of the distance vT_F travelled by the avalanche in the formative time and the gap width. Below this field a larger distance than the gap width would be required for streamer development from a single avalanche, and further avalanches would be required with a consequent

increase in formative time.

Dickey proposed for the results of Fletcher an entirely different explanation, which also went some way to explaining the shape of the voltage fall (and current rise) after the formative period. At around 4 to 5nsec. in figure (1.1) a pronounced kink is visible in the oscillogram as the rate of rise of current falls. Fletcher suggested that a change in mode of electron release from the cathode caused this discontinuity, for instance a change from photon bombardment to positive ion bombardment. Dickey discarded the streamer mechanism of breakdown and chose instead a uniform field model.

In defence of this choice Dickey pointed out some significant inconsistencies in Fletcher's model. The observed currents during voltage fall would require something of the order of 10^{13} electrons compared with Fletcher's critical value of 10^{8}. Further, Dickey suggested that the large space charge fields present would tend to reduce the ionization rate near the centre rather than increase the exponential electron growth. He neglected space charge effects for two reasons. Firstly, Fletcher's distribution was derived from a uniform field development, while space charges would in practice tend to oppose the formation of large space charge fields. Secondly, he considered that the average field was of greater importance than effects caused by spatial variations in the field. The discharge in Dickey's model would develop via a Townsend ionization process up to and possibly beyond the point of voltage drop.

$$N = N_0 \exp\left(\int_0^t \alpha v \, dt\right) \qquad -(1.3)$$

for initial and final electron numbers N_0 and N respectively. Dickey followed Fletcher in assuming $N_0 = 1$. Fletcher had based this assumption on Strigel's experimental finding that every electron (at the 95% overvoltage used) was successful in initiating breakdown. This assumption would be severely criticized in later works.

Numerical results from Dickey's method generally predicted too high a formative lag and Dickey took this to be due either to incorrect values of αv as a function of the field E, or to an initial value $N_0 > 1$. However, Dickey's results showed the discontinuity in the voltage fall attributed by Fletcher to a change in mechanism of electron release. Dickey claimed that this discontinuity appeared when the ionization rate fell to a very low value giving an almost constant electron number and an almost constant resistance.

The methods of Fletcher and Dickey were developed considerably by later authors. Felsenthal and Proud followed work on pulsed microwave investigations of the formative time (see for instance Gould and Roberts) in restricting breakdown processes within the gas, suggesting that pulsed d.c. conditions could achieve similar conditions while extending the possible range, particularly to higher electric fields. They followed Dickey in assuming a space charge free region. Their theoretical results indicated that the value of pT_F should be a function of $\frac{E}{p}$ only, the ratio of applied field to pressure. Experimental results were generally found to be in good agreement over a wide range of electrode spacings. The dependence was later agreed by Mesyats

et al (1972).

Of interest for laser gas mixtures, the values of pT_F for helium and argon were found to lie in the range 10^{-5} to 10^{-4} torr-sec. for $\frac{E}{p}$ of the order of a few 10V/cm-torr. Assuming a pressure of around 1000 torr this would indicate a formative time of around 10 to 100nsec.

The book by Raether (1964) provides an excellent account of the mechanisms of avalanche and breakdown in gases. Contrary to the assumption of Fletcher and Dickey, Raether studied the development of both single and multi-electron avalanches. Indeed experimental results on the formative time of an avalanche initiated by a single electron gave values considerably higher than the results of Fletcher.

Raether suggests that two mechanisms exist for breakdown with variations between, both very dependent upon the effects of space charge. The initial build-up of space charge by electron avalanche causes a reduced field between the positive and negative space charges while increasing the field before and behind the head of the avalanche. Theory predicts that for avalanche sizes greater than $5 - 10 \times 10^6$ the effective value of α is decreased by the retarding effect of the positive ions leading to an under-exponential growth. Beyond the region of 10^8 the effective value of α again increases. The electrostatic repulsion of the electrons was later shown in a numerical calculation by Maurel et al to become significant at values of 10^8 or more for a helium discharge with $\frac{E}{p} = 10\text{V/cm-torr}$, $p = 760\text{torr}$ and $v = 5 \times 10^6\,\text{cm/sec.}$ The value of 10^8 as a critical size agrees with Fletcher's previous work.

The two forms of breakdown depend upon the available gain $e^{\alpha d}$ where d is the gap width. For high values of $e^{\alpha d}$ of the order of 10^8 the avalanche can develop to its critical size. Beyond this stage the effect of the gas ionizing radiation and electrostatic repulsion, together with the enhanced ionizing ability of the electrons in the increased field between avalanche head and anode causes the rapid ($\sim 10^8$ cm/sec) expansion of the avalanche head and the formation of an anode directed streamer with an over-exponential growth of the electrons. Gas ionizing radiation between cathode and avalanche head then quickly causes a cathode directed streamer to complete the discharge channel. This streamer mechanism is characterized by the ability of an avalanche to cause breakdown under the effect of its own space charge.

Should a single avalanche be unable to attain a size of the order of 10^8 electrons the Townsend or generation mechanism becomes operative. Here, secondary avalanches released by photons at the cathode sustain the build-up of positive ion space charge. This slow-moving space charge can provide the conditions necessary for efficient ionization by the electrons leading eventually to breakdown. Should a single avalanche develop sufficiently in a later generation then streamer breakdown could occur. This transition is particularly relevant for laser gases in which the uniform glow is terminated by arcing.

Both forms of breakdown can be modified by the initial electron number N_0. Since it is a critical size which is required, the amplification needed will be lower for higher N_0. For the streamer mechamism, these N_0 electrons must lie

within the diffusion radius of a single avalanche. It was found, in fact, that the critical number of electrons depended on the gas, and that while independent of the pressure it was proportional to the gap width. The critical number also decreased for higher overvoltages.

Raether proposed a criterion for the critical length x_c of the avalanche formation to be given by

$$\exp(\alpha x_c) = 10^8 x_c . \qquad -(1.4)$$

A streamer breakdown mechanism would be likely if $x_c \leqslant d$, although the strict equality would be expected to yield no anode streamer. Equation (1.4) is in close agreement with Fletcher's equation (1.2) since

$$vT_F = x_c \sim \frac{\log_e N_c}{\alpha} . \qquad -(1.5)$$

Raether's results also included measurements of the rapid current rise during streamer breakdown. The current growth was characterized as exponential with a time constant T_K which Raether found to be smaller for higher carrier number in the individual avalanche. He also found decreased values of T_K at higher electron numbers (and therefore current) in the streamer. Typical values of T_K lay in the range 2-20nsec. with αv similar. Values were independent of gap width but generally varied inversely with p to give a product pT_K constant at lower pressures but increasing slightly at higher pressures. T_K was found to decrease for higher overvoltages. These results were applicable to single and multi-electron initiation, but it must be stressed that they applied only up to small currents of say 100μA.

Mesyats et al (1969) developed the argument of discharge mechanism in an attempt to explain the observations of

Fletcher. A variation of Fletcher's experiment had been the inclusion of a dielectric over either electrode which did not effect the formative time and therefore ruled out a streamer discharge channel. Dickey claimed that this was consistent with his model but Mesyats et al criticized the rejection of a streamer discharge without the rejection of the single initiating electron assumption. As Raether had shown, this leads in practice to much longer formation times than Fletcher had observed.

The results of Fletcher were very well reproduced by Mesyats et al in discharges with initial values N_0 of the order of 10^4. The arrangement of initial values was based upon a statistical analysis of fluctuations in the formative time indicating the probability of cathode electron release.

Mesyats et al concluded that all known experimental observations of pulsed air-gap breakdown could be explained by the assumption that a discharge begins with the development of electron avalanches initiated by free electrons in the gap. A large initial number of free electrons would develop during a formative time T_F whereas a smaller initial number of free electrons would require secondary avalanches to build up the number. After several generations, the avalanche mechanism would lead to breakdown as in the multi-electron initiation.

Mesyats et al developed the theoretical treatment from an equivalent circuit to that used by Dickey. For roughly constant voltage, $\alpha v \sim$ constant and by taking values from experiment with $N_0 \sim 10^4$ this yielded

$$T_F = \frac{18}{\alpha v}$$

in excellent agreement with Fletcher's predictions (equation (1.2)).

For single-electron initiation the formative time is considerably longer. Mesyats et al considered the self-arresting effect of the positive ion space charge during avalanche development, leading to a reduction in α and v. This self-arrest occured roughly in the region

$$\alpha N \sim \text{constant} \qquad -(1.6)$$

showing that the avalanche begins slowing down at smaller sizes for larger fields. This would also tend to reduce the number of photons emitted, as would the rapid development to the value N. The initiation of the necessary secondary avalanches is therefore retarded for higher fields.

In a later paper Mesyats et al (1972) commented upon a second criterion for streamer discharge. In addition to equation (1.4) relating the critical avalanche size to the gap width, Mesyats et al pointed out that it was also necessary for the avalanche to radiate enough photons, particularly near its head, to ionize the gas molecules. The characteristic times $T_{exc.}$ of de-excitation of the gas molecules were taken from Raether to be of the order of 1 to 10nsec. If the critical time $\frac{x_c}{v} < T_{exc.}$, a streamer is unlikely and other processes are required. A streamer is likely if

$$\frac{\log_e N_c}{\alpha} < d \text{ and } \frac{\log_e N_c}{\alpha v} > T_{exc.} \qquad -(1.7)$$

From Raether's data for nitrogen, $T_{exc.} \sim 3ns$. Thus for $\log_e N_c \sim 20$ the mechanism would deviate from a streamer if $\alpha v \geqslant 10ns^{-1}$ or $E \geqslant 60kV/cm$.

Mesyats et al in this study restricted themselves to the

high field region where the streamer mechanism no longer operates and where the characteristic development times are of the order of nanoseconds. They showed that the current can reach its maximum before the onset of discharge channels, either by the production of a large number of photoelectrons from the cathode (as in a Townsend discharge) or by the use of a large initial number of electrons when no secondary electrons may be required. They comment that this type of discharge may be useful for pumping high pressure gas lasers.

In the same year, L.E. Kline et al found through computational means that streamer development in nitrogen depended essentially upon photoionization effects producing secondary avalanches as the primary avalanche is slowed by the space charge build-up.

1.3 Discharge Mechanisms in Gas Lasers

The pumping of a high pressure gas laser by fast electric discharge requires a volume stabilized discharge free from the arcing normally associated with the development of a streamer discharge channel. Attempts to solve this problem have normally centred around the use of contoured (e.g. Rogowski profile) electrodes and preionization of the discharge volume, for example by U.V. photoionization from an auxiliarly discharge (see for instance Javan and Levine (1972)).

Recent papers by Palmer (1974) and by Karnyushin et al (1978) have attempted to derive models and suggest criteria for the development of a homogeneous gas discharge over large volumes at high pressures. Both worked with the CO_2 TEA

laser geometry.

If preionization provides an initial electron density n_0, then under the influence of an applied voltage pulse large enough to cause breakdown each electron can be viewed as giving rise to a primary avalanche, the average distance between avalanches being of the order of $n_0^{-1/3}$. Taken separately, each avalanche could eventually lead to streamer formation with secondary avalanches produced by photo-ionization tending to converge towards the primary due to the large field gradients associated with the space charge. In both papers, the requirement for a homogeneous discharge was seen as the need for substantial spatial overlap of the avalanches by transverse diffusion before the onset of streamer breakdown.

Palmer suggested that the diffusion radius and $n_0^{-1/3}$ should be comparable at the critical moment of streamer breakdown, and showed that typical values for CO_2 lasers lead to a requirement $n_0 \geqslant 10^4 cm^{-3}$ in agreement with experimental data. Karnyushin et al, on the other hand, took the avalanche doubling time of the order of $\frac{1}{\alpha v}$ to be the time within which mutual overlap should occur. This led to an upper limit on the electric field rising steeply with preionizing energy as confirmed by experiment. The diffuse nature of this upper limit they attributed to the statistical nature of the avalanche process and the weak dependence of diffusion radius on the field strength.

Karnyushin et al went further in suggesting a second criterion for homogeneous discharge. They saw the breakdown mechanism as involving two stages - a build-up of space

charge via avalanche ionization followed by a quasistreamer breakdown in which photoionization processes would be decisive. The rapid ionization wavefront from anode to cathode was considered essential for the production of replacement electrons behind the head of the avalanche. Without this electron production, the initial value n_0 would be "forgotten" after a time $\frac{d}{v}$, when the electron density would comprise only a background count leading to spark development.

The formation of a positive ion space charge by primary avalanches thus provided long-term storage of information about the initial ionization conditions. By assuming a quasi-streamer criterion in which the space charge field is comparable to the applied field, Karnyushin et al derived a lower limit for the applied field. This they found to be a sharp limit, nearly independent of preionization conditions and again in good agreement with experiment. A lower limit to the electron density n_0 was calculated to be in the region of $4 \times 10^5 cm^{-3}$, higher than that derived by Palmer.

In view of the ability of the gas to "forget" pre-ionization conditions in a time $\frac{d}{v}$ a rapid rise of voltage pulse is clearly essential for the formation of a homogeneous discharge.

J. Hsia (1977) studied the effect of U.V. preionization in electric discharge pumped XeF and KrF lasers and concluded that a fast electron attachment rate by F_2 or NF_3 would suggest the disappearance of electrons produced by pre-ionization within the observed optimum delay times of up to $1\mu s$. He saw the F^- ions as a reservoir of electrons due to

their low electron affinity (3·5eV) compared to the ionization potentials of other species (12 - 24eV). By making an order of magnitude estimate for the rate of collisional detachment

$$F^- + Xe \rightarrow F + Xe + e \qquad -(1.8)$$

Hsia showed that an equilibrium electron density of the order of $10^8 cm^{-3}$ could be achieved from an initial F^- density of $5 \times 10^{11} cm^{-3}$, thereby inhibiting arc formation.

As mentioned at the beginning of the section, attempts to ensure homogeneous discharge development have centred mostly around the use of both uniform fields from contoured electrodes and uniform preionization. By careful attention to both requirements the discharge will be expected to develop simultaneously throughout the volume leading to a homogeneous glow. In a recent paper, Hasson and von Bergmann (1980) reported experiments in which they had been able to control precisely the geometry of high pressure glow discharges in nitrogen obviating the need for precise electrode contouring. By the use of masks over the preionizer they exploited the (logarithmic) dependence of the formative lag on initial electron number to ensure equal "local formation times" in regions throughout the required discharge volume and thereby to ensure a homogeneous discharge. The initial value of electron density could be varied over orders of magnitude and its geometry controlled by these simple U.V. masking procedures.

1.4 Time-Dependent Resistance During Breakdown

While a great deal of data is available on the formative

stage leading to breakdown in a gaseous discharge little is known about the resistive phase during which the resistance of the gas falls rapidly with time, with a consequent drop in voltage and rise in current. Raether (1964) characterized the early rise of current by an exponential growth with time constant T_K, although this he showed to be dependent on electron number and therefore time (section (1.3)). J.C. Martin (1965) gave an empirical expression for the duration of the resistive phase of a spark channel based on observations over a wide range of substances of a largely exponential fall in gap voltage:

$$\text{Resistive phase duration} = \frac{88}{Z^{1/3}E^{4/3}}\left\{\frac{\rho}{\rho_0}\right\}^{1/2} \text{ nsec.} \qquad -(1.9)$$

where Z is the impedance driving the channel (ohms), E is the field (10kV/cm) and ρ, ρ_0 are the densities of the gas and air respectively at N.T.P. Martin claimed a fit of 10% or better.

Much more recently, the time-resolved resistance of a gaseous discharge during spark breakdown was measured by Sorenson and Ristic (1977) for the gases nitrogen and helium. Cary and Mazzie (1979) built upon their work with experiments involving a number of other gases including hydrogen and argon. Both papers included measurements taken when a spark gap was broken down by a pulse charged transmission line with a slow voltage rise time of up to $2\mu s$. The fall of resistance was in each case rapid, dropping to a fraction of an ohm in around 1nsec.

Unfortunately the discharge parameters involved were quite unlike those found in an excimer laser gas mixture - for

instance, a gap width of tens or hundreds of microns and $\frac{E}{p}$ of the order of 100V/cm-torr or more, leading to a very rapid drop in resistance. Furthermore, the mechanisms of spark breakdown may be quite unlike those involved in a "quasistreamer" breakdown. However, the results may be informative in pointing towards a form of time dependence for the resistance suggesting, perhaps, a t^{-m} or an e^{-bt} development, and it is in this spirit that the results are discussed.

For nitrogen at a pressure of $6{\cdot}48 \times 10^5$Pa and with a gap width of 100μm, Sorenson and Ristic found that the resistance of the gap for different values of the transmission line impedance Z_0 could be accurately described by the function

$$R(t) = 2.0 \times 10^4 \left(\frac{p^{1/2}}{EZ_0^{1/3}t}\right)^3 \qquad -(1.10)$$

for E = 374 to 404kV/cm, where R(t) is normalized with respect to the transmission line impedance Z_0. [This comment, it must be said, removes the $\frac{1}{Z_0}$ dependence.] The rise time in the voltage wave reflected from the gap was found for a wide range of parameters to be

$$T_R = \frac{44p^{1/2}}{EZ_0^{1/3}} \text{ nsecs.} \qquad -(1.11)$$

if p is measured in atmospheres, E in 10kV/cm. Z_0 in ohms. This differs from Martin's equation (1.9) but the two predict similar times in the region $E \simeq 80$kV/cm between the ranges studied.

A similar characterization of resistance in a helium discharge was found impossible except, perhaps, for pressures above 8atm.

Cary and Mazzie studied breakdown in the region E =

158 - 669kV/cm; $\frac{E}{p}$ = 50 - 850kV/cm-torr; p = 0·5, 25, 50psig; d = 1,3mils using four gases nitrogen, argon, hydrogen and 95%Ar/5%H_2. Their results were given in graphical form, showing resistance versus time on log-log scales. On such a graph a dependence of the form t^{-m} would appear as a straight line of slope-m. Sorenson and Ristic suggested that m = 3.

The results were inconsistent with those of Sorenson and Ristic, showing straight lines only in the later regions for nitrogen and for other gases. While several different time dependences of a t^{-m} form could be speculated, it is suggested here that a dependence of the form

$$R(t) = R_0 + ae^{-bt} \qquad -(1.12)$$

might be more appropriate, corresponding to an initial exponential rise in conductivity reaching a plateau when $R(t) \rightarrow R_0$. Such a plateau was suggested by Dickey (1952) in explaining the kink observed in Fletcher's oscillograms during the resistive phase. The general shape of such a curve is illustrated on log-log scales in figure (1.2). Figures (1.3) to (1.5) illustrate some of the results of Cary and Mazzie plotted with suggested fits of the form (1.12). The values were taken from log-linear plots of the results where $\log R \rightarrow \log a + bt \log(e)$ in the higher regions of the curves. No great accuracy is implied for the suggested values, in particular the smaller R_0.

Clearly the dependence is not as simple as that of equation (1.12), but some improvement over a straight line fit may be gained in regions of the graphs. The values give rates of the order of 1 to 10$nsec^{-1}$ for the resistance fall

Figure 1.2 A typical trace of the function $R(t) = R_0 + a \exp(-Bt)$.

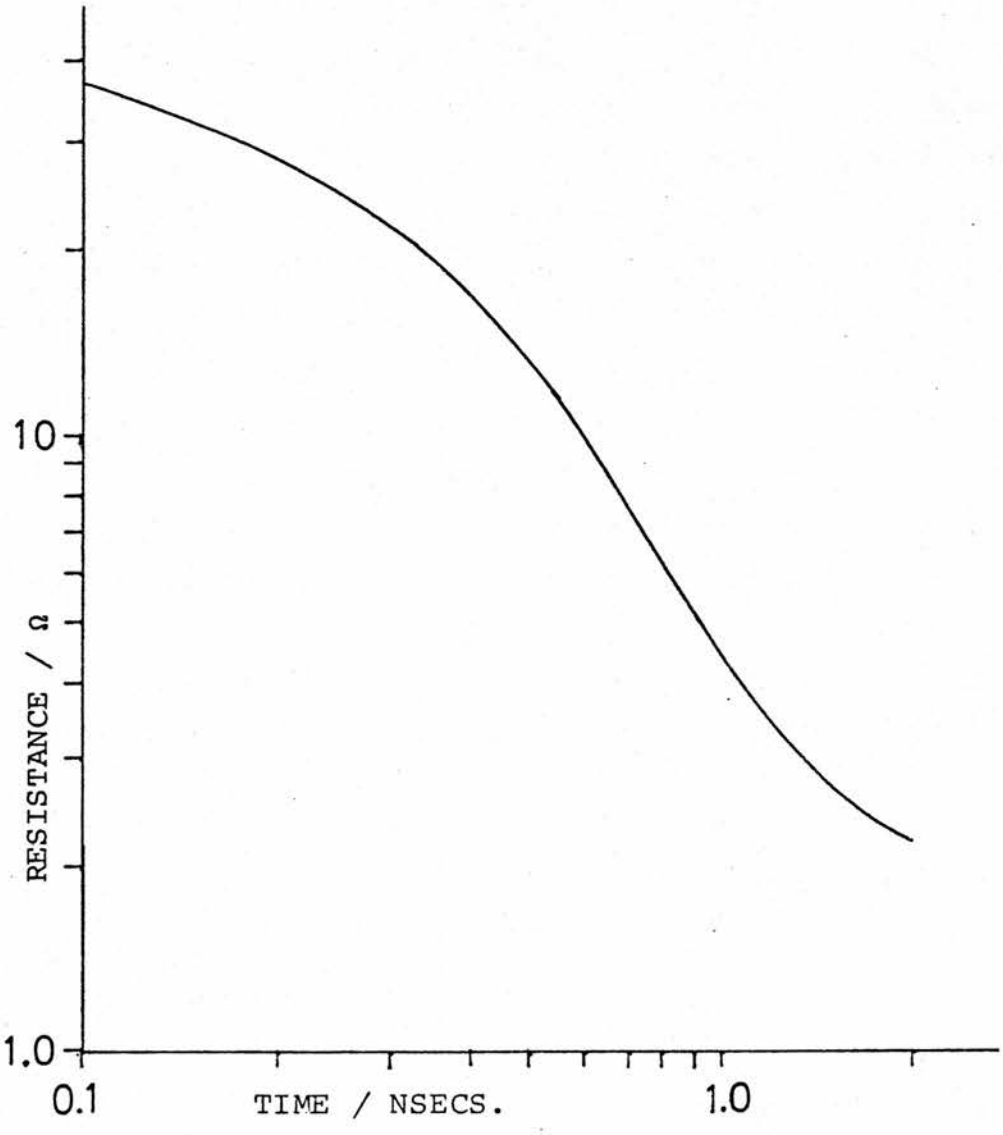

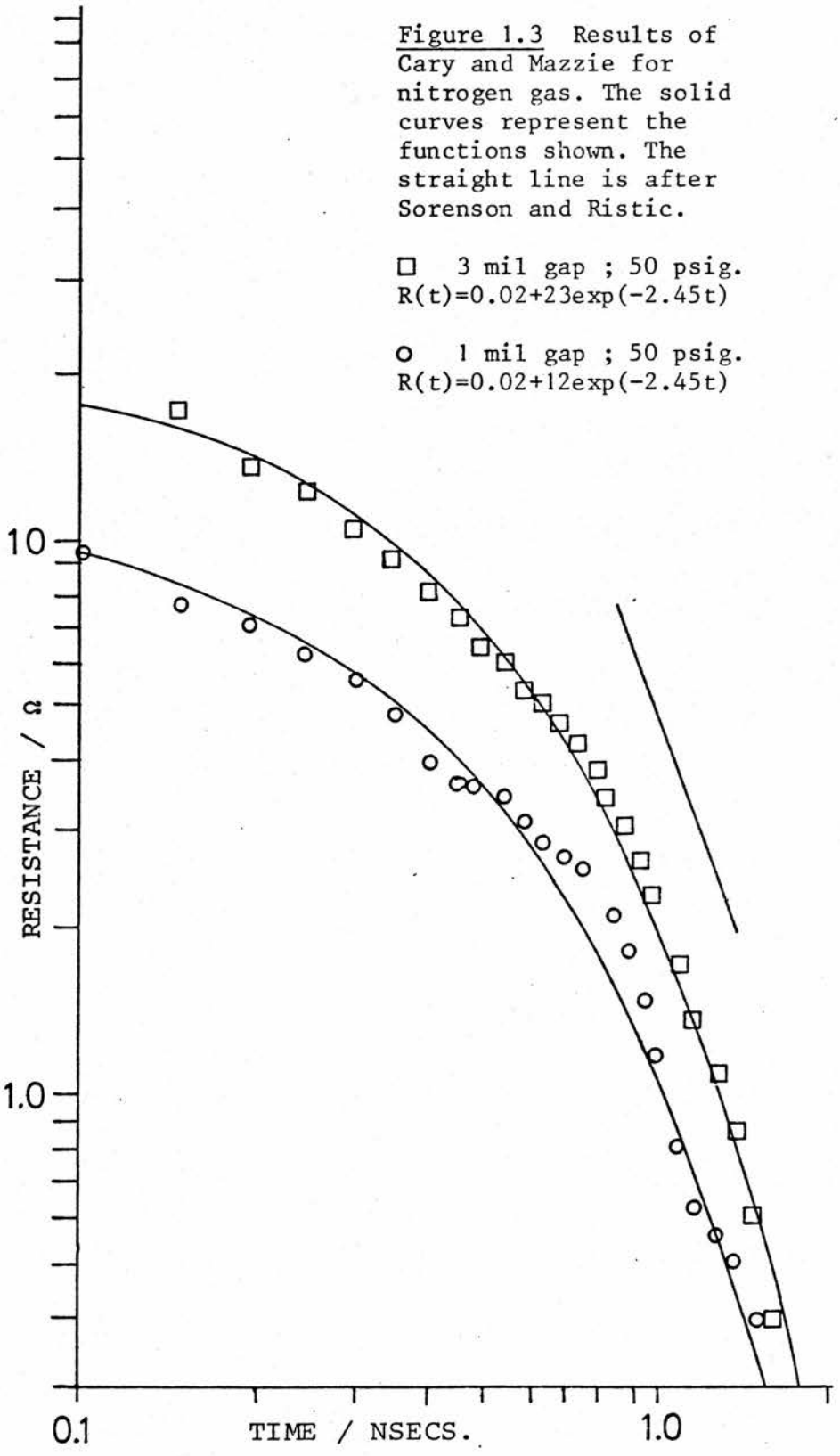

Figure 1.3 Results of Cary and Mazzie for nitrogen gas. The solid curves represent the functions shown. The straight line is after Sorenson and Ristic.

□ 3 mil gap ; 50 psig.
R(t)=0.02+23exp(-2.45t)

o 1 mil gap ; 50 psig.
R(t)=0.02+12exp(-2.45t)

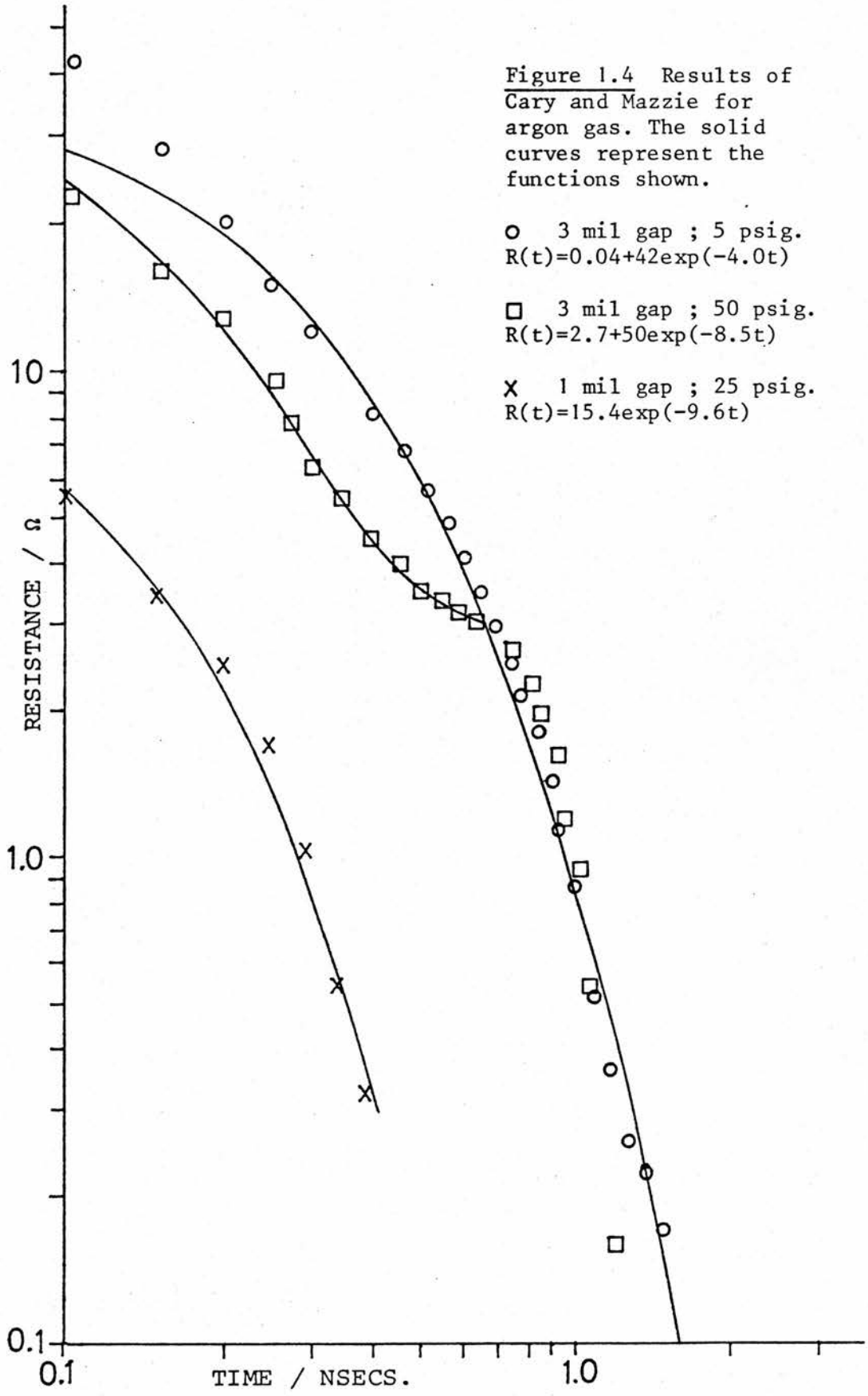

Figure 1.4 Results of Cary and Mazzie for argon gas. The solid curves represent the functions shown.

o 3 mil gap ; 5 psig.
R(t)=0.04+42exp(-4.0t)

□ 3 mil gap ; 50 psig.
R(t)=2.7+50exp(-8.5t)

X 1 mil gap ; 25 psig.
R(t)=15.4exp(-9.6t)

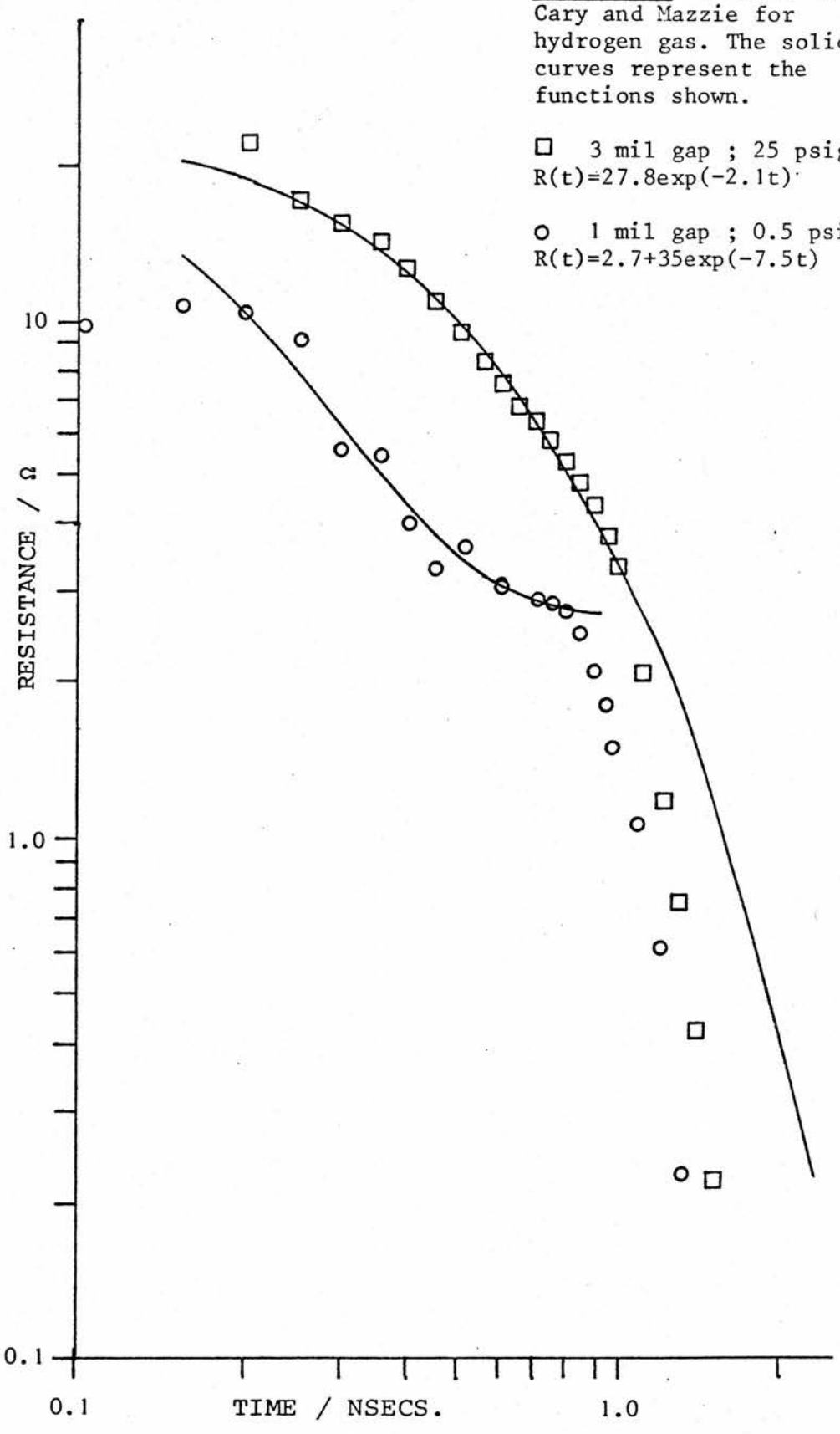

Figure 1.5 Results of Cary and Mazzie for hydrogen gas. The solid curves represent the functions shown.

□ 3 mil gap ; 25 psig.
$R(t)=27.8\exp(-2.1t)$

○ 1 mil gap ; 0.5 psig.
$R(t)=2.7+35\exp(-7.5t)$

corresponding to time constants of the order of 0·1 to 1.0 nsecs. Those time constants suggested by Raether (T_K) lie generally an order of magnitude higher and it is in this region that the excimer laser is taken as lying, with much lower $\frac{E}{p}$ than used by Cary and Mazzie.

1.5 The Excimer Laser

Although several authors have pointed out the rapidly decreasing nature of the resistance of an excimer laser gaseous discharge, little information is available on its time-resolved form. The impedance matching requirements have generally been formulated in terms of depositing as much energy as possible into the gas while the resistance is high before the onset of arcing. This may be compared with the case of an electron beam controlled discharge in which a low ($<1\Omega$) impedance may be well matched to the discharge circuit.

In a properly designed system such as a rare-gas fluoride system, most of the discharge energy will be channelled into excitation of the rare gas atom to the metastable levels rather than into ionization, since this is the preferred channel for excimer upper level formation. For efficient formation this requires a high value of $\frac{E}{p}$ provided by a fast voltage pulse rise leading to substantial overvoltage. In a helium dominated discharge the high overvoltage is particularly important owing to the electron cooling action of the light helium atoms.

While efficiency requirements demand a high value of $\frac{E}{p}$ at breakdown, clearly the energy deposited into the discharge will also be expected to benefit, increasing as the square of

the peak voltage. Sze and Scott (1978) have shown by inductance variations a 0·75% voltage drop per nanosecond increase in voltage rise time, while Sze and Loree (1978) have shown that output energy is well correlated to input energy. Watanabe et al (1979) have shown a similar correlation for variations in electrode separation and pressure, and have commented that this is due not only to an increased voltage but also to an increased discharge impedance since the discharge mechanism would not be expected to vary too much.

At the high level of $\frac{E}{P}$ in an excimer laser discharge, the discharge is particularly unstable, the glow typically lasting only 30-40 nsecs. before the onset of arcing (although Lin and Levatter (1979) have extended this time by using X-ray (very uniform) preionization). The form and scale of the impedance variation with time is therefore of importance in matching the external circuit to the discharge in order to provide as much input energy as possible.

Watanabe et al (1979) gave two time resolved graphs of discharge impedance, showing a rapid fall to a lower plateau level before the collapse with arcing after around 100nsec. The impedance was seen to increase as the gap width and pressure of this $He/Kr/F_2$ mixture were increased.Fits to these curves (see figure (2.6)) have been made by the present author and result in a clear t^{-m} dependence with m slightly greater than unity and without the addition of a separate plateau.

The purpose of this present study is to study mathematically the time evolution of two lumped-parameter

discharge circuits and in particular to study the effect of a time-dependent term in the resistance with reference to excimer laser, and indeed other, discharges. The form of time dependence has been taken as that of equation (1.12) in most cases.

CHAPTER 2

Gaseous Discharges in LCR Circuit Geometry

Gaseous Discharges in LCR Circuit Geometry

2.1 Introduction

There exist a variety of discharge circuits employed in the pumping of pulsed gas discharge lasers, not necessarily devised for the pumping of excimer lasers. The fast capacitor dumping (capacitor transfer) design has been used by Andrews et al (1977) for KrF and also by Fitzsimmons et al (1976) with nitrogen. A cable fed version was used by Sze and Scott (1978). The LC-inversion circuit has been particularly popular along with the closely related Blumlein circuit, examples including Sze and Loree (1978), Burnham et al (1976) and Schwab and Hollinger (1976), the last again for the nitrogen laser. A distributed liquid transmission line storage element has been used by Taylor et al (1978). The performances of these various circuits can differ widely depending upon factors such as voltage rise time, over-voltage, power storage which in turn will depend upon the inductances involved in circuit components - particularly the spark gap - and upon capacity. Different demands on output energy, efficiency and repetition rate will clearly influence the design.

In studying these different circuit designs, the general circuit equations governing the discharge will be complicated by the number of loops (generally at least two) involved in the application of Kirchhoff's laws, if lumped parameter methods are applicable at all. If the designs have a common feature at all, however, it is in the simple LCR circuit discharge and this circuit has

been used by several authors in formulating models of discharges in gas lasers (e.g. Johnson et al (1979), Gerry (1965), Ali (1969)) and has been applied to more complicated designs (Sze and Loree (1978)) in deriving circuit parameters. This is based on the assumption that after the voltage rise a main discharge loop will exist which can be treated approximately by LCR methods. This is extremely attractive mathematically since few analytical results exist for more complicated circuits.

It is the purpose of this chapter to study the effect of a rapidly decreasing resistance for a discharge in LCR circuit geometry, mainly by numerical means. In chapter 3 an attempt will be made to approximate these results mathematically.

2.2 The Circuit Equation

The LCR circuit consists of a capacitor C and inductance L in series with a time dependent resistance R(t). The capacitor is charged to a voltage V_0 prior to breakdown and has then a charge Q given by $Q_0 = CV_0$. The resistance R(t) is defined by

$$R(t) = R_0 + ae^{-Bt} \qquad -(2.1)$$

$$R_0 = R_0(\text{ext.}) + R_0(\text{laser}) \qquad -(2.2)$$

where $R_0(\text{laser}) + ae^{-Bt}$ defines the discharge resistance and $R_0(\text{ext.})$ an external circuit resistance. No specific allowance is made for the discharge head inductance although Sze and Loree have taken this to be a substantial fraction of the total. The circuit is switched by a spark gap whose resistance is assumed to fall immediately from infinity to some value included in $R_0(\text{ext.})$. Clearly this is not a

realistic assumption and an improvement to the circuit would include a time dependent term. The results of Cary and Mazzie might be particularly useful in this respect. The inductance of the spark gap would be expected to form a large part of L and would in reality be time dependent.

The circuit equation in Q is

$$L\frac{d^2Q}{dt^2} + R(t)\frac{dQ}{dt} + \frac{Q}{C} = 0 \qquad -(2.3)$$

yielding for the current I

$$L\frac{d^2I}{dt^2} + R(t)\frac{dI}{dt} + [\dot{R}(t) + \frac{1}{C}]I = 0 \,. \qquad -(2.4)$$

2.3 Integration of the Solutions

The initial rise from zero involves dropping virtually all of V_0 across the larger resistance a. In equation (2.4) this represents neglecting terms other than R, $\dot{R}$ to yield

$$I \sim \frac{1}{R} \sim e^{Bt} \qquad -(2.5)$$

which has been found valid for values of R down to around 500Ω. The solutions were actually generated from a value of $a = 10^8\Omega$ but this was found to be equivalent to a time delay during which equation (2.5) applied - a resistance of $10^3\Omega$ would have sufficed to generate the same solutions. The use of $a = 10^8$ therefore generated its own "formative" time for current build up.

Rather than beginning from a boundary condition $I(0) = 0$, the current then effectively begins at $I(0) = \frac{V_0}{a}$ apart from a very rapidly decreasing term negigible for $t \neq 0$. A Gear method integration (for stiff equations) confirmed this. In practice the solutions were generated by Merson's method

from values predicted by the function (2.5) until after the stiff region. The program described in Appendix 2 checked the solutions by using the ringing arm LCR circuit and a high resistance R_2.

The solutions were generated for a range of the parameters L, C, R_0 (laser) and B. The inductance was varied from 10nH to 40nH while the capacitance was varied from 15nF to 40nF. The value of R_0 (laser) was taken as $0{\cdot}2 - 0{\cdot}5\Omega$; Sze and Scott (1978) report an impedance of $\frac{1}{3}\Omega$ to $\frac{1}{10}\Omega$ at the peak of the current pulse in a KrF laser. R_0 (ext.), including the spark gap impedance, was taken similarly as $0{\cdot}5\Omega$. The value of B has been discussed in Chapter 1 as likely to lie in the range $\frac{1}{b} = 1 - 10$nsecs. An estimate may be taken from the paper by Sze and Loree (1978). A kink is observed in the voltage waveform during the fall after breakdown, with some 20nsec. between breakdown and kink. This may be compared to the results of Fletcher (1949) and following Dickey's suggestion of a constant resistance effect, it will be assumed that this kink is caused by the lower plateau R_0 (laser). The resistance must then fall to the order of 1Ω say within around 20nsecs. from its value at the voltage peak. As mentioned at the beginning of this section the threshold resistance for a measurable effect on the circuit (i.e. for breakdown) is about 500Ω in this analysis. Thus $e^{B(20ns.)} \sim 500$ or $B \sim 0{\cdot}3ns^{-1}$. In fact B is taken in the range $0{\cdot}10 - 0{\cdot}20ns^{-1}$ in this analysis.

2.4 The Computed Solutions

The graph of figure (2.1) shows the derived current and

Figure 2.1 Current and voltage waveforms in the LCR circuit.

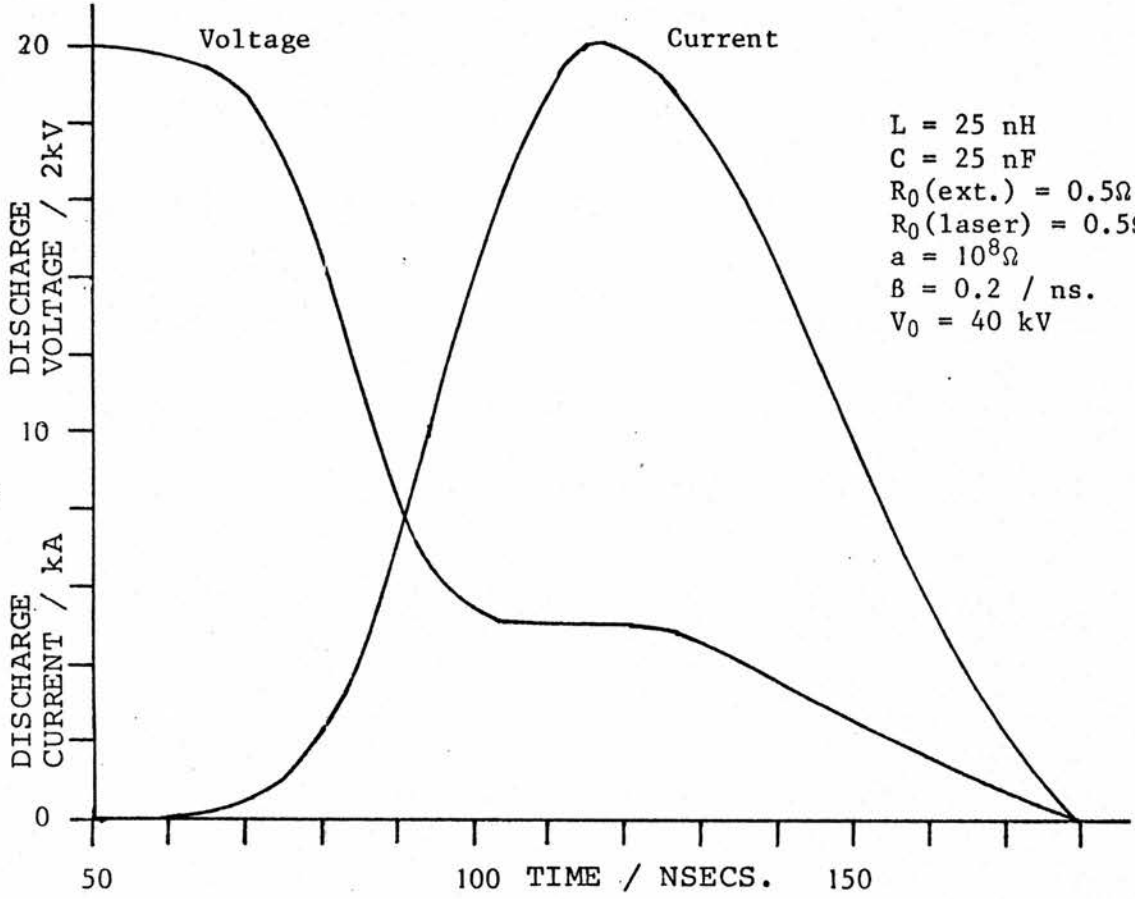

Figure 2.2
Time evolution of the LC inversion circuit for KrF.

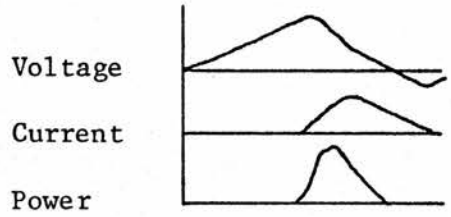

From Sze & Loree (1978).

voltage waveforms for a 25nF capacitor charged to 40kV (other values are shown on the graph). A kink in the voltage curve is clearly visible beginning at around 100nsecs. as an effect of the plateau level R_0. Indeed at 100nsecs. $ae^{-Bt} \sim 0{\cdot}21$ such that the discharge resistance is mainly R_0 (laser) and the fall of the resistance is effectively over by the peak of the current pulse. As mentioned in the last section such a discontinuity is visible in the oscillograms of Fletcher (1949) and of Sze and Loree (1978) [figure (2.2)] using in the latter case an LC-inversion circuit. Since a lower value of B has been used to that roughly derived from the experimental results of Sze and Loree a longer delay of around 40nsecs. exists between breakdown and discontinuity. A kink may also be seen in the discharge power graph shown as one of the examples in figure (2.3). This kink is seen to precede the voltage kink which in turn precedes the current peak and this behaviour seems to be visible in the results of Sze and Loree. The power peak, on the other hand, is predicted here to occur slightly before the current peak whereas the difference is more marked in the experimental case where power deposition is almost over by the peak of the current. The fact that inductance is not included for the discharge head would be expected to have some effect upon the shape of the voltage and therefore the power curves.

The remaining two graphs in figure (2.3) demonstrate the effect on power deposition of lowering the plateau level R_0 (laser). The very evident kink is exaggerated as the ratio R_0 (laser) : R_0 (ext.) is reduced, developing into a separate peak for a ratio 2 : 5. It has been found that this effect

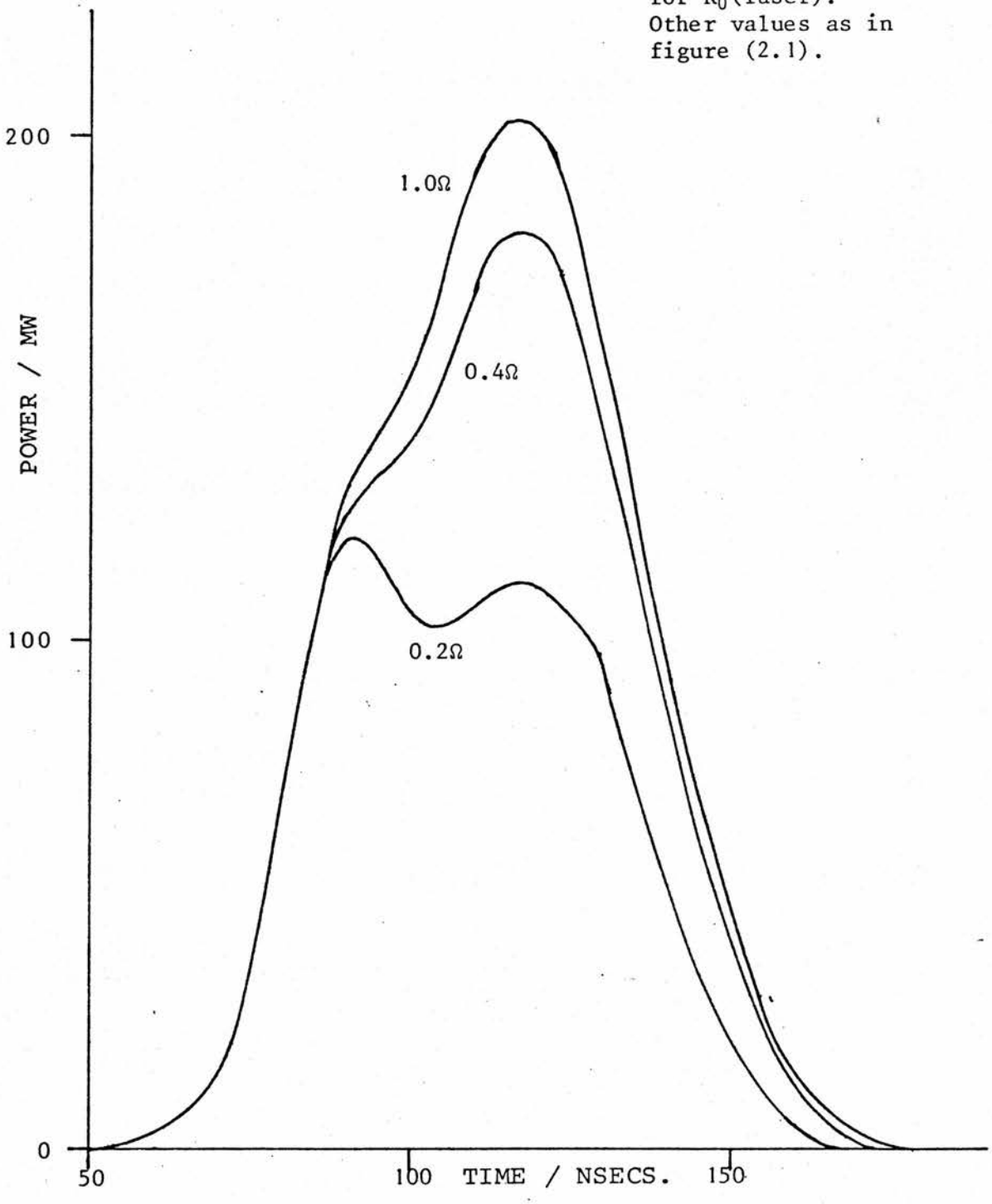

Figure 2.3 Power deposited into the discharge in the LCR circuit.

Values shown are for R_0(laser). Other values as in figure (2.1).

is smoothed somewhat by a lower value of B as might be expected from the less rapid fall to the plateau level, and also by faster rise times associated with a lower value of L or C.

The general effect upon current pulse shape of introducing an exponential term into the resistance can be seen in the figures (3.1) and (3.2) where two examples of current pulse shape are shown alongside the result provided by a constant resistance approximation. (The constant resistance result is positioned in time such that the zeros on the falling edge of the pulses coincide. Also shown is an approximate solution to be described in chapter 3.). The extra resistive term is seen to reduce the peak of the pulse whilst increasing the pulse width. In fact the width of the pulse for B = 0·2 is consistently around 27nsecs. longer than the constant resistance case for variations in capacitance. This result is indeed also true for inductance variations other than those of the order of 10nH when the difference increases. The pulse widths for capacitance variations are illustrated in figure (3.3).

In figure (3.4) the current peaks are shown for variations in capacitance as a function of the constant resistance prediction. (Note that the boundary conditions used in figure (3.4) are ones of equal initial charge CV_0 rather than charging voltage V_0.) Unlike the case of pulse width, however, the results derived from variations of inductance show a quite different form. Assuming an equal initial capacitor charge Q_0 the difference is generally increased for the shorter pulses i.e. for lower capacitance

or for lower inductance, the latter having the greater effect.

Energy deposition in a constant resistance circuit leads to energy sharing in the ratio of the resistances, with faster rates of rise associated with lower inductance. A higher capacitance leads to greater energy deposition than a smaller capacitor charged to the same voltage, but at a slower rate as a fraction of the originally stored energy. When the exponential term is included in the discharge resistance the discharge takes a greater share of the energy corresponding to the speed with which the current in the circuit rises, depositing energy while the discharge resistance is still high. This high region endures generally during the rise of the current only. For variations in inductance this leads not only to a faster rise for lower inductance but also to a greater energy total. For variations in capacitance the faster rise for a smaller capacitor implies that the energy deposition is more efficient, although the greater energy originally stored in a greater capacitance (assuming equal charging voltages) increases the actual value of discharge energy. In all cases the introduction of an exponential term into the resistance decreases the peak power from the value reached using a constant discharge resistance and the extra energy derives from the increased pulse width. For the example shown in figure (2.1) the peak power is reduced by 15% while the total energy deposited is increased by 12%. Generally speaking, around half of the energy deposited into the discharge is deposited before the current peak during the

resistance fall. This fraction increases for faster rise times and increases markedly if the ratio R_0 (laser) : R_0 (ext.) is reduced.

The graphs in figure (2.4) illustrate the energy deposition (normalized to originally stored energy) for variations in capacitance while figure (2.5) illustrates the effect of inductance.

Variations in the rate constant B lead to predictable effects whereby slower rates of fall broaden the current pulse and reduce the peak whilst the longer time spent in the high resistance region increases the total deposited energy. A fall in deposition rate is observed in reducing B from infinity (a constant discharge resistance) to 0·10. Any physical interpretations must include the possibility of reduced excimer formation efficiency associated with a slow fall of resistance. For instance Sze (1979) has commented that for the rare gas halide lasers the ionization rate may be reduced by the use of a lower value of $\frac{E}{p}$ at breakdown but that this also reduces the excitation of rare gas metastables. Laser output is adversely affected despite the apparent gain in input energy.

2.5 A t^{-m} Form of Resistance

In Chapter 1 mention was made of the time-resolved impedance measurements made by Watanabe et al. Measurements were made for two gap widths, 30mm at 1·5atm. and 45mm at 1·7atm. for a gas mixture of F_2/Kr/He = 0·2/5/94·8 in a preionized LC-inversion circuit charged to 40kV. The impedance was considerably higher at all times in the larger gap, falling to roughly 0·6Ω after 100nsecs. compared with a

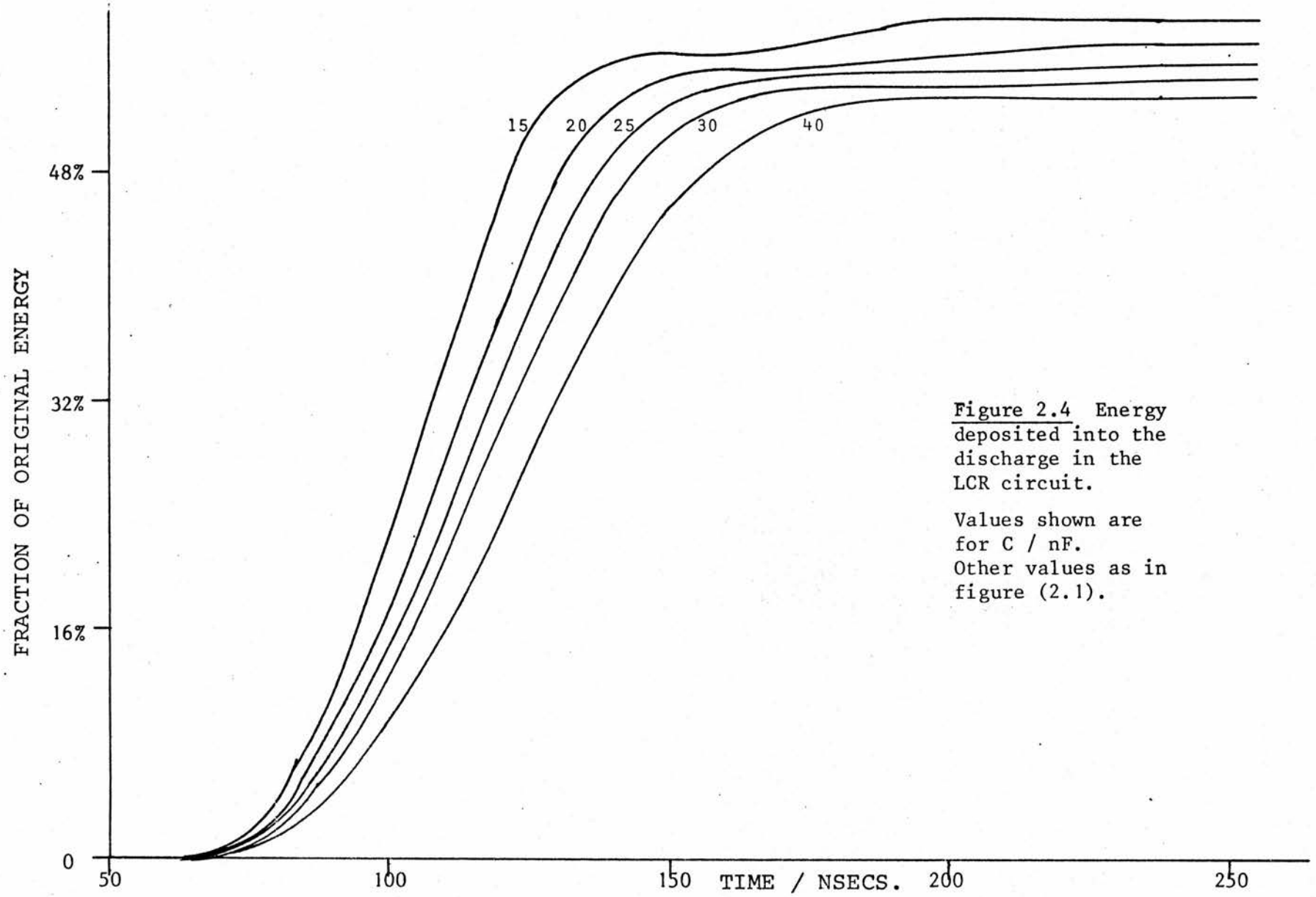

Figure 2.4 Energy deposited into the discharge in the LCR circuit.

Values shown are for C / nF.
Other values as in figure (2.1).

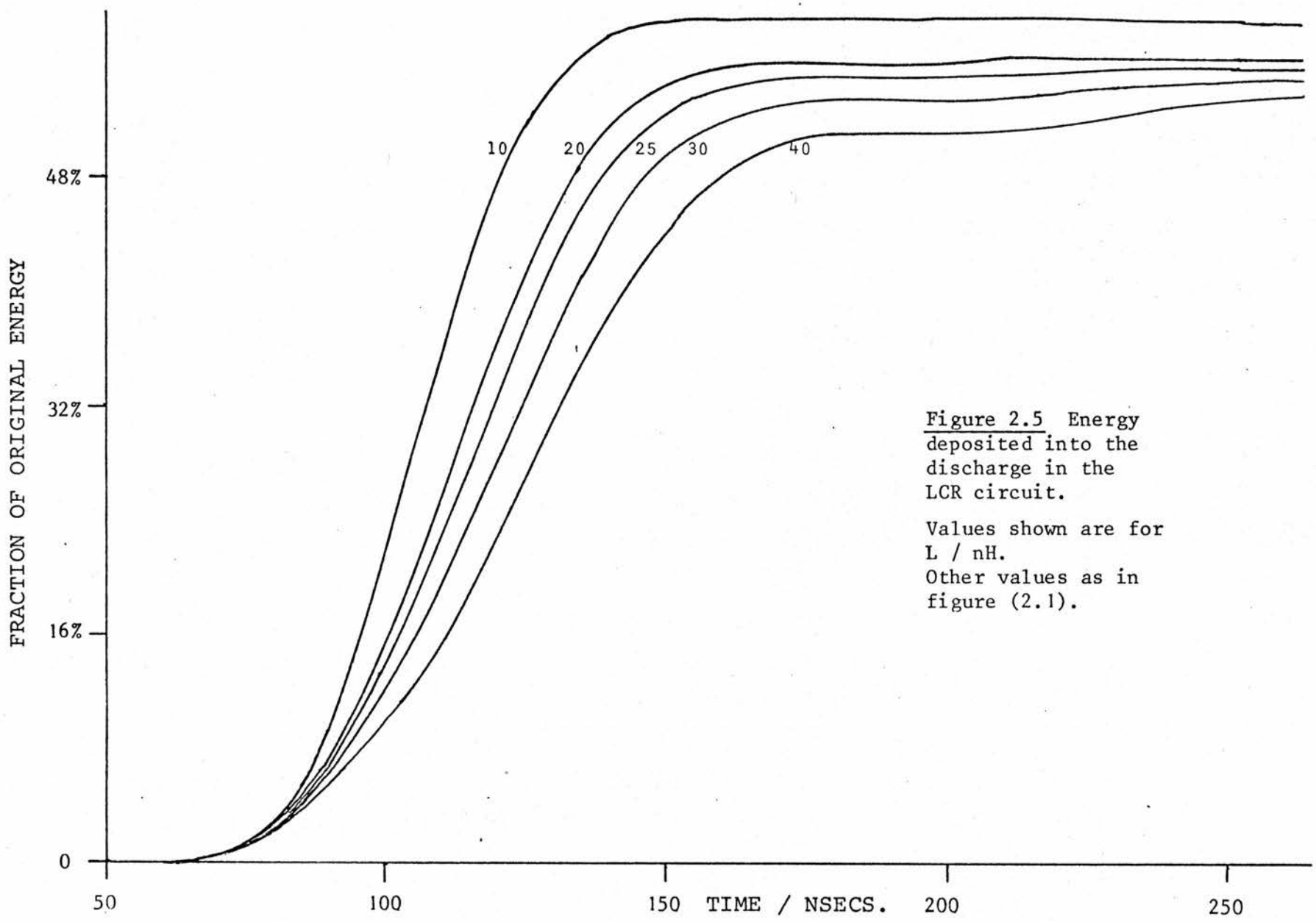

Figure 2.5 Energy deposited into the discharge in the LCR circuit.

Values shown are for L / nH.
Other values as in figure (2.1).

Figure 2.6 Points taken from Watanabe et al (1979) for a KrF amplifier. The solid lines have slopes as shown.

□ 45mm gap ; 1.7atm
Slope = -1.3

○ 30mm gap ; 1.5atm
Slope = -1.15

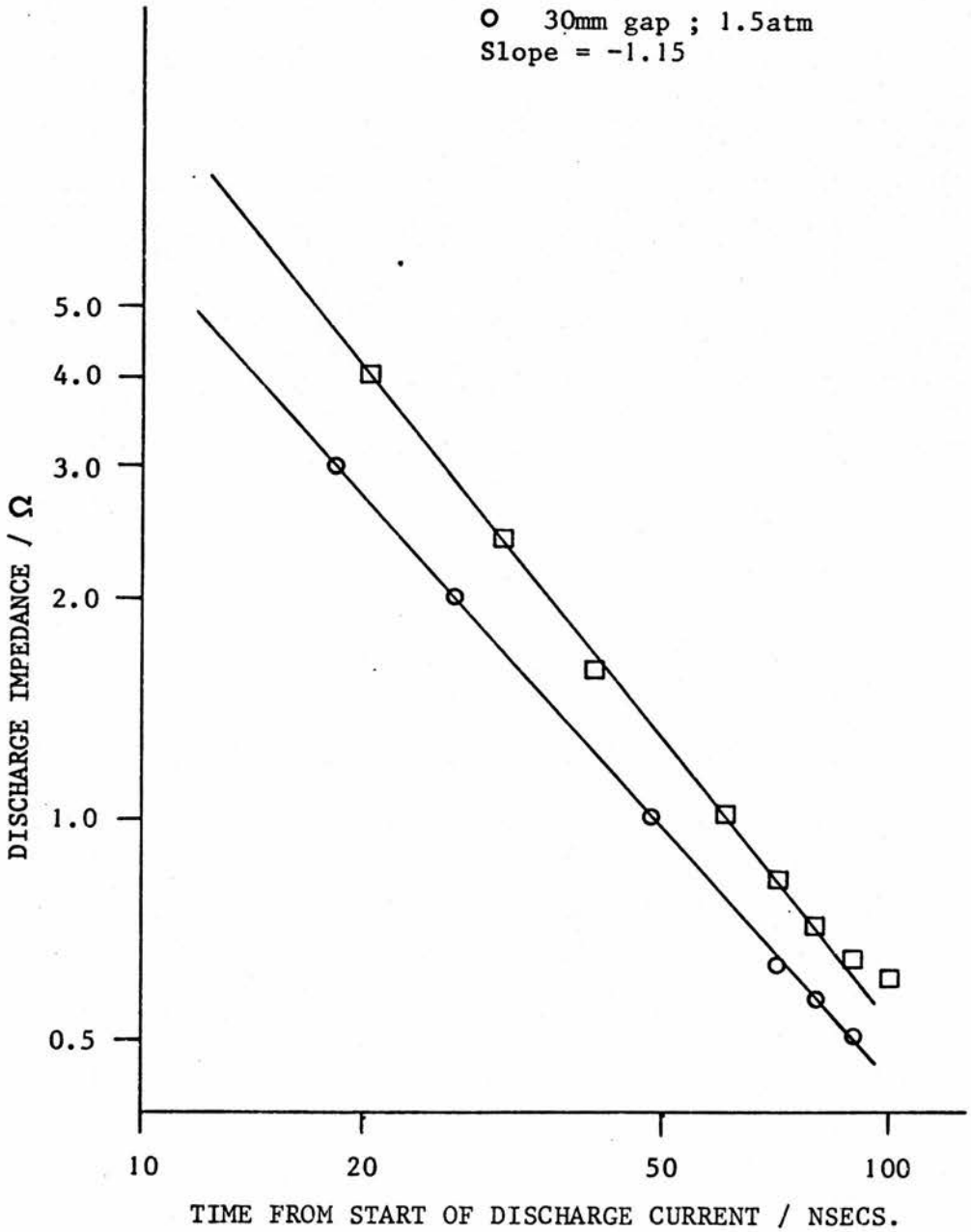

value of $0{\cdot}4\,\Omega$ for the 30mm gap.

Fits made to these curves by the present author indicate a time dependence of the form t^{-m} with m lying in the region of 1.15 to 1.3 (the smaller gap and pressure give the lower value) and without the addition of a lower plateau level. While solutions for such a time dependence are not considered here, it is possible to solve exactly the case of an LCR circuit discharge obeying a dependence with $m \leqslant 1$ in the form of a series, allowing a wide scope of mathematical analysis. Indeed a sum of terms obeying $m \leqslant 1$ could be envisaged.

The method of series solutions is given in mathematical texts, for instance the book by Mathews and Walker (page 13). Briefly, a solution is possible for $m \leqslant 1$ since the point at $t = 0$ is then a regular singular point (unless $m \geqslant 0$ in which case it is an ordinary point). A series solution has been found for the case

$$R(t) \equiv R_0 + \frac{\lambda}{t} \qquad -(2.6)$$

a sum of two terms with $m = 0$ and $m = 1$. It is interesting to note the similarity of the differential equation for capacitor charge Q to a Bessel's equation of order zero:

$$L\frac{d^2Q}{dt^2} + (R_0 + \frac{\lambda}{t})\frac{dQ}{dt} + \frac{Q}{C} = 0\,. \qquad -(2.7)$$

Differentiating, the equation in current I becomes

$$L\frac{d^2I}{dt^2} + (R_0 + \frac{\lambda}{t})\frac{dI}{dt} + (\frac{1}{C} - \frac{\lambda}{t^2})\,I = 0\,. \qquad -(2.8)$$

A series solution defined by

$$I = \sum_{n=0}^{\infty} g_n\, t^{n+s} \qquad -(2.9)$$

gives upon substitution into the differential equation

$$s = 1 , -\frac{\lambda}{L} \qquad \text{—(2.10)}$$

and the two solutions are defined by the relations

$$g_1 = -\frac{R_0}{[\lambda + L(1+s)]}\, g_0$$

$$g_{n+2} = -\frac{[\, R_0\, g_{n+1}(n+s+1) + \frac{g_n}{C}\,]}{(n+s+1)\,[\, L(n+s+2) + \lambda\,]} \,. \qquad \text{—(2.11)}$$

Since the solution with negative s yields infinite current at t = 0 it is not appropriate. In fact consideration of equation (2.8) shows that $I \sim t$ as $t \to 0$, an infinite resistance demanding zero current.

The coefficients fall as n^{-1} for the higher n. A series of coefficients falling as n^{-2} can be derived by removing the expected (as $t \to \infty$) $\exp(-\frac{R_0 t}{2L})$ dependence from I in an attempt to discover a more rapidly converging series.

2.6 Discussion

The effect of a time dependent resistance in an LCR circuit has been discussed in the light of the well known behaviour of the constant resistance circuit. The high resistance region reduces the current and power peaks from those associated with a constant resistance only, while lengthening the current and power pulses. The effect is greater when the high resistance region endures through a larger proportion of the pulse i.e. when L, C or the constant B are smaller.

Some agreement has been found with qualitative aspects at least of experimental results. The delay of about 40nsecs. between breakdown and the kink in the voltage curve of

figure (2.1) is consistent with the method used in section (2.3) to estimate a value for B.

Finally, mathematical techniques have been suggested for the solution of the LCR circuit over a range of time dependences of the form t^{-m}. An approximate solution for more general time dependences, including an exponential resistive term, will be detailed in Chapter 3.

CHAPTER 3

The WKB Method Applied to the LCR Circuit

The WKB Method Applied to the LCR Circuit

3.1 Introduction

The results of the previous chapter are based upon numerical solutions to a linear second order differential equation with non-constant coefficients. The mathematical solution for a constant parameter LCR circuit was first proposed by Lord Kelvin in 1853. For a gaseous discharge, however, the resistance at least is a time varying quantity and mathematical solutions are exceedingly difficult if not impossible. The WKB (Wentzel, Kramers, Brillouin) method used extensively in wave theory provides for the approximate treatment of such a second order differential equation. The general mathematical technique had been used earlier by Liouville, Rayleigh and Jeffreys.

This chapter reports upon the application of the WKB method to various examples studied numerically in the previous chapter. The respective solutions are compared and empirical improvements to the method suggested. The method is also compared to the much simpler approximation of a constant discharge resistance for which an exact solution is known.

The WKB approximation is briefly reviewed and its application to this problem described in Appendix 4.

3.2 The Current Pulse Shape

Figures 3.1 and 3.2 illustrate two examples of the WKB solutions shown against the numerically derived results of the previous chapter. The monotonically decreasing

Figure 3.1 Solution and approximations to the LCR circuit.

Values as shown in figure (2.1).

– – – – – Computed solution.
·---------- Solution for R(t) = constant.
———————— W.K.B. approximation.

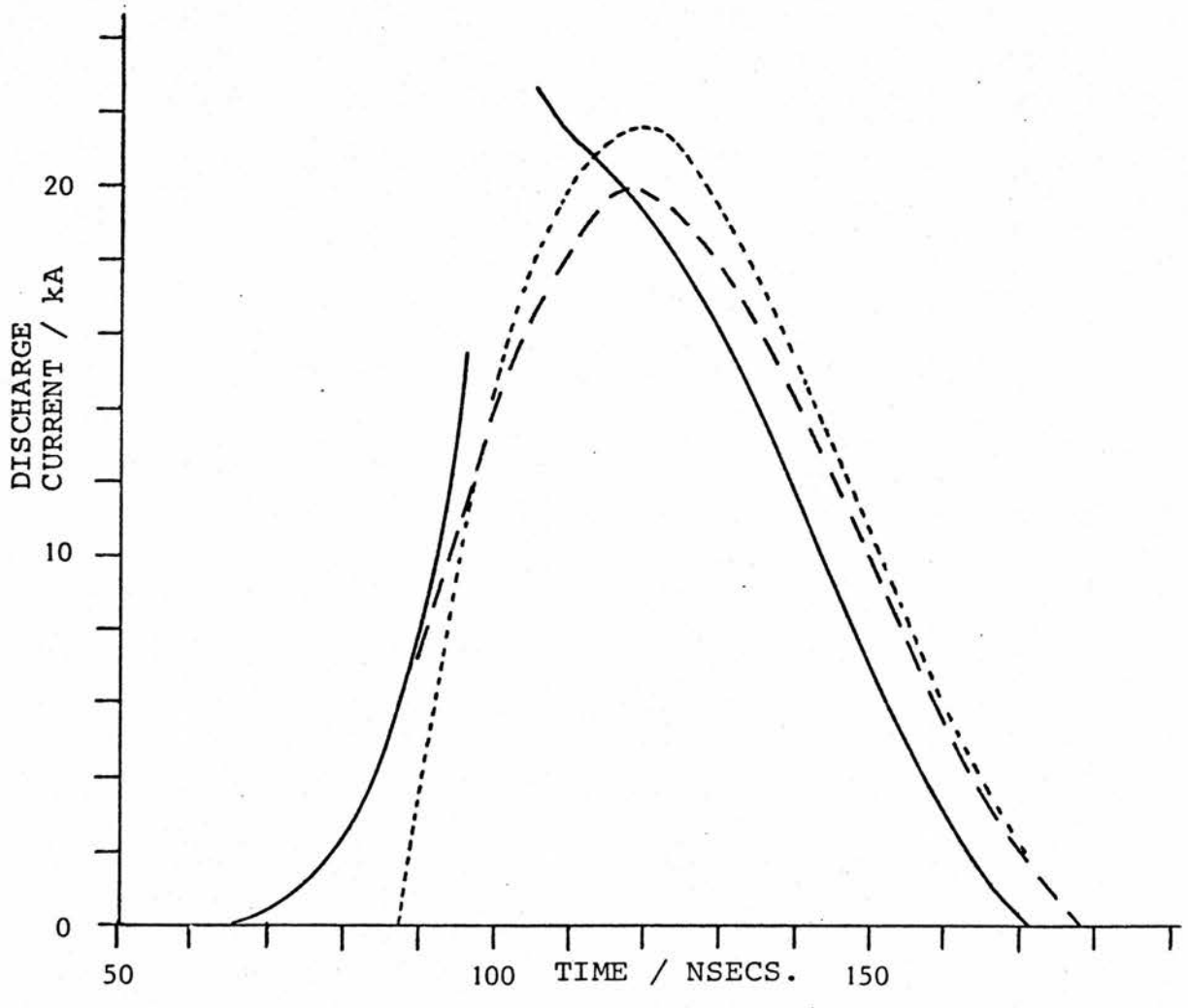

Figure 3.2 Solution and approximations to the LCR circuit.

L = 10 nH.
Other values as shown in figure (2.1).

— — — — Computed solution.

---------- Solution for R(t) = constant.

———— W.K.B. approximation.

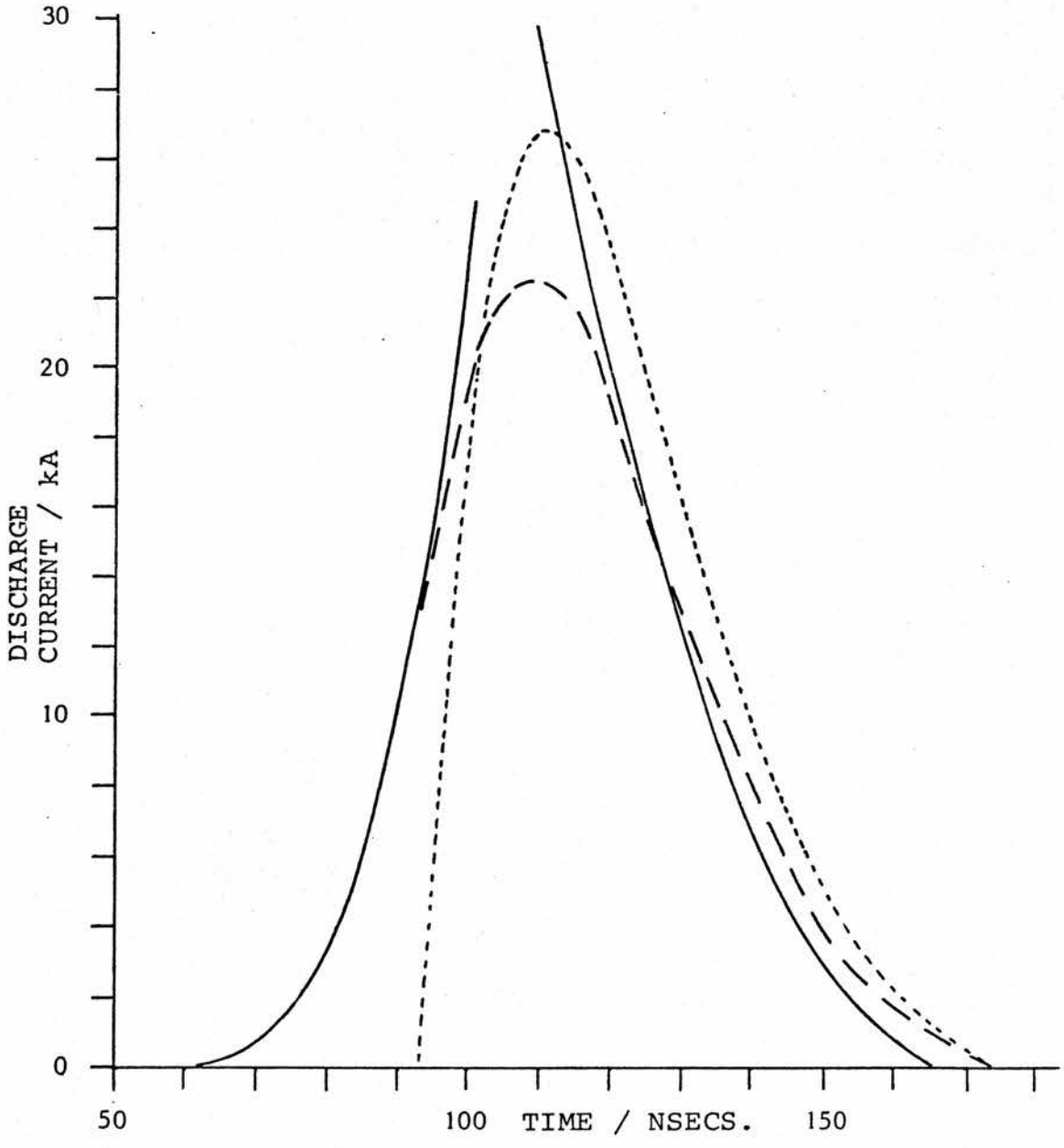

resistance splits the solution into two distinct regions around a turning point t_0; an initial exponential growth of current is followed by an oscillatory region, both forms rising to infinity at the turning point due to the term in the denominator. It should be noted that this point is not determined by the condition $R^2(t_0) - \frac{4L}{C} = 0$ although the value of t_0 will be close.

The rise from t = 0 where the boundary conditions are given mimics exactly the scale and form $I \sim e^{Bt}$ of the correct solution. While this form soon becomes a large overestimate in the region of interest beyond about 60nsecs, the WKB approximation continues to follow the correct curve for some distance towards the turning point.

The differential equation near to this turning point may be written in the form of the Stokes differential equation. This allows the Stokes' regions to be identified for the problem and by integration around what Kemble called a "good path" the required coefficients for the oscillatory region $t > t_0$ may be derived. [See for example the book by Mathews and Walker, page 27.] The necessary coefficients are in fact complex and a phase of $-\frac{\pi}{4}$ is introduced.

Beyond the turning point the oscillatory solution quickly becomes a simple underdamped oscillation as the resistance becomes essentially constant. The phase, however, is incorrect, with the current oscillating ahead of the numerical solution.

The approximate solution with constant discharge resistance (ignoring the ae^{-Bt} term) is also shown in figures 3.1 and 3.2 positioned such that the end of the current pulse coincides with that of the numerical solution.

This corresponds to beginning the pulse when the two terms in $R(t) = R_0 + ae^{Bt}$ are of comparable magnitude. The effect of the exponential addition to the resistance is clearly to broaden the current pulse and reduce the peak.

3.3 The Current Pulse Width and Phase Error

The WKB method provides a particularly accurate fit to the current rise derived from numerical methods. The fall of the current pulse is, however, predicted early. This suggests that the phase constant $\frac{\pi}{4}$ mentioned in the last section is an underestimate and that a further constant is required. Since the resistance is essentially constant by the end of the current pulse this phase factor may be deduced from the error $T_{err.}$ in the position of the current zero.

The WKB solution was calculated for several values of capacitance (15, 20, 25, 30, 40nF) to compare with results of the previous chapter. Figure 3.3 shows the pulse width determined by this approximation plotted against $\frac{\pi}{\omega}$, the width predicted by a constant resistance R_0 with

$$\omega^2 = \frac{1}{LC} - \frac{R_0^2}{4L^2} \quad . \qquad -(3.1)$$

This latter approximation is itself represented by a straight line. Also included are the numerically derived values showing a reasonably linear relationship. Indeed the numerical values are given by $(\frac{\pi}{\omega} + 27\text{nsecs.})$ in these examples. The remaining graph of $T_{err.}$ against $\frac{\pi}{\omega}$ is also linear, indicating that the phase error $\omega T_{err.}$ varies linearly with ω.

The WKB method thus provides a reasonable estimate of the pulse width assuming an exponentially decreasing

Figure 3.3 Pulse widths and error against $\frac{\pi}{\omega}$ for variations in capacitance. L = 25 nH.

X Actual width.

□ W.K.B. predicted width.

O $T_{err.}$

..... $\frac{\pi}{\omega}$.

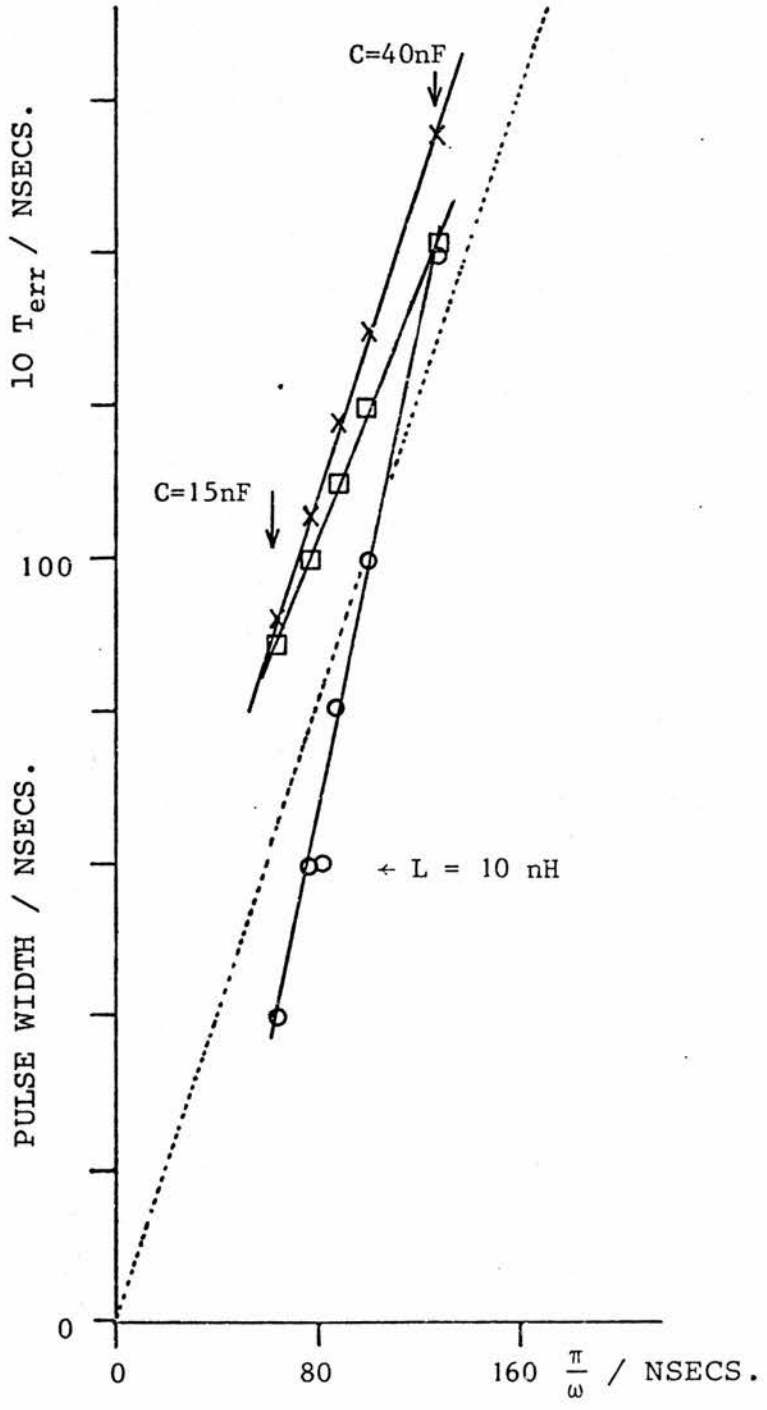

resistive term. In the cases shown, the error lies between 4% and 9% (4nsecs. and 14nsecs.) and appears to be well-characterised in terms of ω or the WKB-predicted width itself for these variations in capacitance. The constant resistance approximation, on the other hand, provides a constant error of around 27nsecs. for these variations. Other examples have shown that similar characterisations can be applied to variations of inductance, but requiring separate empirical rules. The point on figure 3.3 showing the position of the L = 10nH example of figure 3.2 suggests, however, that the same WKB characterisation in terms of ω alone would not be unreasonable for inductance variation, leaving, in this example, only around 1-2nsecs. error. The phase error is in fact much less sensitive to inductance variation than to capacitance, as indeed is ω.

3.4 The Current Peaks

The connection formula between the two regions $t < t_0$ and $t > t_0$ mentioned in section 3.2 and Appendix 4 predicts both the magnitude and the phase of the current oscillations in the later region. In section 3.3 the phase was demonstrated to be incorrect causing an underestimate in the pulse width, and it is to be expected that the predicted size of the current peak will also be in error.

Since the WKB approximation tends to infinity near to the turning point t_0 no current peak may be apparent. However, a point of inflection is apparent suggesting the movement towards a peak; on the scale of the graph in figure 3.1 this point of inflection is visible at around 111nsecs. If the

current at this point is taken as a prediction of the current peak, then for the examples of the previous chapter the errors lie between 5% and 11%.

A second method of deriving a current peak from the WKB approximate solution is to work backwards via a constant resistance method from the later regions of the solution. This can provide improvements over the latter method, the errors for the capacitance variations ranging from 1% to 9%. Both estimates are given in graphical form in figure 3.4 for variations in capacitance. They are plotted against the current peak for constant discharge resistance, given by

$$I(\text{peak}) = \omega C V_0 \left[1 + \frac{1}{\left(\frac{4L}{R^2C} - 1\right)} \right] \exp\left[-\frac{R}{2L\omega} \tan^{-1}\left(\frac{2L\omega}{R}\right) \right] \sin\left[\tan^{-1}\left(\frac{2L\omega}{R}\right) \right] \quad \text{—(3.2)}$$

Also included are the numerical solutions to the peaks and the constant resistance solution itself which appears as a straight line.

In the region shown it is evident that the WKB predictions follow closely the behaviour of the numerical solutions. The predictions from the points of inflection, while less accurate than those of the back-extrapolation method, do follow a roughly parallel curve about 1 to 1·5kA above the correct value. The constant discharge resistance method, while more accurate for lower peaks, appears to diverge from the correct value at higher peaks. The back-extrapolation values, on the other hand, appear to improve towards the higher peaks.

Examples on inductance variation indicate that characterisations in terms of the constant resistance peaks do not suffice, and that separate empirical rules are

Figure 3.4 Current peaks against the constant resistance predictions for variations in capacitance.

Q_0 = 25nF . 40kV = 1mC.

X Actual peak.

□ W.K.B. predicted peak.

o W.K.B. "back extrapolated" peak.

--------- Constant resistance peak.

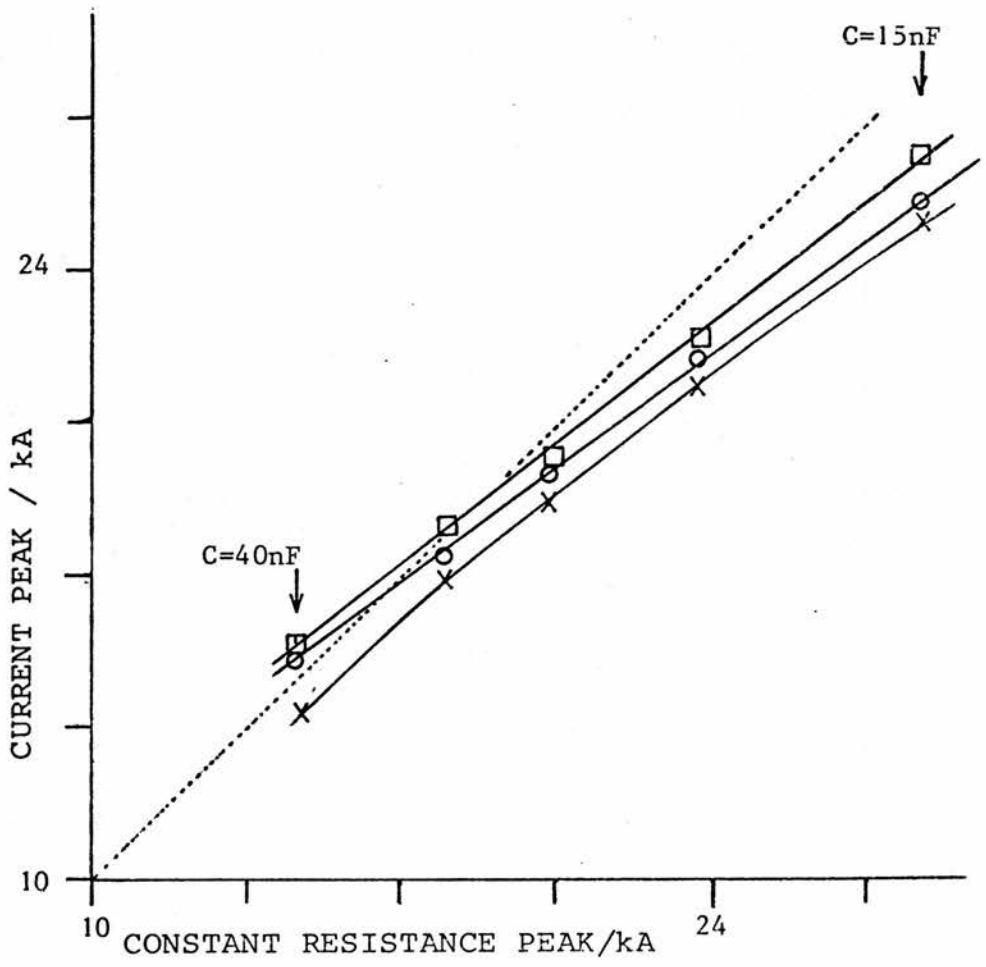

required. The predictions deteriorate for the faster rising cases of lower inductance.

3.5 Artificially Improved Versions

Knowledge of the phase error and current peak error as described in the last two sections allows a greatly improved WKB version of the region $t > t_0$ to be obtained. The introduction of the extra phase factor significantly improves the form of the current peak providing a much more realistic picture of the pulse, while the peak error provides the necessary scaling. An example of the result is given in figure 3.5 alongside the numerical solution and a scaled, positioned version of the constant resistance approximation. While the latest offers no approximation to the current rise, it would be expected to improve upon the WKB shape around the peak and this is seen to be the case. A combination of the two approximations based only upon the two empirical WKB factors leaves a small region unspecified, roughly between 90 and 105nsecs. in figure 3.5.

3.6 Discussion

For the particular case of an exponentially decreasing term in the discharge resistance, the WKB method has been shown to provide reasonable estimates for the pulse height and width of a gaseous discharge from a charged capacitor. These estimates can improve significantly upon those derived from a constant discharge resistance approximation. The shape of the pulse is predicted well, in particular the initial rise from zero. The peak and subsequent oscillation

Figure 3.5 Artificially improved approximations for the example of figure (3.1).

— — — — Computed solution.

---------- Solution R(t) = constant.

———— W.K.B. approximation.

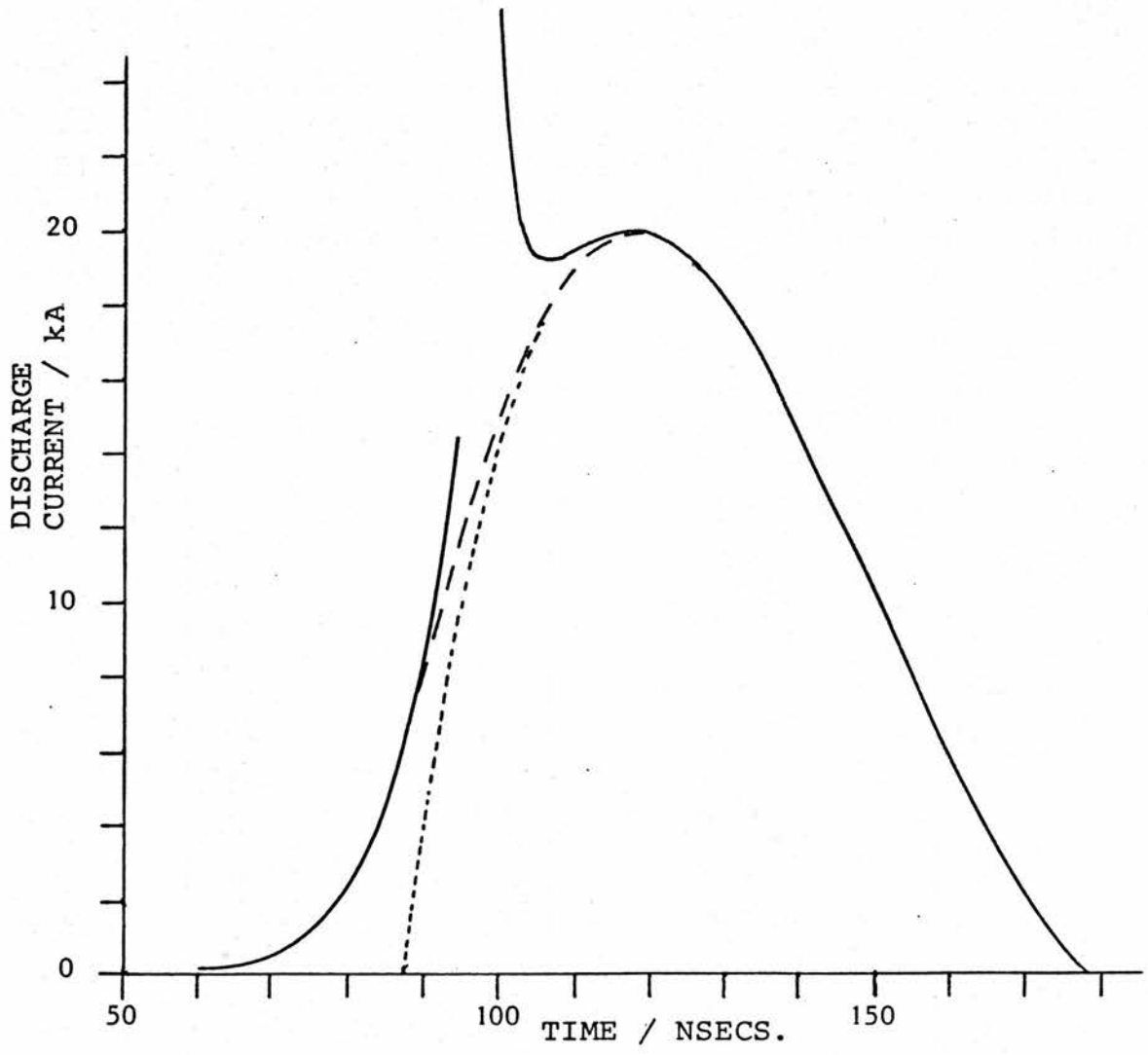

are greatly improved by the inclusion of two empirical but well-characterised factors of phase and scale, although the same could be said for a constant resistance. These factors arise mainly in the region around t_0 where the WKB approximation becomes invalid, and may be predictable to some extent mathematically.

The examples studied in this chapter involve a relatively slow fall in resistance $\exp[-\frac{t}{5ns}]$ although to a high base level of 1Ω. For a fast fall the resistance approaches a step-down from infinity to a ground level and a constant resistance approximation would be expected to become more suitable. The validity of the WKB approximation must also be considered for fast rates of change.

While the method has been applied to an exponential decay of resistance, other forms of decay have been suggested - for example the t^{-3} experimental results of Sorenson and Ristic - and it is hoped that the method may be usefully applied to some of these. To this end, much of the analysis of Appendix 4 is carried out for the general case.

CHAPTER 4

Gaseous Discharges in the LC-Inversion Circuit

Gaseous Discharges in the LC-Inversion Circuit

4.1 Introduction

Several authors have reported discharge models of the LC-inversion circuit. Greene and Brau (1978) in a companion paper to the experimental report by Sze and Loree (1978) performed a numerical analysis based upon equations coupling the discharge kinetics to the discharge circuitry and indicated the extent to which theory could be used to predict results not only for discharge characteristics but also for laser performance. While this work applied specifically to a lumped component circuit, it has been suggested by Burnham et al (1976) that the Blumlein circuit could lose its transmission line nature over the relatively long rise times involved in an excimer laser discharge. A lumped parameter model would then be appropriate, closely related to the LC-inversion geometry.

In addition to more involved numerical analyses based upon circuit and discharge coupling [for instance Greene and Brau (1978) for rare gas fluorides, Chubb and Michels (1979) for rare gases], models of the LC-inversion circuit have also been based upon a constant discharge resistance following gas breakdown [Schwab and Hollinger (1976) for nitrogen, Burnham et al (1976) for rare gas fluorides]. This latter model lends itself to exact analysis for the circuit and some results are detailed in Appendices 1 and 3 leading to an exact solution of equations for energy deposited into the discharge for general boundary conditions.

It is the purpose of this chapter, however, to attempt a

middle ground between,on the one hand,the simplest model of a constant discharge resistance and,on the other hand,the much more complicated treatment of gas discharge kinetics. A time-dependent discharge resistance will be used in order to study circuit behaviour and in particular to predict energy deposition into the gas discharge.

4.2 The Circuit and Method of Solution

Figure (4.1) shows the discharge circuit used to model the LC-inversion circuit. The inductances L_1, L_2 and l the resistances R_1, R_2 and r and the capacitances C_1 and C_2 are as may be found in figure (A1.1). L_2 is composed of L_2 (ext.) from the external circuit and L_2 (laser) of the discharge head while R_2 is similarly composed of R_2 (ext.) and R_2 (laser). The definition

$$R_2(\text{laser}) = R_{20}(\text{laser}) + ae^{-Bt} \qquad -(4.1)$$

allows a time-dependent form for the discharge resistance. Using charges Q_1 and Q_2 on the two capacitors C_1 and C_2 respectively as the dependent variables, the discharge equations are given by Kirchhoff's laws as

$$L_1\ddot{Q}_1 + R_1\dot{Q}_1 + l(\ddot{Q}_1 + \ddot{Q}_2) + r(\dot{Q}_1 + \dot{Q}_2) + \frac{1}{C_1}(Q_1 + Q_2) = 0 \qquad -(4.2)$$

$$L_2\ddot{Q}_2 + R_2(t)\dot{Q}_2 + l(\ddot{Q}_1 + \ddot{Q}_2) + r(\dot{Q}_1 + \dot{Q}_2) + \frac{1}{C_1}(Q_1 + Q_2) + \frac{1}{C_2}Q_2 = 0 \qquad -(4.3)$$

$$\text{with } I_1 = \dot{Q}_1 \text{ and } I_2 = \dot{Q}_2 . \qquad -(4.4)$$

The two differential equations (4.2) and (4.3) can be uncoupled to yield a single fourth order differential equation in Q_1 or Q_2. For constant coefficients the assumption $Q \sim e^{kt}$ yields a quartic equation in k which is exactly soluble. In practice numerical solutions are preferable to the exact solutions and the analysis of

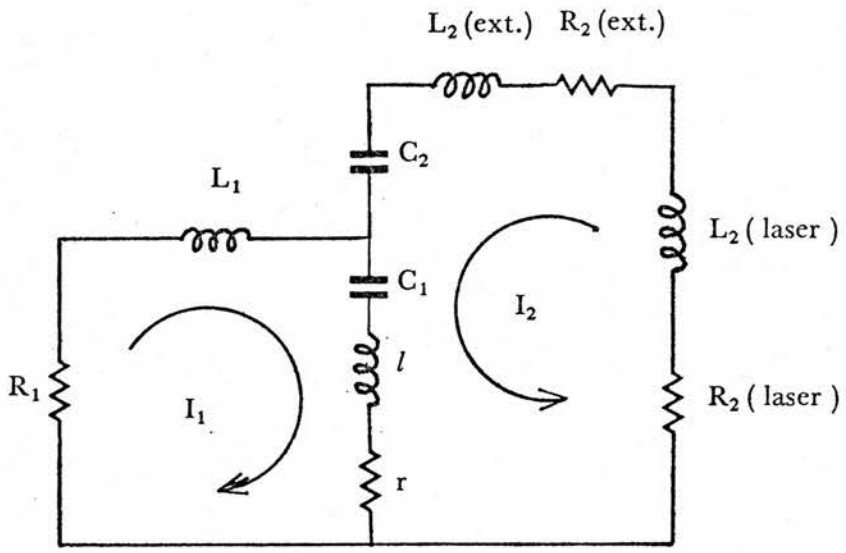

Figure 4.1 Model of the LC-Inversion Circuit

Appendix 1 simply assumes that the four roots k_i are known. The four coefficients required to complete the solution are determined in Appendix 1 from initial boundary conditions on currents I_1, I_2 and charges Q_1, Q_2. The result is a mathematical expression for the behaviour of the LC-inversion circuit with constant circuit parameters.

This analysis is employed in a step by step fashion to solve the LC-inversion circuit for the more general time dependent circuit parameters already discussed. The method is described in Appendix 2.

4.3 Simulation of Experimental Waveforms

In Chapter 2 the results of Sze and Loree (1978) were used to estimate a time constant for the resistive phase of breakdown in an excimer laser discharge. An LCR circuit discharge was then modelled and a comparison was made of qualitative aspects at least of the experimental and modelled waveforms. In this section an attempt will be made to simulate as closely as possible the waveforms (figure (2.2)) observed by Sze and Loree with the aid of the companion paper by Greene and Brau (1978) mentioned in the introduction. Circuit parameters are taken from the two papers when possible.

In section (2.3) a value of $B \sim 0{\cdot}3ns^{-1}$ was estimated for the rate constant (1/time constant). This value is used here. The ringing arm capacitance C_1 and the discharge arm capacitance C_2 are taken from the experimental paper to be 19nF and 24nF respectively both charged to 25kV. Greene and Brau in their model took L_1 to be 47nH, the value used here. (Note that their notation differs.) Similarly $0{\cdot}15\Omega$ is

attributed to the spark gap (to R_1) and to both capacitors C_1 (to r) and C_2 (to R_2 (ext.)). The value R_{20} (laser) is taken as $0{\cdot}3\Omega$ in accordance with the estimate of Sze and Loree and L_2 (laser) as 7nH. Since l is not included in either paper it is set to zero. The value of L_2 (ext.) is reduced from the given 26nH to 20nH in the light of trial results and bearing in mind the rough derivation by Sze and Loree.

The initial stage of the program involves setting R_2 high during the ringing of the switching loop. In theory the circuit can reverse the voltage across C_1 to build up a discharge voltage almost twice the charging voltage before breakdown. In practice, while a considerable overvoltage is achieved above the static breakdown level, the gas breaks down before voltage doubling. Clearly the peak voltage level will depend upon the rise time of the voltage pulse and therefore upon L_1. Sze and Loree comment that the gas actually begins to break down at around 10kV in all cases. The finite time taken for current to build up in the discharge allows the overvoltage to develop.

To model this effect the resistance fall is initiated at a discharge voltage of 20kV with the initial value of R_2 (laser) as a = 1000Ω. This allows a "formative period" before R_2 decreases to a level at which I_2 is appreciable. The formative period can be increased by increasing a (or decreasing B). Clearly the constant B is itself a function of overvoltage but, in so far as no discharge coupling is used, the model does allow a period for overvoltage, with increasing overvoltage for faster rise times. The time taken

for the exponential term ae^{-Bt} to fall to the same order as the plateau level R_{20} (laser) is, with these values of circuit parameters, around 27nsecs.

The results of this analysis are shown in figure (4.2) alongside the results of Sze and Loree. In accordance with the practice of Greene and Brau in their simulation, the waveforms have been adjusted in time so that the peaks of the voltage curves agree. Also the experimental current waveform has been normalized since absolute measurements were not made. The difference in voltage rise times may be partly attributed to the finite rise time of the spark gap. In fact the program provides an exponential facility for R_1 but this is not used.

The estimated 28kA current of Sze and Loree is not seen, the predicted peak being under 20kA. The relative timing of the voltage and current pulses is reasonably predicted but the current pulse is some 5 - 10nsecs. early. These discrepancies, however, may also be found in the predictions of Greene and Brau.

The peak voltage is predicted to be 25kV as given by Sze and Loree. This represents a voltage overshoot of 5kV above the 20kV level assigned to the beginning of the resistance fall. The kink in the voltage curve is visible at around 80 nsecs. on the rise of the current pulse but is early compared to the experimental kink. The negative overshoot is clearly reduced. Following Sze and Loree's suggestion, the peak current and the voltage at that time do yield a value of $0{\cdot}3\Omega$ for the resistance of the gas at that point. Modelling the discharge arm by an LCR approximation after

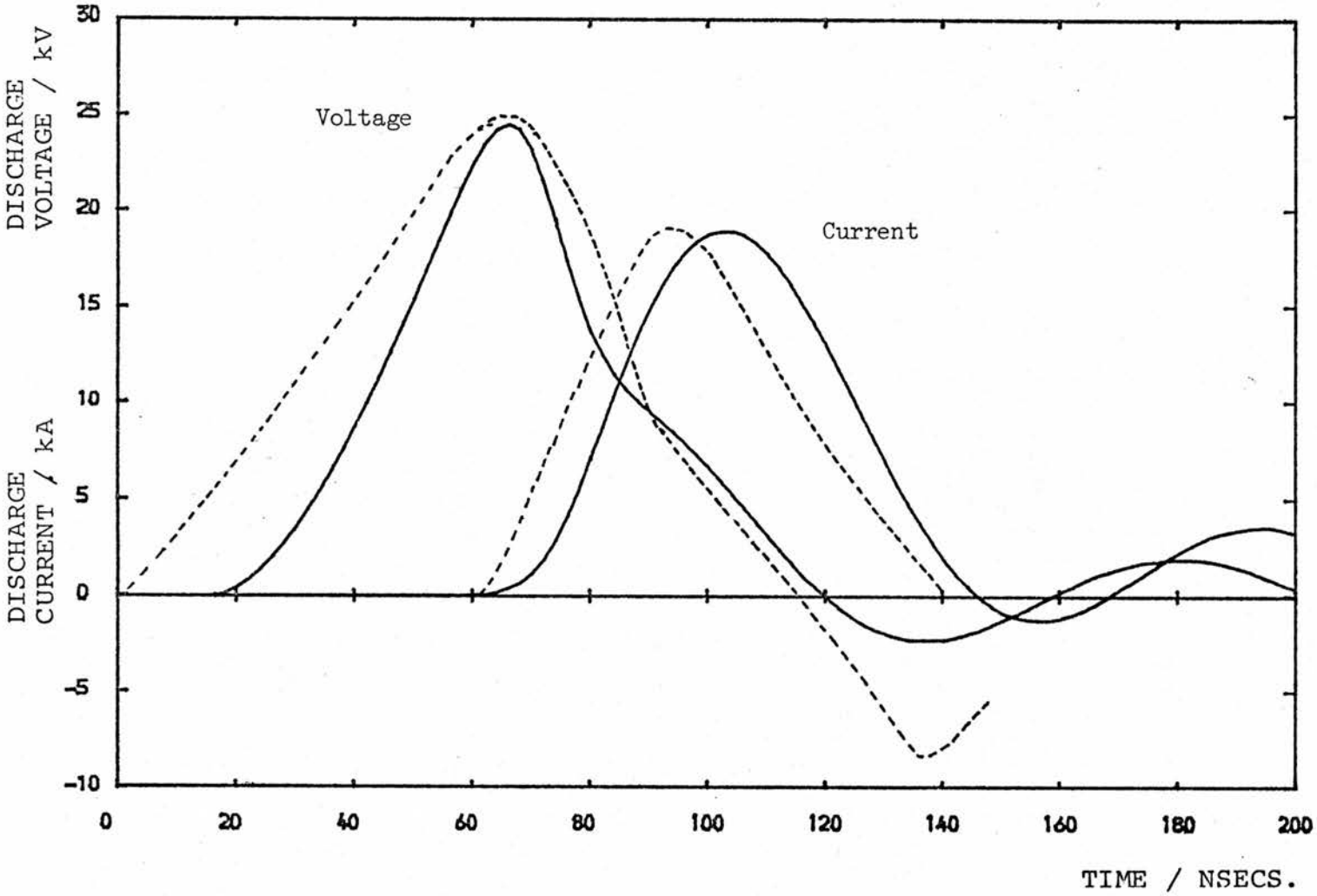

Figure 4.2 Discharge current and voltage waveforms in the LC inversion circuit.

-------- Experimental results from Sze and Loree (1978).

——— Present results.

L_1 = 47 nH.
L_2(ext.) = 20 nH.
L_2(laser) = 7 nH.
l = 0.
C_1 = 19 nF.
C_2 = 24 nF.
R_1 = 0.15Ω.
R_2(ext.) = 0.15Ω.
R_{20}(laser) = 0.3Ω.
r = 0.15Ω.
a = 1 kΩ.
B = 0.3 / nsec.
V_0 = 25 kV.

breakdown is shown to be dubious, however, by the form of I_1 (shown as one of the curves of figure (4.7)) which is held high during the discharge implying significant coupling between the two loops. This justifies the use of a different value for L_2 (ext.) from the one derived by the LCR approximation in which Sze and Loree ignored the ringing arm after breakdown.

Two theoretical power curves are given in figure (4.3), one defined as I_2V_L the product of discharge current and voltage while the other is defined as $I_2^2R_2$ (laser). The former is also given by Sze and Loree in their results. The rise of power a few nanoseconds before the current rise is in agreement with these. The kink caused by the plateau level R_{20} (laser) is visible in the purely resistive power curve but is smoothed out by the presence of the inductive term in I_2V_L. The position of the discontinuity at around 80 nsecs. agrees with the experimental results. However the peak of the power in the experimental case follows closely afterwards contrary to prediction. This may be in line with the late prediction of current peak.

It is interesting from the point of view of laser performance that the product I_2V_L exaggerates considerably the peak power actually deposited into the discharge resistance while underestimating the rise time.

The paper by Greene and Brau makes predictions of the experimental results of a slightly different circuit with C_1 replaced by a 24nF capacitor and with L_2 taken as 17nH. With these corrections (still keeping L_2 (laser) = 7nH) an analysis was performed by the present method and the

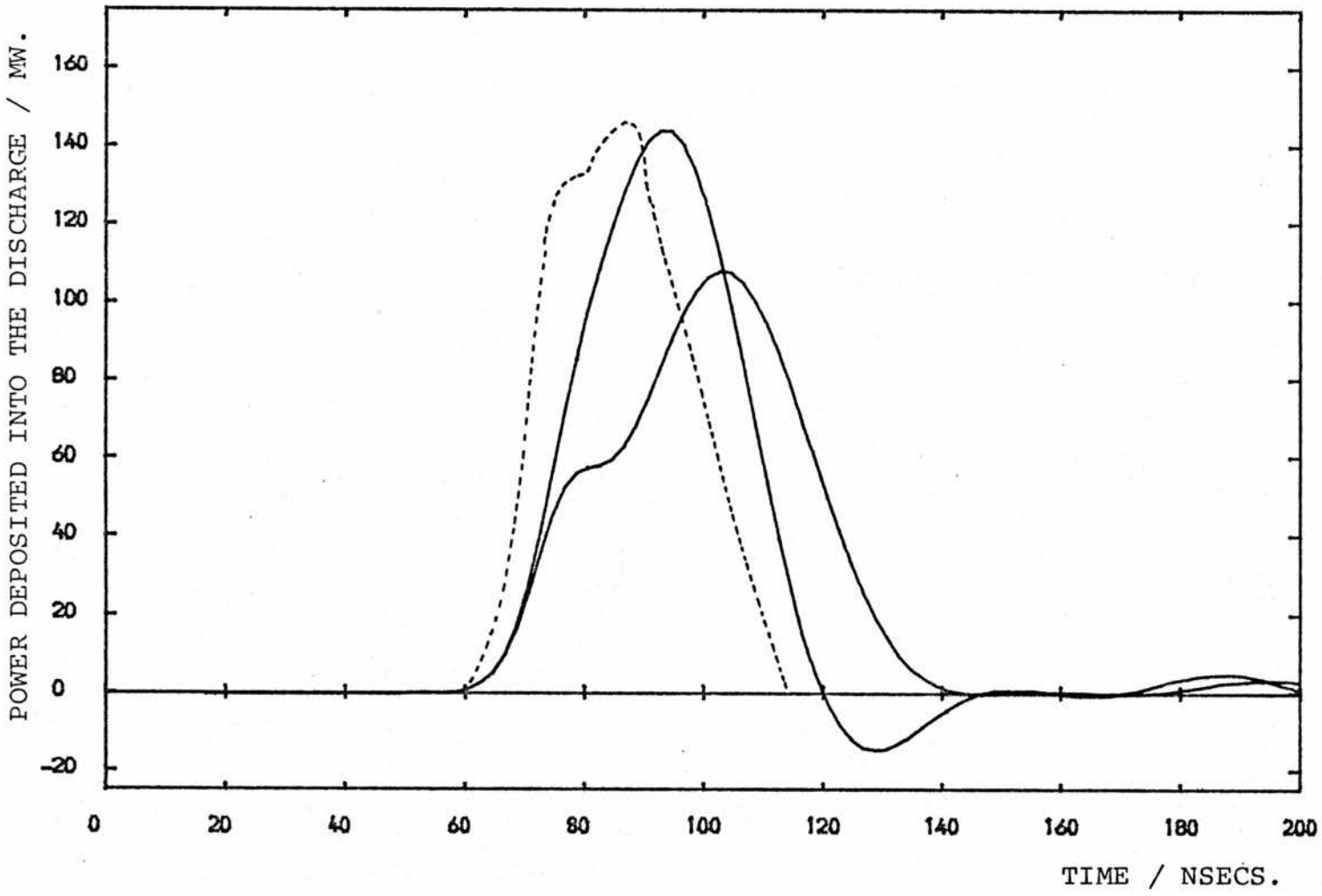

Figure 4.3 Power deposited into the discharge in the LC inversion circuit.

Values as in figure (4.2).

-------Experimental results from Sze and Loree (1978).

——— (Upper trace) Power $I_2 V_L$.

——— (Lower trace) Power $I_2^2 R_2$.

resulting voltage and current waveforms are illustrated in figure (4.4) alongside the experimental results.

4.4 Variations in Circuit Parameters

Beginning with the values for parameters used for the simulation of experimental results by Sze and Loree, individual parameters were varied and the effects on circuit behaviour are discussed in this section. In the next section the consequences for energy deposition are discussed more quantitatively.

Chubb and Michels (1979) have studied a Blumlein circuit for a rare gas discharge and have commented that the three important circuit parameters are switch inductance (L_1), switch resistance (R_1), and the capacitance ratio $\frac{C_2}{C_1}$. Sze and Scott (1978) have commented for a KrF laser that L_1 determines the voltage rise time while after breakdown L_2 determines the current rise time, adding that a 1nsec. increase in voltage rise time can lead to a 0·75% fall in peak voltage.

The discharge voltage curves of figure (4.5) illustrate the effect on voltage rise time of varying the ringing arm inductance L_1. The three values used - 30, 47 and 100nH - give voltage rise times of 42, 50 and 68nsecs. with peaks of 25·7, 24·4 and 22·8kV respectively. On the basis of a 0·75% per nsec. decrease in peak, the highest value of 25·7kV would be reduced to 24·2kV and 21·1kV for the two higher inductances. This shows excellent agreement in the region 30nH to 47nH in which practical inductances may lie.

The current peaks are similarly reduced as L_1 increases but rise time remains constant at around 35nsecs. Sze and

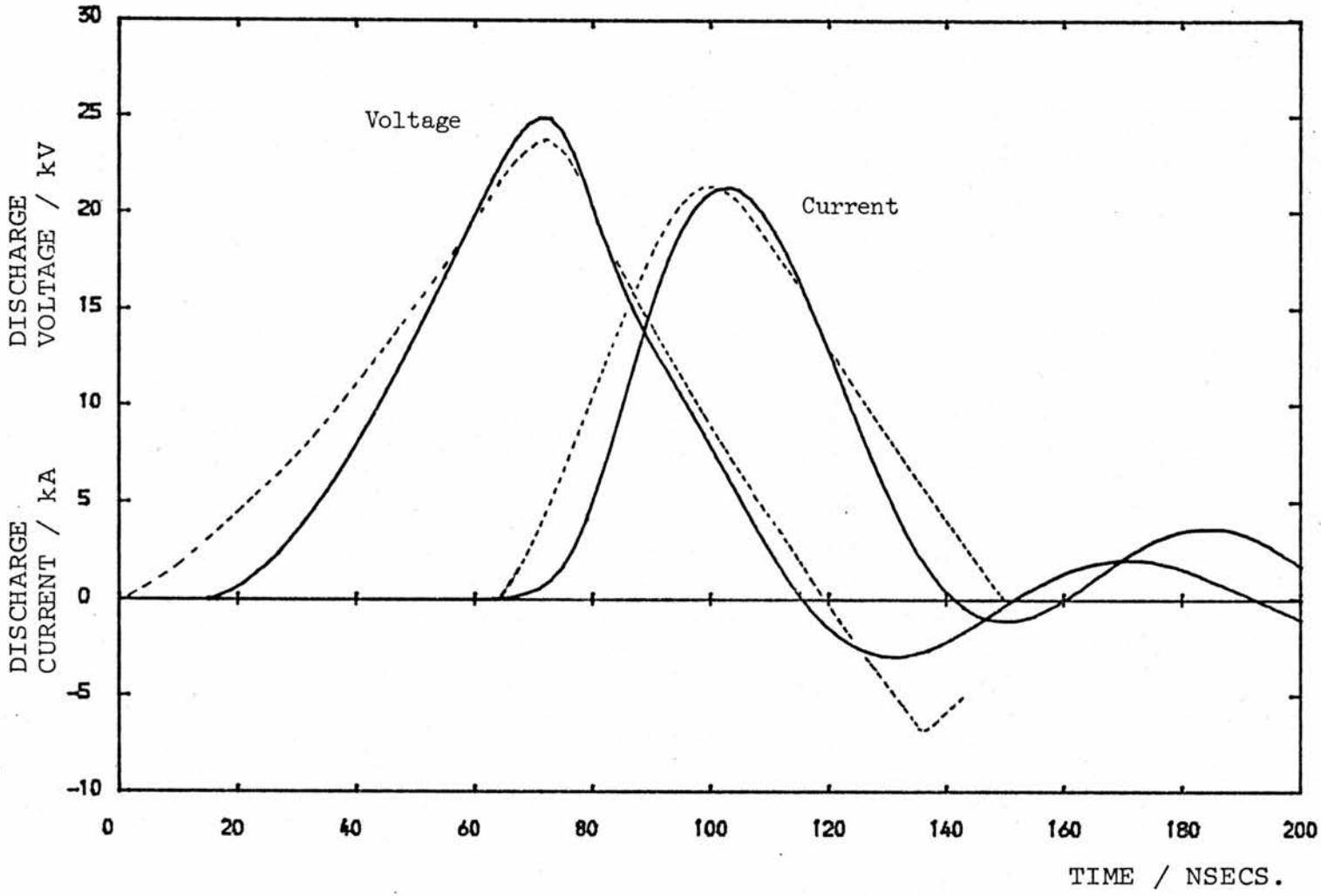

Figure 4.4 Discharge current and voltage waveforms in the LC inversion circuit.

-------Experimental results from Sze and Loree (1978).

———Present results.

C_1 = 24 nF.
L_2(ext.) = 10 nH.

Other values as in figure (4.2).

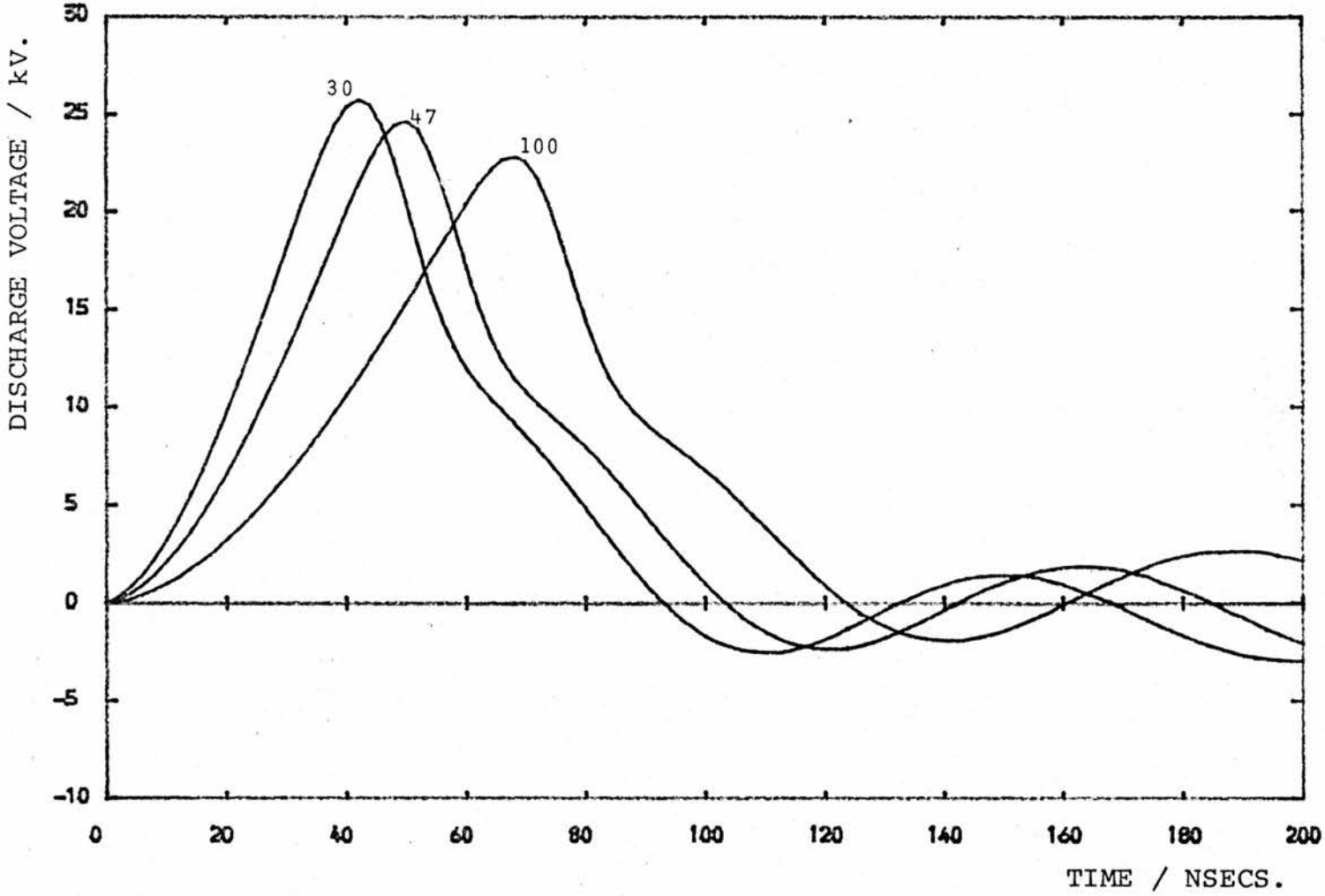

Figure 4.5 Discharge voltage waveforms in the LC inversion circuit.

Values shown are for L_1 / nH. Other values as in figure (4.2).

Scott (1978) comment that this rise time is given by $\frac{L_2}{R_2}$ yielding here $\frac{27nH}{0{\cdot}6\Omega}$ = 45nsecs. using the lowest value of R_2. The power peak (I_2V_L) is significantly reduced as L_1 is increased, falling some 27% in the range 30nH to 100nH with no significant change in pulse width. The curves are shown in figure (4.6) and may be compared with similar curves in the paper by Sze and Loree who also varied voltage rise time by varying L_1.

It might be suggested that a small value of L_1 should lead not only to a rapid reversal in the voltage across C_1 before breakdown but also to a rapid reversal back depleting the discharge voltage. This effect is not seen, however, owing to the strong coupling between the two loops after breakdown. The curves of figure (4.7) illustrate the I_1 waveforms and show that breakdown occurs well before the ringing arm has reversed, when I_1 would in theory have dropped to zero. The subsequent coupling holds I_1 high (as mentioned in Section (4.2)) and the ringing arm does not actually reverse until well after the region of interest.

The effect on current rise time of the discharge arm inductance was tested by varying L_2 (ext.). The current pulses are shown in figure (4.8) for values of 10, 20 and 40nH and clearly the effect is large. The voltage peak is similarly increased for lower inductances, with some 2 - 3nsecs. lengthening of the initial rise as may be seen in figure (4.9). The rapid build-up of current afforded by the lower inductance actually holds the voltage high while the resistance is falling. (The effect on power is particularly great with a drop in peak of some 55% between cases L_2 (ext.) =

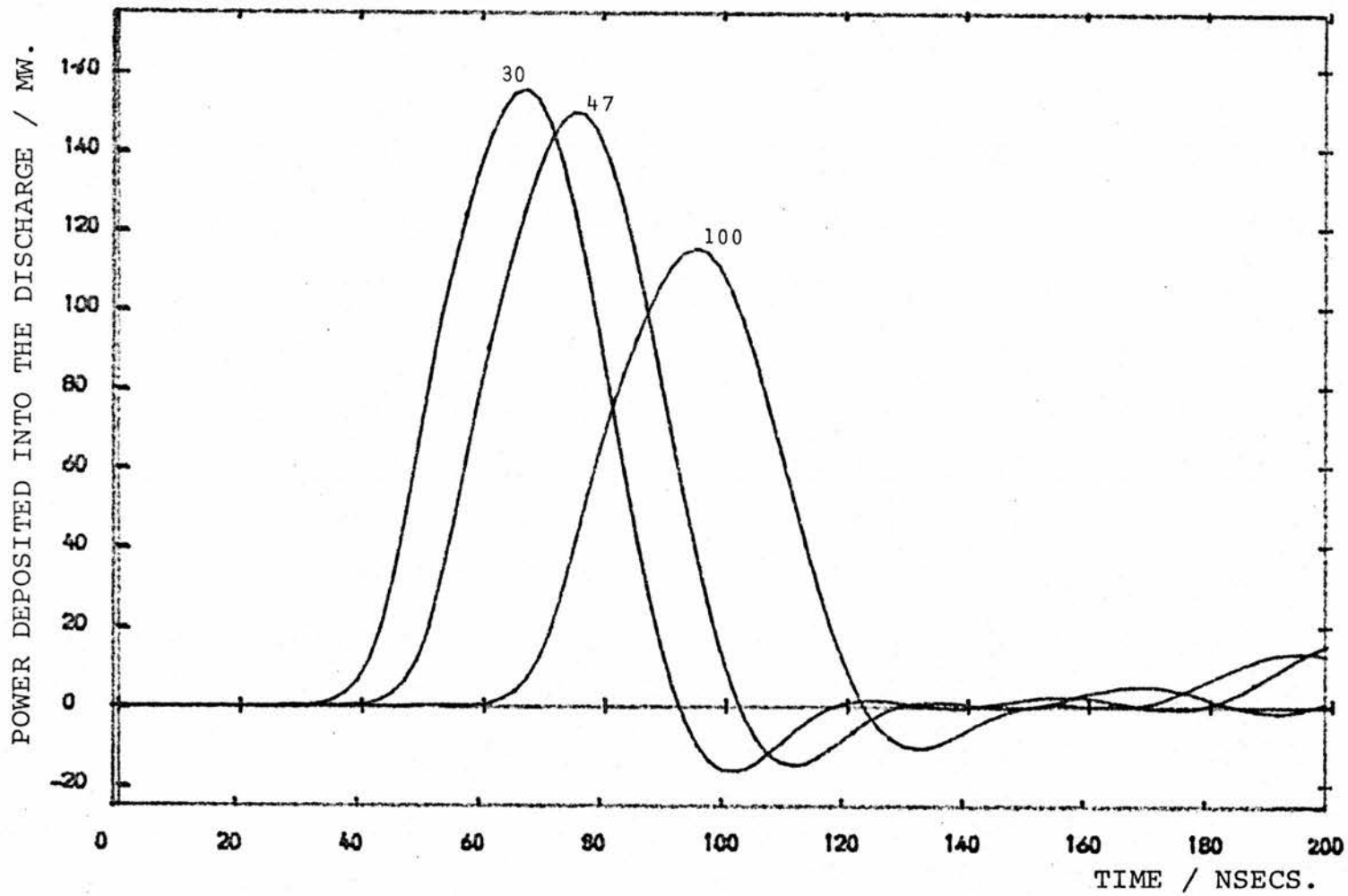

Figure 4.6 Power deposited into the discharge in the LC inversion circuit.

Values shown are for L_1 / nH. Other values as in figure (4.2).

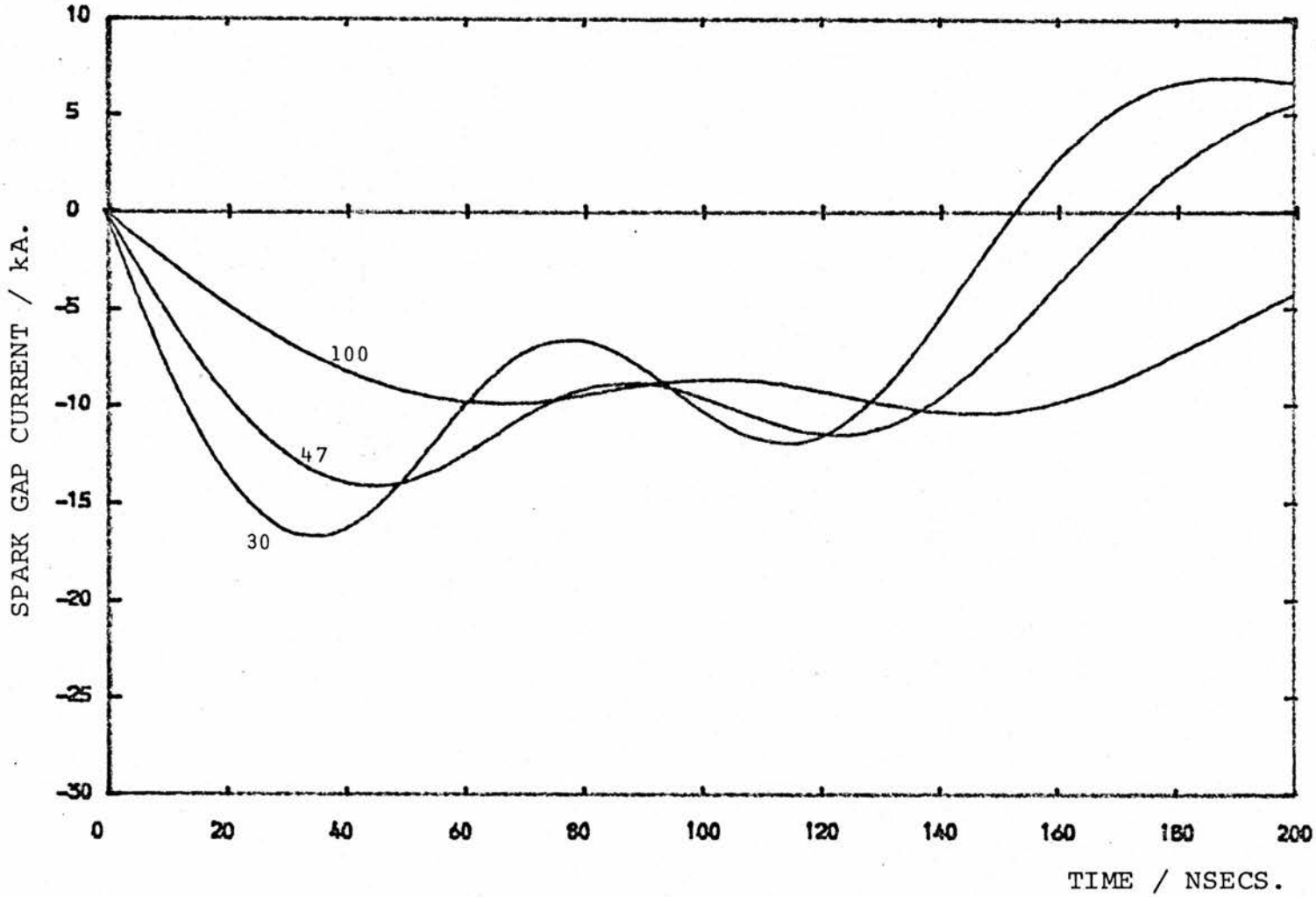

Figure 4.7 Spark gap current waveforms in the LC inversion circuit.

Values shown are for L_1 / nH. Other values as in figure (4.2).

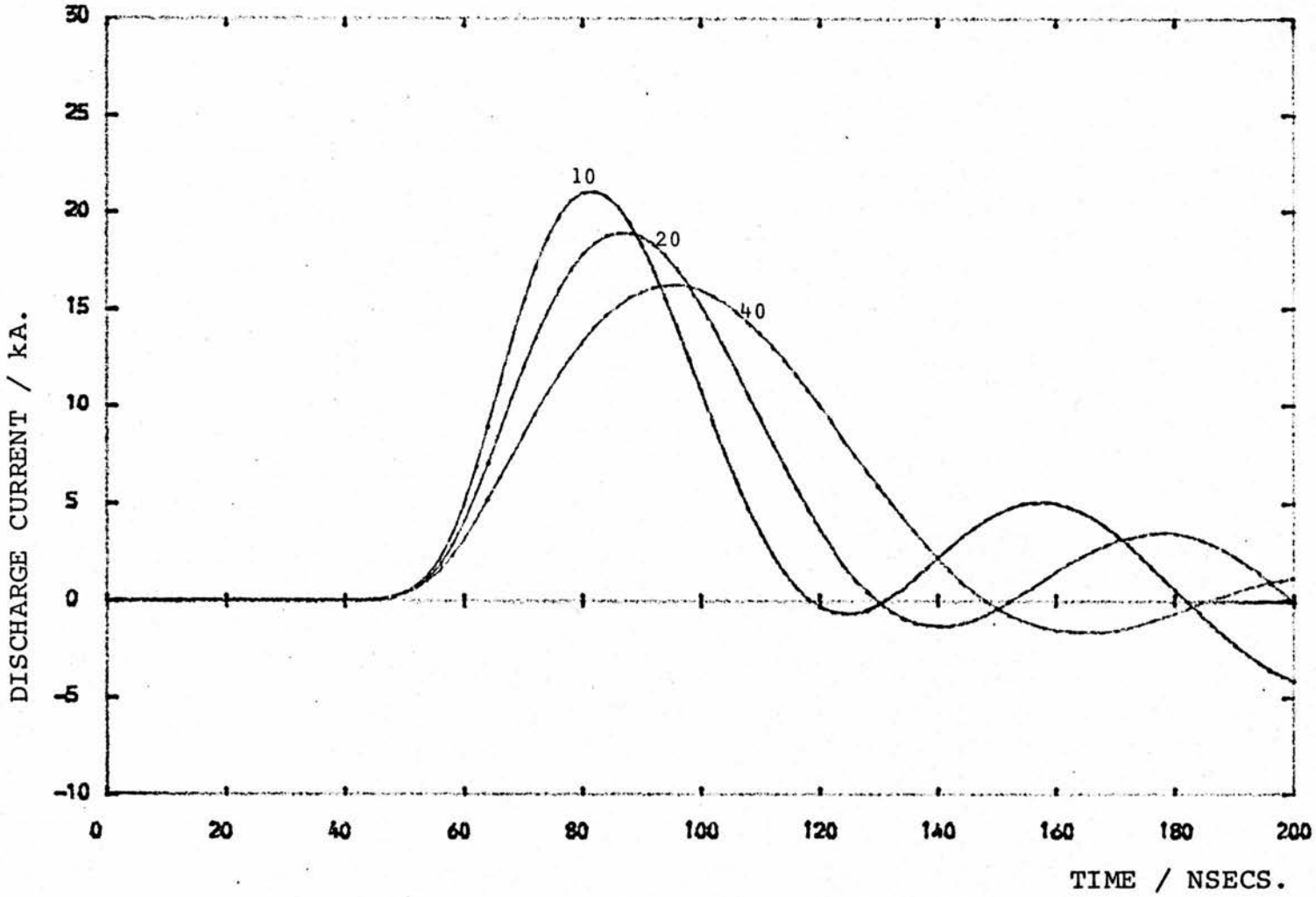

Figure 4.8 Discharge current waveforms in the LC inversion circuit.

Values shown are for L_2(ext.) / nH. Other values as in figure (4.2).

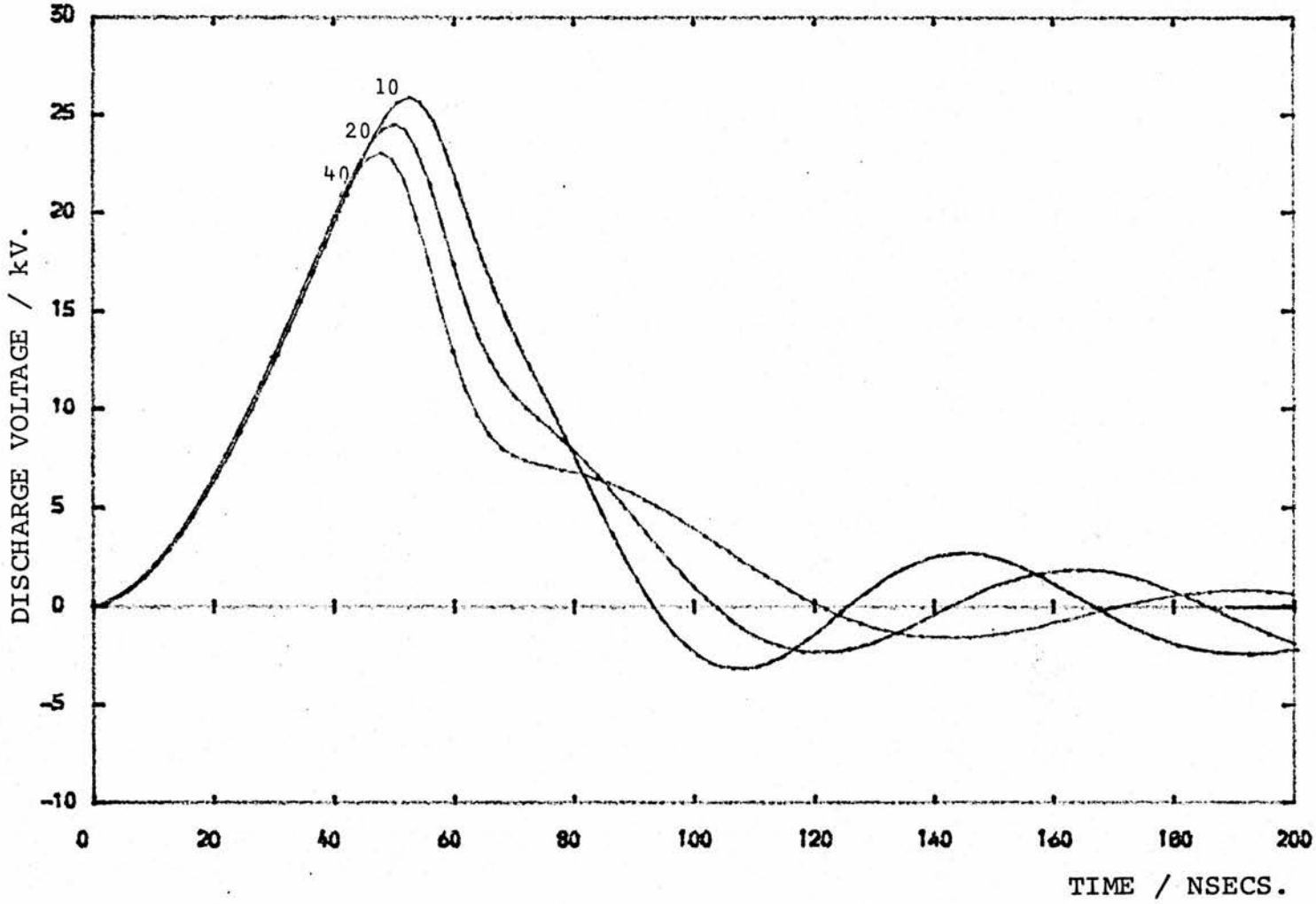

Figure 4.9 Discharge voltage waveforms in the LC inversion circuit.

Values shown are for L_2(ext.) / nH. Other values as in figure (4.2).

10nH and 40nH with a 25nsec. increase in rise time.)

Perhaps the most important parameter involved in the circuitry is the capacitance ratio $C_2 : C_1$. While the effect of inductance is of major importance for the performance of the laser, it is not a freely variable quantity but should be generally as small as possible within geometry and design limitations. The values of C_1 and C_2, however, are much more accessible to the user for variations. Given a number of doorknob capacitors for instance it would be of value to know the optimum ratio in which to place them. Of course inductance would undoubtedly be altered too in practical terms.

The effects of varying both C_1 and C_2 separately were studied. An increase in C_1 was found to lead to an increase in voltage rise time because of the ringing arm time constant and consequently to a drop in peak voltage. The effect on current and power, however, is particularly interesting. The power curves are shown in figure (4.10) for C_1 = 12, 24 and 48nF around a C_2 value of 24nF. The peak power for C_1 = 24nF is only nominally higher than that for C_1 = 12nF despite an overall increase of one third in the original energy stored. Doubling C_1 again to 48nF leads to an actual drop in the peak power. The discharge current follows this behaviour. Furthermore the rise times for power and current as well as voltage are considerably increased by a larger C_1. This suggests an optimum value for C_1 between, on the one hand, a rise in stored energy as C_1 is increased and, on the other hand, a rise in circuit time constants.

Variations in C_2 were found not to affect voltage rise

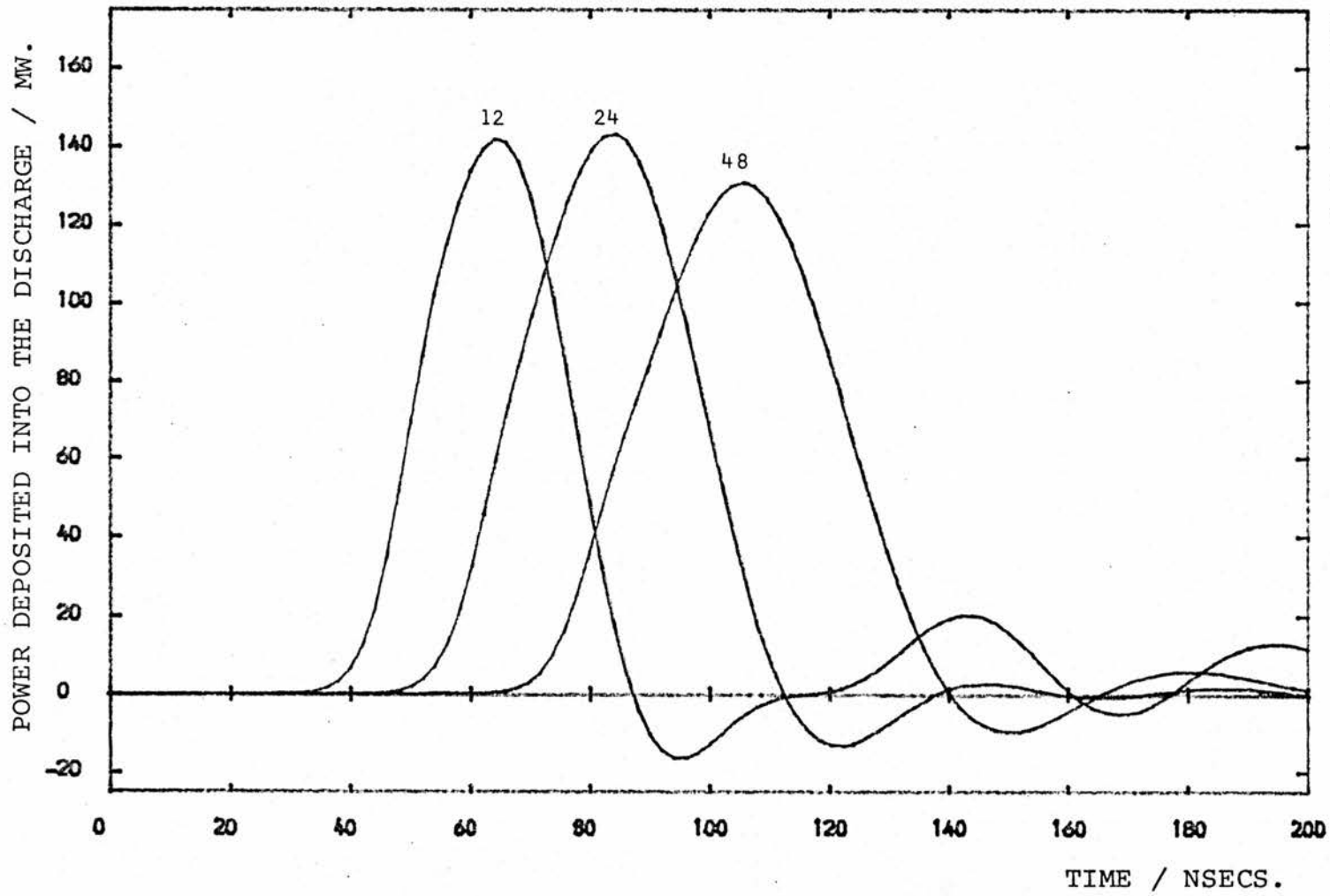

Figure 4.10 Power deposited into the discharge in the LC inversion circuit.

Values shown are for C_1 / nF. Other values as in figure (4.2).

time or peak for values of 10, 20 and 40nF. After the kink during voltage fall the voltage is held somewhat higher for higher C_2. The curves of figures (4.11) and (4.12) show the evolution of the current and power pulses. Increasing C_2 from 10nF to 40nF represents a total capacitance increase from 29nF to 59nF or roughly double. This does not, however, lead to a doubling of current or power peak. The higher C_2 leads instead to a higher time constant for the discharge loop and therefore to a longer rise to peak current. This analysis suggests that large increases in C_2 will not lead to ever larger laser outputs. The lengthening of the current pulse is not expected to maintain the stable discharge region and arc formation will terminate lasing. This has been mentioned by Sze (1979) who maintained a high current using high energy storage but found that for much of the time the discharge voltage was zero. He thus suggested that optimum capacitance is determined by the stable discharge time.

The effect shown in figure (4.11) whereby the discharge current does not turn negative is also seen for variations in C_1 and seems to be associated with a ratio $\frac{C_2}{C_1} \sim 2$.

Finally the two discharge parameters $R_{20}(\text{laser})$ and B were varied. On this model a variation of B leads to larger overvoltages for slower rates of fall whereas this effect would tend to be associated with lower overvoltages. Generally, though, an increase in $R_{20}(\text{laser})$ or a decrease in B leads to an increase in the average resistance and therefore to an increase in rise time. The paper by Greene and Brau provides experimental waveforms (from Sze and Loree) for both KrF and

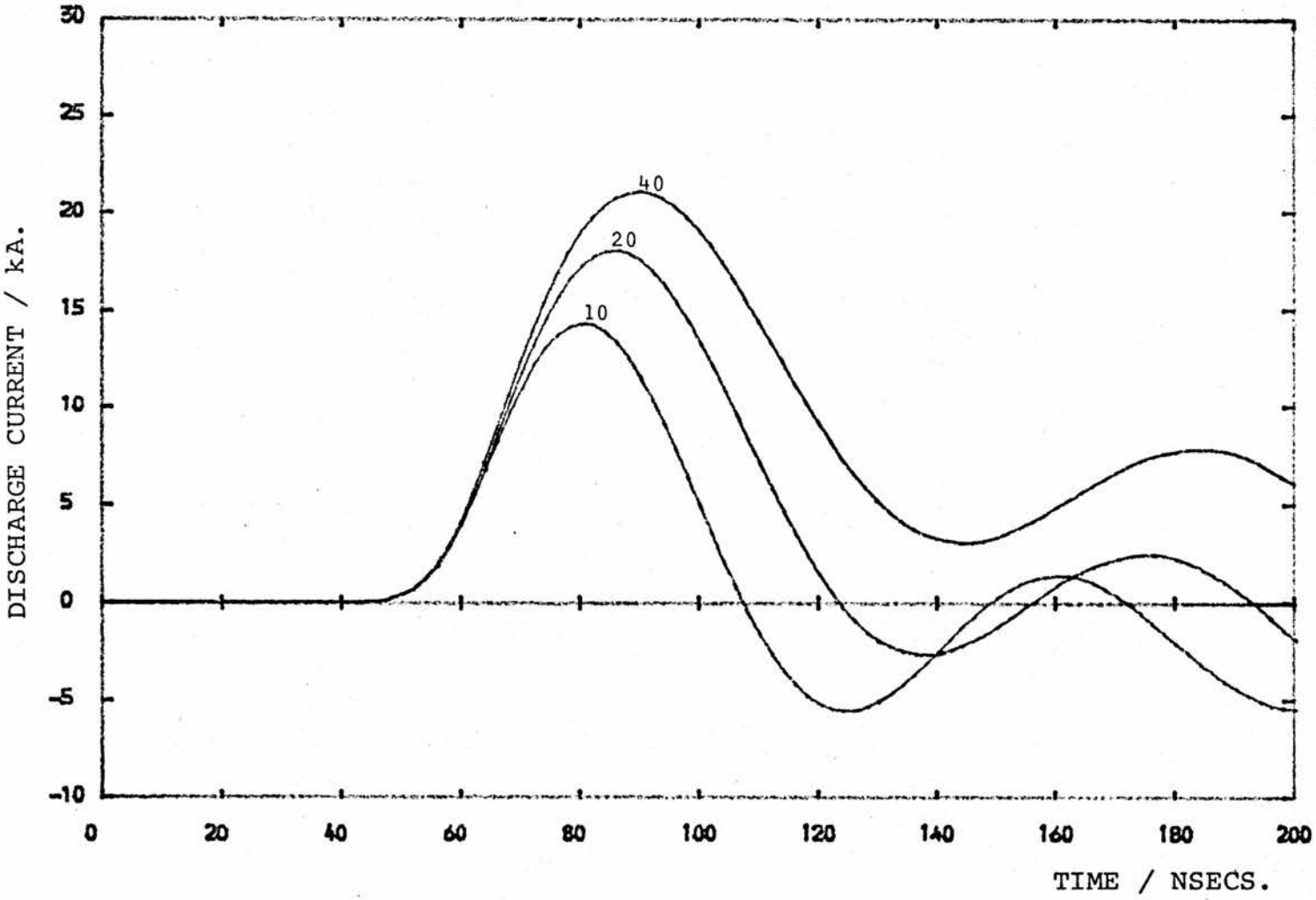

Figure 4.11 Discharge current waveforms in the LC inversion circuit.

Values shown are for C_2 / nF. Other values as in figure (4.2).

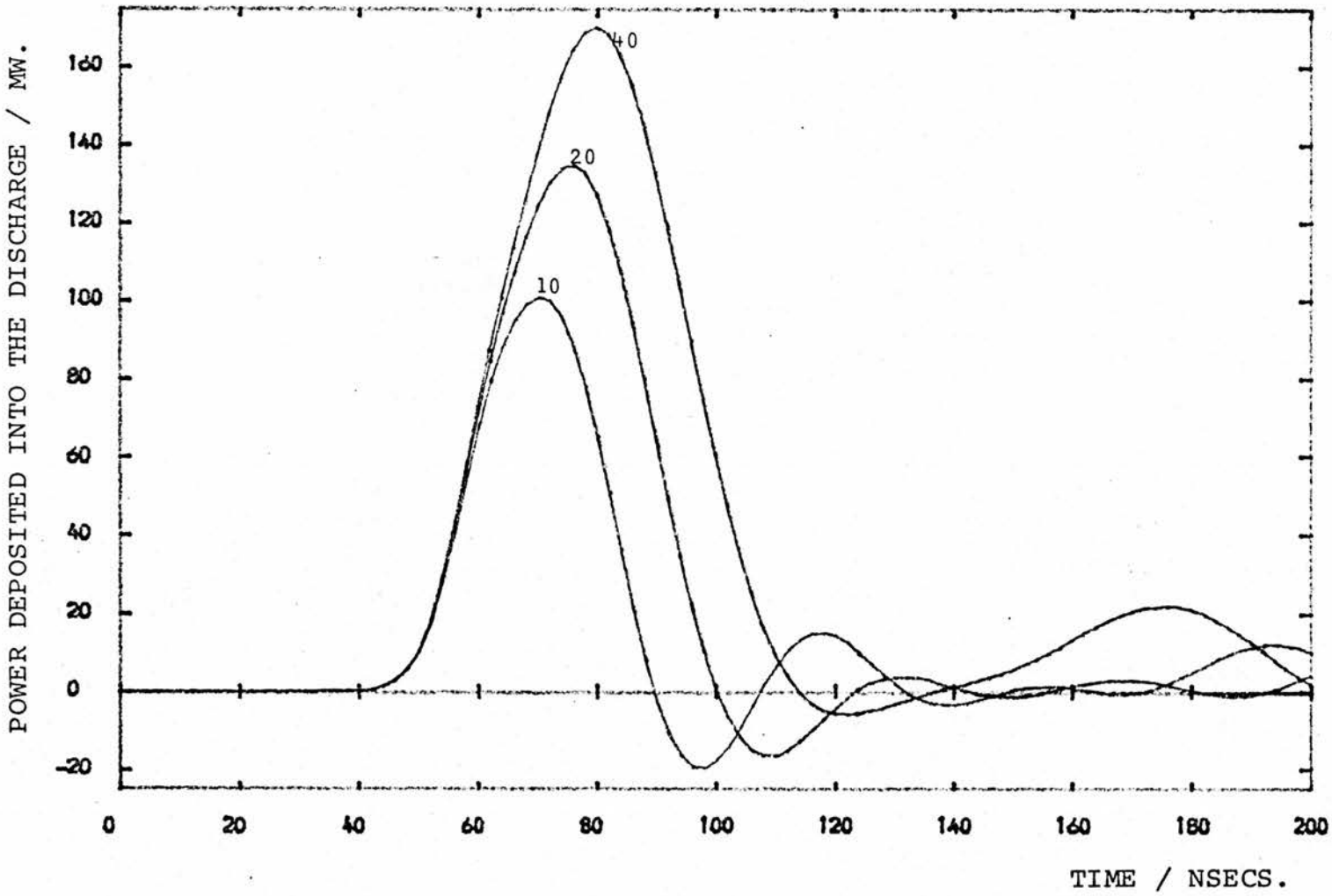

Figure 4.12 Power deposited into the discharge in the LC inversion circuit.

Values shown are for C_2 / nF. Other values as in figure (4.2).

ArF laser discharges. The ArF discharge involves a higher voltage rise time and peak but is followed by a much more rapid fall in voltage and presumably resistance. The current rise time is lowered. Clearly then the value of B is very dependent upon the nature of the discharge and its characteristic parameters such as $\frac{E}{p}$. The paper by Sze makes reference to work by Martin (AWRE report SSNA (JCM/704/49)) involving resistive phase time constants determined by pressure and discharge dimensions. The effect of these two parameters on resistance has already been mentioned with reference to Watanabe et al (1979) and Raether (1964).

4.5 Energy Deposition

The high concentration of excited molecules required for threshold gain in an excimer laser demands the rapid deposition of large amounts of energy into the laser medium and it has already been stated that the high value of $\frac{E}{p}$ necessary for efficient excitation limits the stable glow region following breakdown to typically 30 - 40nsecs. Localized space charge fields caused by non-uniform pre-ionization or statistical fluctuations then lead to the formation of streamer arcs and the destruction of lasing. The efficiency of formation of the excited states is a function of the time varying $\frac{E}{p}$ requiring careful analysis. However Sze and Loree have suggested that the primary effect afforded by a low $\frac{E}{p}$ in the rare gas fluorides is the decrease in energy deposited into the discharge and not the decrease in excitation efficiency. They showed for the KrF laser that output energy bears a strong correlation to input energy for different voltage rise times. Watanabe et al

(1979) have shown excellent correlations for variations in pressure and electrode separation.

The paper by Sze and Loree provides results on the variations with voltage rise time of input energy, output energy and the value of $\frac{E}{p}$ at breakdown. The deposited energy was measured during the first ringing of the voltage pulse. The associated power variations have already been discussed in section (4.3). In this section the energy deposited during the first ringing of the voltage pulse is modelled and plotted graphically in figure (4.13) alongside the experimental results of Sze and Loree. The corresponding values of $\frac{E}{p}$ at breakdown are also shown (scaled on the assumption that an $\frac{E}{p}$ of 8·2kV/cm-torr is equivalent to a discharge voltage of 25kV).

A more rapid fall in $\frac{E}{p}$ is evident in the experimental results than is seen in the modelled results. However, the model imposes a minimum value of 20kV on $\frac{E}{p}$ which is too high for the lower experimental values, indicating a likely improvement necessary for the model. Although Sze and Loree have fitted a straight line to their curve it is suggestive of the modelled shape, more appropriate to the notion of a 0·75% decrease per nanosecond increase in rise time. It must be borne in mind that the rise times measured experimentally are generally longer than the modelled rise times. Conversely, as energy values are normalized, it is likely that the higher rise time results are too high because of the overestimate of $\frac{E}{p}$. If these were lowered the modelled curve would resemble more the experimental curve with underestimated rise time. The general trend is, however,

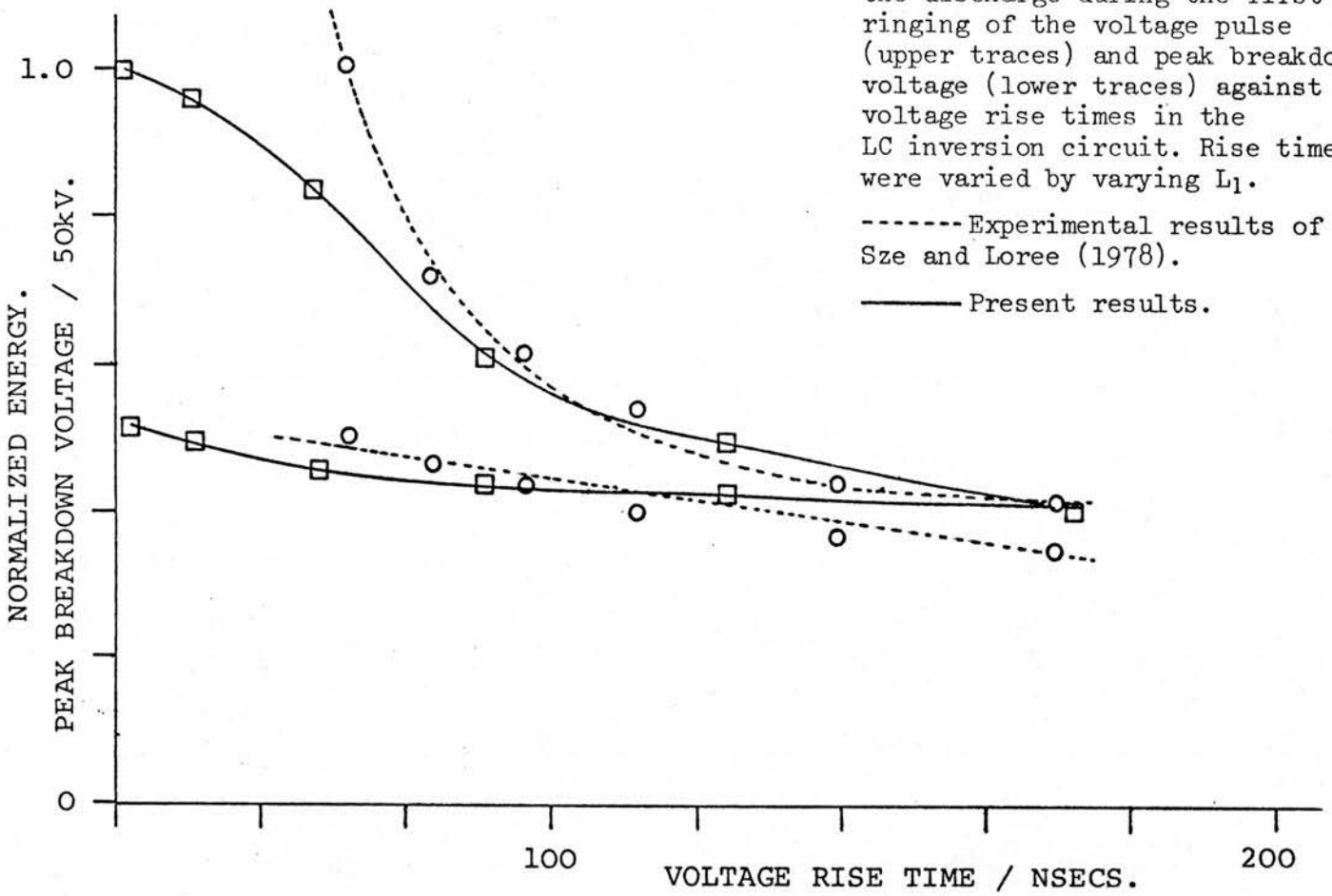

Figure 4.13 Energy deposited into the discharge during the first ringing of the voltage pulse (upper traces) and peak breakdown voltage (lower traces) against voltage rise times in the LC inversion circuit. Rise times were varied by varying L_1.

-------Experimental results of Sze and Loree (1978).

———— Present results.

observed and is followed in parallel fashion by deposited energies calculated during the first current pulse and in total.

Sze (1979) has pointed out that much of the deposited energy is wasted owing to a delay between the current and laser pulses, with the flow of electrical power at a peak before the current peak. Side-light fluorescence indicated that the KrF* upper laser level density followed closely the current curve. A substantial increase in performance was observed by Sze and Scott (1978) using a cable-fed device with much faster current rise and therefore more nearly synchronous current and lasing pulses.

The effect of capacitance ratio $\frac{C_2}{C_1}$ upon energy deposition has been tested by variations in both parameters. The results are shown in figures (4.14) and (4.15) for both actual energy deposited during the first ringing of the voltage pulse and for efficiency based upon original energy stored. Variations in C_1 (figure (4.14)) indicate a maximum both in absolute terms and in terms of efficiency. The most efficient ratio is seen to be in the region of $\frac{C_2}{C_1} = \frac{3}{2}$ with a rapid fall for a ratio below 1 or above 2 . The analysis was repeated for a greatly reduced value of L_1 = 27nH with very similar results suggesting an optimum value of $\frac{3}{2}$.

The variations of C_2 in figure (4.15) show an increasing deposition of energy with increasing capacitance up to 80nF. The efficiency, however, reaches a plateau region between C_2 = 25nF and C_2 = 50nF. An estimate of $\frac{C_2}{C_1} = \frac{3}{2}$ would indicate an optimum in the region of C_2 = 30nF.

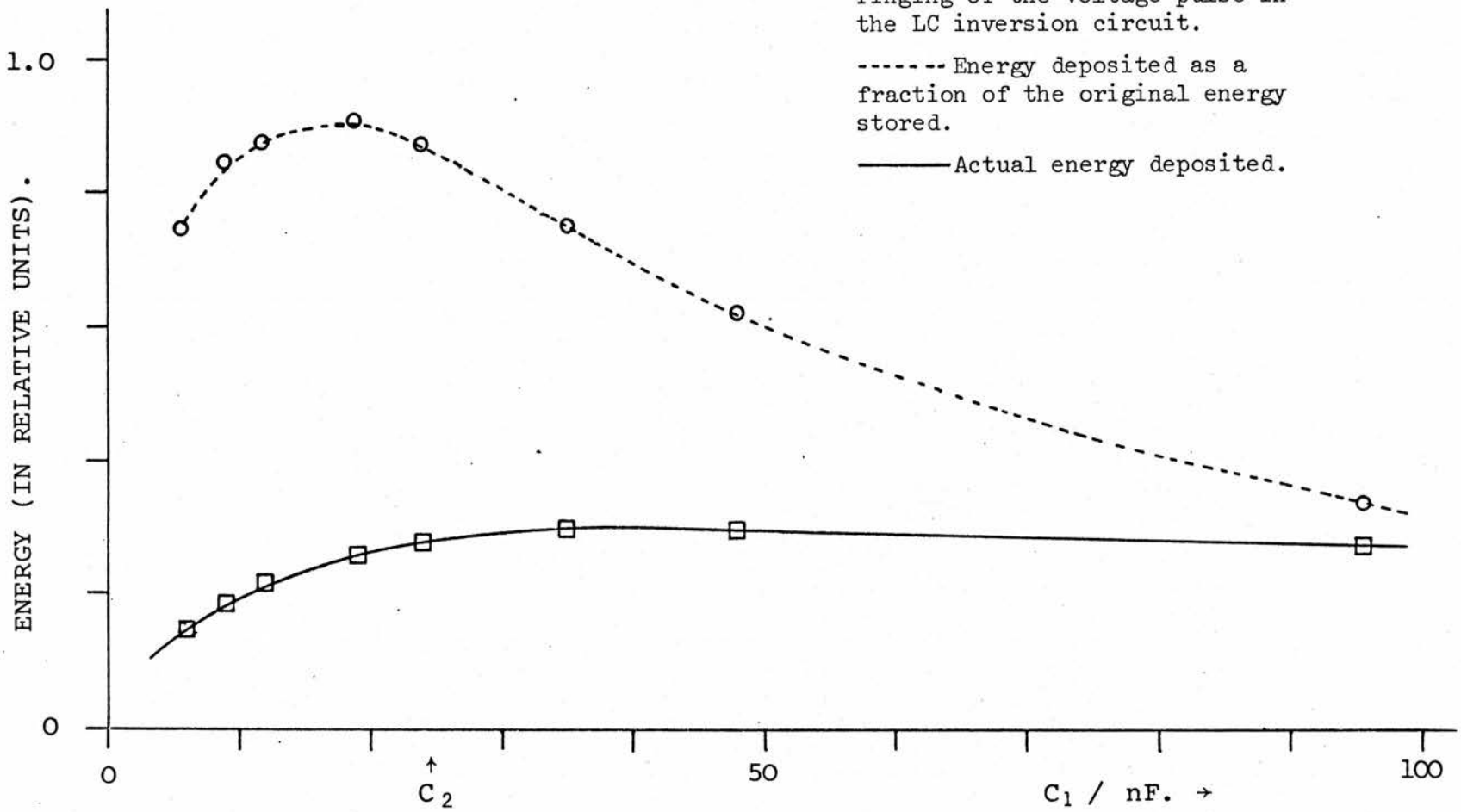

Figure 4.14 Energy deposited into the discharge during the first ringing of the voltage pulse in the LC inversion circuit.

- - - - - - - Energy deposited as a fraction of the original energy stored.

——— Actual energy deposited.

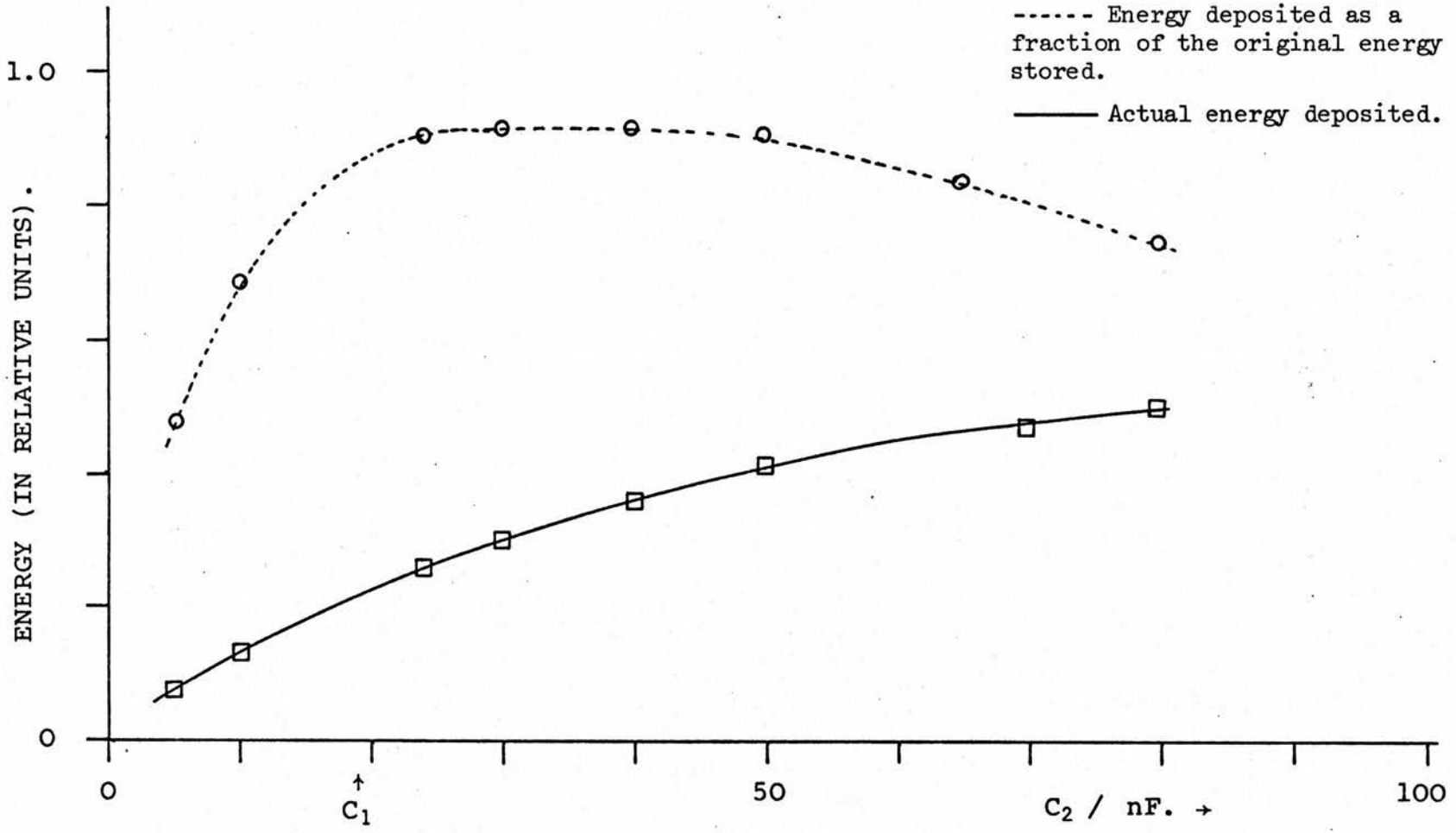

Figure 4.15 Energy deposited into the discharge during the first ringing of the voltage pulse in the LC inversion circuit.

------ Energy deposited as a fraction of the original energy stored.

——— Actual energy deposited.

4.6 Discussion

The inclusion of a time dependent term for the resistance of a gas discharge has allowed reasonable simulations to be made of the LC-inversion circuit behaviour based upon a simple model together with given circuit details and a rough calculation of the resistive phase time constant. The accuracy of the model is comparable to the results of discharge kinetics coupled analysis but provides no lasing details.

The model has allowed reasonable predictions to be made concerning the effect of voltage rise time on energy deposition in the belief that the deposited energy is a major factor in determining laser output. The effect of other circuit parameters on discharge behaviour has been predicted, in particular the effect of the capacitance ratio $\frac{C_2}{C_1}$. It is suggested that a ratio of $\frac{3}{2}$ provides optimum efficiency for the circuit studied, although separate variations of C_1 and C_2 indicate that it is not only the ratio which is important. The equation (A3.24) would seem to confirm this.

CHAPTER 5

Conclusions and Suggestions for Further Work

Conclusions and Suggestions for Further Work

5.1 Introduction

It has been shown in Chapter 4 that the use of a time dependent term to describe the resistance of a gaseous discharge after breakdown can provide some insight into the behaviour of an LC-inversion circuit driving an excimer laser discharge. In particular,a simple model provides an estimate of the laser cavity peak voltage. This is not possible in a constant resistance model in which the laser cavity voltage collapses immediately following breakdown nor in the LCR circuit discharge if no voltage rise is modelled.

The deposition of energy into the discharge is very dependent upon the size of the overvoltage and the extent of the high resistance region. In the simulation of section (4.3) the discharge resistance reaches its lower level shortly before the discharge voltage falls to zero and over two thirds of the input energy is deposited during this higher resistance phase. Large time constants can, however, cause a considerable amount of energy to remain in the circuit after the ringing of the first voltage pulse. A slow rise of discharge current does not allow significant energy deposition during the high resistance region and most of the energy deposited during the first ringing of the voltage pulse is deposited while the resistance is only moderately higher than its plateau level. The falling voltage and rising current produce a power peak preceding the current peak and Sze (1979) has commented that this effect can waste electrical energy before lasing begins. A fast current rise

is needed to synchronise the power, current and lasing pulses for greater efficiency.

The external resistances used in the analyses of Chapter 4 are of the same order as the lower level of the discharge resistance and consequently remove a significant amount of energy from the circuit. In a constant discharge resistance model of their very low inductance Blumlein circuit, Burnham et al (1976) predicted a 70 - 80% deposition of originally stored energy into the 0·5Ω discharge resistance during the first 50nsecs. after breakdown. The spark gap resistance of 0·05Ω took 15% with the remainder deposited afterwards. With suggested inductances of only 2nH this represents a much more efficient deposition than could be realized in the higher inductance circuits discussed in Chapter 4.

It is hoped that the use of a time dependent resistance for the discharge resistance can provide a useful means to optimize energy deposition in the LC-inversion circuit, and various effects of inductance and capacitance values are discussed in Chapter 4. It must be remembered that in a real circuit,values are unlikely to be alterable at will and that values of capacitance, inductance and resistance will be physically linked. Furthermore it is not necessarily true that circuit parameters can be assumed constant. Rothe and Gibson (1977) have mentioned the fall in capacitance of barium titanate capacitors as applied voltage is increased and this phenomenon has been studied more closely by Matsumoto et al (1980). The doorknob capacitors used by Sze and Loree (1978) showed this behaviour, possibly affecting the results cited in Chapter 4. In their experiments the

peak voltage rose linearly with charging voltage V_0 and it might have been expected that the output energy would rise as V_0^2 or more(given more favourable formation of the upper laser level). In fact the output energy rose less than linearly with V_0. (Their argument is misleading however, in that the linear relationship between peak voltage and V_0 over the range studied involves a non-zero intercept and a gradient much less than unity - not a simple proportionality. This was confirmed by application of the model of Chapter 4.)

Circuit analysis and optimization can be improved if mathematical expressions are available to supplement or even replace numerical techniques requiring solutions by computer. The results of Appendices 1 and 3 describe the LC-inversion circuit behaviour and energy deposition for constant circuit parameters and their use is discussed in the following two sections. The mathematical techniques for describing the LCR circuit are well known and suggestions have been made in Chapters 2 and 3 for developing the analysis.

5.2 A Mathematical Analysis of the LC-Inversion Circuit

A simple model of the laser cavity resistance involves a single step-down of resistance from a high value prior to breakdown to a low value following breakdown, typically of the order of a fraction of an ohm. Schwab and Hollinger (1976) have used a step down from 1MΩ to 0·3Ω in their model of a Blumlein circuit. Burnham et al (1976) have used a step down from infinity.

On this model the results of Appendix 1 can be used to

provide mathematical expressions for circuit behaviour during the entire process. Before breakdown the ringing arm behaves as a pure LCR circuit unaffected by the much smaller current in the discharge arm. The voltage across the laser cavity is derived from the calculated voltage across C_1, l and r and from the constant voltage V_0 across C_2. This total acts as a driving term for R_2 (and to a very small extent L_2) while R_2 is high. Once the breakdown voltage is reached the known boundary conditions can then be used in the analysis of Appendix 1 to solve for the subsequent behaviour of the full LC-inversion circuit while R_2 is low.

5.3 An Improved Analysis

The simple model described in the last section requires prior knowledge of the breakdown voltage. In the last chapter it was shown that the use of a resistive phase time constant goes some way towards providing a voltage overshoot dependent upon the rate of voltage rise across the cavity, as is seen experimentally. Unfortunately such a time dependent resistance is beyond the scope of Appendix 1 and requires numerical computation of results.

A very good approximation to the computed peak voltage is, however, possible. It has been found that the ringing arm behaves quite separately from the discharge arm at least until the peak of the cavity voltage. The low current I_2 furthermore implies a constant voltage V_0 across C_2. It is therefore possible to calculate the total voltage across C_1, C_2, l and r to a very good approximation and to use the resultant expression, U(t) say, as a driving force for L_2

and R_2. This voltage sum was found to be correct to within 1% near the cavity voltage peak in the simulation of the Sze and Loree (1978) results.

Equating this driving force to the voltage across R_2 and L_2 leads to a first order differential equation in I_2 which is always soluble. As a first approximation the current may be taken as

$$I_2(t) \cong \frac{U(t)}{R_2(t)} \qquad -(5.1)$$

since R_2 is large. Differentiation can then yield $L_2\dot{I}_2$ as the voltage across the inductance L_2. Clearly this yields a total greater than U(t) and the two voltages I_2R_2 and $L_2\dot{I}_2$ must be scaled (in proportion) to sum to U(t). Although a rough approximation, this was found to give a peak voltage of 24·3kV as compared with 24·5kV in the simulation of the results of Sze and Loree (1978), and with the correct timing. Indeed the approximation was not unreasonable a little beyond the voltage peak. By the time R_2 had fallen from 1kΩ to around 30Ω the error was only 2%.

Lower values of R_2 lead to appreciable currents I_2 and the coupling in the LC-inversion circuit becomes significant. At this stage it is possible to postulate a constant resistance level for R_2 and to employ the methods of Appendix 1.

While not providing the correct resistance level during the important build up to current peak this approximation analysis does, therefore, estimate the over-voltage so important for efficient energy deposition into the laser discharge. Using the derived boundary conditions the energy deposition can be described by integration of the expression for I_2 or the total energy deposited may be evaluated by an

immediate application of the results of Appendix 3.

5.4 Discussion and Suggestions for Further Work

Although mathematical expressions for deposited energy in the LC-inversion circuit can be complicated as is clear from Appendix 3, it should be possible in the simpler cases to derive an expression such as that expanded in section (A3.3). This formula (A3.24) is based upon the reasonable assumption that $I_2 = 0$ at breakdown but the less reasonable though ideal assumption that the ringing arm has completely reversed and that $I_1 = 0$. Alternatively, should only one or two circuit parameters be in question - say C_1 and C_2 - then an expression involving these parameters only should not be difficult to expand from equation (A3.18) incorporating, if desired, the methods outlined in the last two sections. Differentiation would then suggest an optimum value for total energy deposition.

In any case the methods outlined in sections (5.2) and (5.3) should allow reasonable predictions of the LC-inversion circuit behaviour to be made without recourse to computer methods. The behaviour of the LCR circuit was the subject of Chapters 2 and 3 and it is envisaged that the modelling of the ringing arm may be improved by the similar use of a time dependence for the spark gap resistance. Certainly the voltage rise times in the LC-inversion circuit are longer than those predicted in Chapter 4.

Although an exponential fall in resistance has been used here, characterized by a time constant $\frac{1}{B}$, other time dependences such as t^{-m} have been suggested and should not

further complicate the analysis. Work is necessary to study the nature of the time dependence in an excimer laser discharge and to identify, if possible, a reasonably simple form. Should it be possible to identify the main mechanisms involved this should help to estimate time constants rather than adopt an entirely empirical approach. Raether (1964) for instance has compared early time constants with αv, the product of Townsend ionization coefficient and drift velocity.

In furthering the mathematical analysis, series solutions such as those described in section (2.5) should be possible for the LC-inversion circuit. The WKB method has been used to approximate the solutions of two coupled second order differential equations (see for instance the book by Budden), although the coupling in the LC-inversion circuit would seem large. It may be possible to improve the analysis of the behaviour immediately following breakdown since coupling is then small. For instance, a method of feeding a first approximation back into the differential equations may improve upon the approach adopted in section (5.3).

The LCR and LC-inversion circuits comprise only two of the discharge schemes used to power excimer lasers. It should be possible to extend the idea to other systems such as the C-to-C transfer system and indeed to other laser gases of which carbon dioxide is an important example.

APPENDIX 1

Solution of the LC-Inversion Circuit for Constant Circuit Parameters

Solution of the LC-Inversion Circuit for Constant Circuit Parameters

A1.1 The Circuit Equations

The LC-inversion circuit may be modelled by a two-loop circuit in which a ringing arm contains the switch and a discharge arm contains the laser cavity. In the illustration below r, R_1, R_2 represent resistances; l, L_1, L_2 represent inductances; C_1, C_2 represent capacitances. I_1 and I_2 represent currents in the ringing arm and discharge arm respectively.

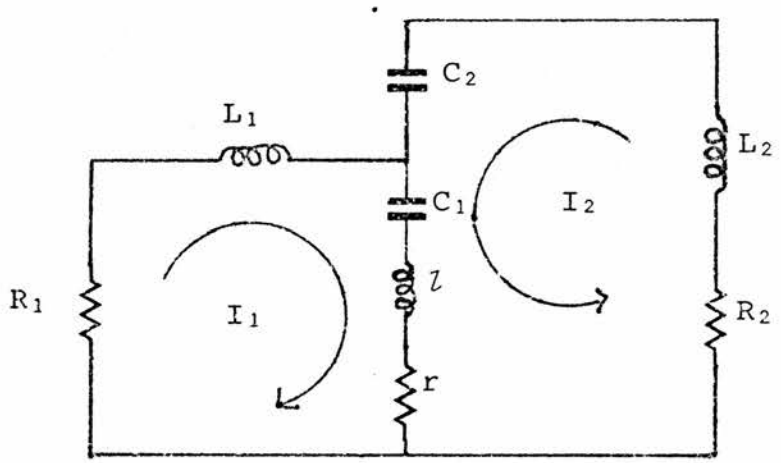

Fig. A1.1 Model of LC-Inversion Circuit

If charges Q_1 and Q_2 are associated with the currents I_1 and I_2 respectively, then the circuit obeys the differential equations

$$L_1\ddot{Q}_1 + R_1\dot{Q}_1 + l(\ddot{Q}_1 + \ddot{Q}_2) + r(\dot{Q}_1 + \dot{Q}_2) + \frac{1}{C_1}(Q_1 + Q_2) = 0$$

$$L_2\ddot{Q}_2 + R_2\dot{Q}_2 + l(\ddot{Q}_1 + \ddot{Q}_2) + r(\dot{Q}_1 + \dot{Q}_2) + \frac{1}{C_1}(Q_1 + Q_2) + \frac{1}{C_2}Q_2 = 0 \; . \qquad -(A1.1)$$

Assuming behaviour of the form

$$Q_1 = e^{kt} \quad \text{and} \quad Q_2 = He^{kt} \quad \text{then} \qquad -(A1.2)$$

$$L_1 k^2 + R_1 k + l k^2 (1+H) + rk(1+H) + \frac{1}{C_1}(1+H) = 0$$

$$L_2 k^2 + R_2 k + l k^2 (1+H) + rk(1+H) + \frac{1}{C_1}(1+H) + \frac{1}{C_2} H = 0 \ .$$

By rearranging terms to give

$$(l+L_1)k^2 + (r+R_1)k + \frac{1}{C_1} = -H(lk^2+rk+\frac{1}{C_1})$$

$$(l+L_2)k^2 + (r+R_2)k + \frac{1}{C_1} + \frac{1}{C_2} = -\frac{1}{H}(lk^2+rk+\frac{1}{C_1}) \qquad \text{—(A1.3)}$$

it is clear that k is a solution of the quartic equation

$$[(l+L_1)k^2 + (r+R_1)k + \frac{1}{C_1}][(l+L_2)k^2 + (r+R_2)k + \frac{1}{C_1} + \frac{1}{C_2}] = (lk^2+rk+\frac{1}{C_1})^2 \ . \qquad \text{—(A1.4)}$$

The right hand side appears as a coupling term between the two loops. It is interesting to note that this would be absent for two unconnected loops. as in the illustration below. Then k would be a solution of the quartic equation

$$[(l+L_1)k^2 + (r+R_1)k + \frac{1}{C_1}][(l+L_2)k^2 + (r+R_2)k + \frac{1}{C_1} + \frac{1}{C_2}] = 0 \ . \qquad \text{—(A1.5)}$$

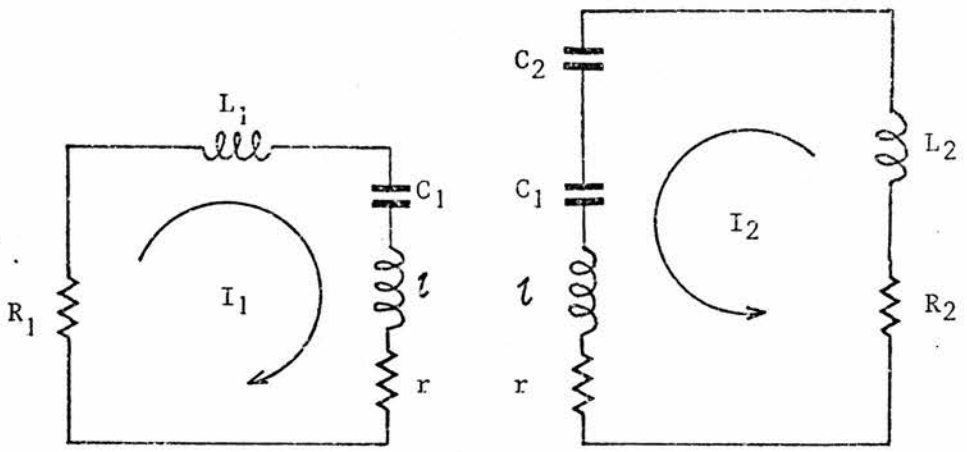

Fig. A1.2 Uncoupled loops of LC-Inversion Circuit

Given the four solutions k_i of the quartic equation (A1.4) the charges Q_1 and Q_2 may be defined by

$$Q_1 = \sum_{i=1}^{4} A_i \exp(k_i t) \text{ and } Q_2 = \sum_{i=1}^{4} X_i \exp(k_i t) \qquad \text{—(A1.6)}$$

and the currents I_1 and I_2 by

$$I_1 = \sum_{i=1}^{4} B_i \exp(k_i t) \quad \text{and} \quad I_2 = \sum_{i=1}^{4} Y_i \exp(k_i t) \; . \qquad \text{—(A1.7)}$$

Clearly $B_i = k_i A_i$ and $Y_i = k_i X_i$. —(A1.8)

Equations (A1.2) and (A1.3) show that A_i and X_i (and similarly B_i and Y_i) are related by the factor H. The equations (A1.8) and (A1.2) thus provide 12 independent relations between the 16 coefficients A_i, B_i, X_i, Y_i. The four equations still necessary for the solution of all the coefficients are supplied by the boundary conditions at t = 0.

$$\sum_{i=1}^{4} A_i = Q_1(0) \qquad \sum_{i=1}^{4} B_i = I_1(0)$$

$$\sum_{i=1}^{4} X_i = Q_2(0) \qquad \sum_{i=1}^{4} Y_i = I_2(0) \qquad \text{—(A1.9)}$$

It is proposed to write the relations (A1.2) and (A1.3) as

$$X_i = m_i A_i$$

$$\text{where } -m_i = \frac{[(l+L)k_i^2 + (r+R)k_i + \frac{1}{C_1} + \frac{1}{C}]}{(lk_i^2 + rk_i + \frac{1}{C_1})} = 1 + \frac{(Lk_i^2 + Rk_i + \frac{1}{C})}{(lk_i^2 + rk_i + \frac{1}{C})} \qquad \text{—(A1.10)}$$

and where $L = L_1$, $R = R_1$, $\frac{1}{C} = 0$. —(A1.11)

Then the boundary conditions (A1.9) may be written in the matrix form

$$\begin{bmatrix} 1 & 1 & 1 & 1 \\ m_1 & m_2 & m_3 & m_4 \\ k_1 & k_2 & k_3 & k_4 \\ m_1k_1 & m_2k_2 & m_3k_3 & m_4k_4 \end{bmatrix} \begin{bmatrix} A_1 \\ A_2 \\ A_3 \\ A_4 \end{bmatrix} = \begin{bmatrix} Q_1(0) \\ Q_2(0) \\ I_1(0) \\ I_2(0) \end{bmatrix} . \qquad \text{—(A1.9)}$$

The following analysis will solve these equations for A_1 as a function of k_1 only, and thus by analogy for A_2, A_3 and A_4. The form in which m_i was defined in equation (A1.10) also allows an immediate deduction of the coefficients X_i via the

observation that m_i becomes $\frac{1}{m_i}$ (i.e. H becomes $\frac{1}{H}$) upon the substitutions

$$R = R_2,\ L = L_2,\ \frac{1}{C} = \frac{1}{C_2} \qquad \text{—(A1.12)}$$

as is evident from equations (A1.3). With the reversal of $Q_1(0)$ and $Q_2(0)$ and of $I_1(0)$ and $I_2(0)$ in the solution, A_i then becomes X_i.

A1.2 Results from the Theory of Equations

The analysis relies heavily upon the theory of equations. If we define

$$\begin{aligned}
\sigma_1 &= k_1 + k_2 + k_3 + k_4 \\
\sigma_2 &= k_1k_2 + k_1k_3 + k_1k_4 + k_2k_3 + k_2k_4 + k_3k_4 \\
\sigma_3 &= k_1k_2k_3 + k_1k_2k_4 + k_1k_3k_4 + k_2k_3k_4 \\
\sigma_4 &= k_1k_2k_3k_4
\end{aligned} \qquad \text{—(A1.13)}$$

then the expanded form of equation (A1.4) becomes

$$k^4 - \sigma_1 k^3 + \sigma_2 k^2 - \sigma_3 k + \sigma_4 = 0 \qquad \text{—(A1.4)}$$

with

$$\begin{aligned}
\sigma_1 &= -\frac{[(l+L_1)R_2 + (l+L_2)R_1 + r(L_1+L_2)]}{[l(L_1+L_2) + L_1L_2]} \\
\sigma_2 &= \frac{[\frac{l}{C_2} + L_1(\frac{1}{C_1} + \frac{1}{C_2}) + \frac{L_2}{C_1} + r(R_1+R_2) + R_1R_2]}{[l(L_1+L_2) + L_1L_2]} \\
\sigma_3 &= -\frac{[R_1(\frac{1}{C_1} + \frac{1}{C_2}) + \frac{r}{C_2} + \frac{R_2}{C_1}]}{[l(L_1+L_2) + L_1L_2]} \\
\sigma_4 &= \frac{1}{C_1C_2[l(L_1+L_2) + L_1L_2]} \quad .
\end{aligned} \qquad \text{—(A1.14)}$$

A1.3 Solution of the Coefficients

Matrix manipulation of (A1.9) provides the simultaneous equations

$$\begin{bmatrix} (k_3-k_1)(m_4-m_1) & (k_3-k_2)(m_4-m_2) \\ (k_4-k_1)(m_3-m_1) & (k_4-k_2)(m_3-m_2) \end{bmatrix} \begin{bmatrix} A_1 \\ A_2 \end{bmatrix} = \begin{bmatrix} [m_4 Q_1(0)-Q_2(0)]\ k_3+I_2(0)-m_4 I_1(0) \\ [m_3 Q_1(0)-Q_2(0)]\ k_4+I_2(0)-m_3 I_1(0) \end{bmatrix}. \quad \text{—(A1.15)}$$

Using differences (m_i-m_j) typified by

$$(m_4-m_1) = \frac{(k_1-k_4)}{Z_1 Z_4}\left\{(Lr-Rl)k_1 k_4 + (\frac{L}{C_1}-\frac{l}{C})(k_1+k_4) + (\frac{R}{C_1}-\frac{r}{C})\right\} \quad \text{—(A1.16)}$$

with the shorthand form

$$Z_i = lk_i^2 + rk_i + \frac{1}{C_1} \quad \text{—(A1.17)}$$

the square matrix in equation (A1.15) is found to have the determinant

$$T = \frac{(k_1-k_2)(k_1-k_3)(k_1-k_4)(k_2-k_3)(k_2-k_4)(k_3-k_4)}{Z_1 Z_2 Z_3 Z_4}\left\{(\frac{L}{C_1}-\frac{l}{C})^2 - (Lr-Rl)(\frac{R}{C_1}-\frac{r}{C})\right\}. \quad \text{—(A1.18)}$$

Thus (A1.15) may be inverted to yield for A_1

$$A_1 = \frac{1}{T}[(k_4-k_2)(m_3-m_2) \quad (k_2-k_3)(m_4-m_2)] \begin{bmatrix} [m_4 Q_1(0)-Q_2(0)]\ k_3+I_2(0)-m_4 I_1(0) \\ [m_3 Q_1(0)-Q_2(0)]\ k_4+I_2(0)-m_3 I_1(0) \end{bmatrix}. \quad \text{—(A1.19)}$$

A common factor $\frac{1}{Z_2}(k_2-k_4)(k_2-k_3)$ is immediately apparent from the form of (m_3-m_2) and (m_4-m_2) shown in equation (A1.16). By further placing Z_3Z_4 in the denominator the numerator may be expanded and several terms cancelled to yield a common factor (k_3-k_4). A_1 thus includes a factor

$$\frac{(k_2-k_3)(k_2-k_4)(k_3-k_4)}{Z_2 Z_3 Z_4\, T} = \frac{Z_1}{(k_1-k_2)(k_1-k_3)(k_1-k_4)\,[(\frac{L}{C_1}-\frac{l}{C})^2-(Lr-Rl)(\frac{R}{C_1}-\frac{r}{C})]}. \quad \text{—(A1.20)}$$

Now the quartic equation (A1.4) is

$$(k-k_1)(k-k_2)(k-k_3)(k-k_4) = 0 \quad \text{—(A1.4)}$$

The derivative of the left hand side evaluated at $k = k_1$ is

$(k_1-k_2)(k_1-k_3)(k_1-k_4)$

and thus (A1.20) may be written as

$$\frac{Z_1}{(4k_1^3-3k_1^2\sigma_1+2k_1\sigma_2-\sigma_3)\,[(\frac{L}{C_1}-\frac{l}{C})^2-(Lr-Rl)(\frac{R}{C_1}-\frac{r}{C})]} \quad . \qquad -(A1.20)$$

The expanded form of the numerator clearly contains terms in k_2, k_3 and k_4. These, however, are necessarily symmetrical and may be reduced using the results from the theory of equations in section A1.2 to terms in k_1 only. In particular the following are necessary:

$$k_2k_3k_4 = \frac{\sigma_4}{k_1} \qquad -(A1.13)$$

$$k_2+k_3+k_4 = \sigma_1-k_1 \qquad -(A1.13)$$

$$k_2k_3+k_2k_4+k_3k_4 = \sigma_2-k_1(k_2+k_3+k_4) = \sigma_2-k_1(\sigma_1-k_1). \qquad -(A1.21)$$

Variations on the above are possible to avoid for example terms in $\frac{1}{k_1}$. However, these are simply substitutions for k_1^n via the quartic equation (A1.4). The generalized solution becomes

$$A_1 = \frac{Z_1}{[4k_1^3-3\sigma_1k_1^2+2\sigma_2k_1-\sigma_3]\,[(\frac{L}{C_1}-\frac{l}{C})^2-(Lr-Rl)(\frac{R}{C_1}-\frac{r}{C})]} \times$$

$$\Big\{Q_1(0)[(Lr-lR)(\frac{1}{C_1}+\frac{1}{C})\;[\sigma_2-k_1(\sigma_1-k_1)] + [(R+r)(Lr-Rl)-(l+L)(\frac{L}{C_1}-\frac{l}{C})]\frac{\sigma_4}{k_1}$$

$$+(\frac{1}{C_1}+\frac{1}{C})(\frac{L}{C_1}-\frac{l}{C})(\sigma_1-k_1)+(\frac{1}{C_1}+\frac{1}{C})(\frac{R}{C_1}-\frac{r}{C})]$$

$$+Q_2(0)[(Lr-lR)\frac{1}{C_1}\,[\sigma_2-k_1(\sigma_1-k_1)] + [r(Lr-Rl)-l(\frac{L}{C_1}-\frac{l}{C})]\frac{\sigma_4}{k_1}$$

$$+\frac{1}{C_1}(\frac{L}{C_1}-\frac{l}{C})(\sigma_1-k_1)+\frac{1}{C_1}(\frac{R}{C_1}-\frac{r}{C})]$$

$$+I_1(0)[(l+L)(\frac{L}{C_1}-\frac{l}{C})[\sigma_2-k_1(\sigma_1-k_1)] + (l+L)(Lr-Rl)\frac{\sigma_4}{k_1}$$

$$+(l+L)(\frac{R}{C_1}-\frac{r}{C})(\sigma_1-k_1)+(R+r)(\frac{R}{C_1}-\frac{r}{C})-(\frac{1}{C}+\frac{1}{C_1})(\frac{L}{C_1}-\frac{l}{C})]$$

$$+ I_2(0)\left[l\left(\frac{L}{C_1}-\frac{l}{C}\right)[\sigma_2-k_1(\sigma_1-k_1)] + l(Lr-Rl)\frac{\sigma_4}{k_1}\right.$$

$$\left.+ l\left(\frac{R}{C_1}-\frac{r}{C}\right)(\sigma_1-k_1) + r\left(\frac{R}{C_1}-\frac{r}{C}\right) - \frac{1}{C_1}\left(\frac{L}{C_1}-\frac{l}{C}\right)\right]\Bigg\} . \qquad \text{—(A1.22)}$$

With interpretations (A1.11) for A_1 and (A1.12) for X_1 this gives

$$A_1 = \frac{\left(lk_1^2 + rk_1 + \frac{1}{C_1}\right)}{\left[4k_1^3 - 3\sigma_1 k_1^2 + 2\sigma_2 k_1 - \sigma_3\right]\left[\frac{L_1^2}{C_1^2} - (L_1 r - R_1 l)\frac{R_1}{C_1}\right]} \quad \times$$

$$\Bigg\{ Q_1(0)\left[\frac{1}{C_1}(L_1 r - R_1 l)\,[\sigma_2 - k_1(\sigma_1 - k_1)] + \left[(R_1 + r)(L_1 r - R_1 l) - (l + L_1)\frac{L_1}{C_1}\right]\frac{\sigma_4}{k_1}\right.$$

$$\left. + \frac{L_1^2}{C_1^2}(\sigma_1 - k_1) + \frac{R_1}{C_1^2}\right]$$

$$+ Q_2(0)\left[\frac{1}{C_1}(L_1 r - R_1 l)[\sigma_2 - k_1(\sigma_1 - k_1)] + \left[r(L_1 r - R_1 l) - \frac{lL_1}{C_1}\right]\frac{\sigma_4}{k_1} + \frac{L_1^2}{C_1^2}(\sigma_1 - k_1) + \frac{R_1^2}{C_1^2}\right]$$

$$+ I_1(0)\left[\frac{L_1}{C_1}(l + L_1)[\sigma_2 - k_1(\sigma_1 - k_1)] + (l + L_1)(L_1 r - R_1 l)\frac{\sigma_4}{k_1}\right.$$

$$\left. + \frac{R_1}{C_1}(l + L_1)(\sigma_1 - k_1) + \frac{R_1}{C_1}(R_1 + r) - \frac{L_1}{C_1^2}\right]$$

$$+ I_2(0)\left[\frac{L_1 l}{C_1}[\sigma_2 - k_1(\sigma_1 - k_1)] + l(L_1 r - R_1 l)\frac{\sigma_4}{k_1} + \frac{lR_1}{C_1}(\sigma_1 - k_1) + \frac{rR_1}{C_1} - \frac{L_1}{C_1^2}\right]\Bigg\} \qquad \text{—(A1.23)}$$

$$X_1 = \frac{\left(lk_1^2 + rk_1 + \frac{1}{C_1}\right)}{\left[4k_1^3 - 3\sigma_1 k_1^2 + 2\sigma_1 k_1 - \sigma_3\right]\left[\left(\frac{L_2}{C_1} - \frac{l}{C_2}\right)^2 - (L_2 r - R_2 l)\left(\frac{R_2}{C_1} - \frac{r}{C_2}\right)\right]} \quad \times$$

$$\Bigg\{ Q_1(0)\left[(L_2 r - R_2 l)\left(\frac{1}{C_1} + \frac{1}{C_2}\right)[\sigma_2 - k_1(\sigma_1 - k_1)] + \left[(R_2 + r)(L_2 r - R_2 l) - (l + L_2)\left(\frac{L_2}{C_1} - \frac{l}{C_2}\right)\right]\frac{\sigma_4}{k_1}\right.$$

$$\left. + \left(\frac{1}{C_1} + \frac{1}{C_2}\right)\left(\frac{L_2}{C_1} - \frac{l}{C_2}\right)(\sigma_1 - k_1) + \left(\frac{1}{C_1} + \frac{1}{C_2}\right)\left(\frac{R_2}{C_1} - \frac{r}{C_2}\right)\right]$$

$$+ Q_2(0)\left[(L_2 r - R_2 l)\frac{1}{C_1}[\sigma_2 - k_1(\sigma_1 - k_1)] + \left[r(L_2 r - R_2 l) - l\left(\frac{L_2}{C_1} - \frac{l}{C_2}\right)\right]\frac{\sigma_4}{k_1}\right.$$

$$\left. + \frac{1}{C_1}\left(\frac{L_2}{C_1} - \frac{l}{C_2}\right)(\sigma_1 - k_1) + \frac{1}{C_1}\left(\frac{R_2}{C_1} - \frac{r}{C_2}\right)\right]$$

$$+ I_1(0)\left[(l + L_2)\left(\frac{L_2}{C_1} - \frac{l}{C_2}\right)[\sigma_2 - k_1(\sigma_1 - k_1)] + (l + L_2)(L_2 r - R_2 l)\frac{\sigma_4}{k_1}\right.$$

$$\left. + (l + L_2)\left(\frac{R_2}{C_1} - \frac{r}{C_2}\right)(\sigma_1 - k_1) + (R_2 + r)\left(\frac{R_2}{C_1} - \frac{r}{C_2}\right) - \left(\frac{1}{C_1} + \frac{1}{C_2}\right)\left(\frac{L_2}{C_1} - \frac{l}{C_2}\right)\right]$$

$$+ I_2(0)\left[l\left(\frac{L_2}{C_1} - \frac{l}{C_2}\right)[\sigma_2 - k_1(\sigma_1 - k_1)] + l(L_2 r - R_2 l)\frac{\sigma_4}{k_1}\right.$$

$$+ l\left(\frac{R_2}{C_1}-\frac{r}{C_2}\right)(\sigma_1-k_1)+r\left(\frac{R_2}{C_1}-\frac{r}{C_2}\right)-\frac{1}{C_1}\left(\frac{L_2}{C_1}-\frac{l}{C_2}\right)\Big]\Big\}. \qquad -(A1.24)$$

Equations (A1.8) subsequently provide the solutions for B_i and Y_i.

A1.4 An Alternative Formulation

It is a necessary condition for the solutions to the coefficients that their sums obey the boundary conditions. Taking B_i as an example $\Sigma B_i = I_1(0), \Sigma k_i B_i = \dot{I}_1(0)$ and so on for higher powers of k_i. This observation leads to a particularly simple formulation of the coefficients. B_i will be taken as an example but the interpretation of the results for the other coefficients is quite straightforward.

The solutions to the coefficients are of the form

$$B_1 = \frac{\alpha k_1^3+\beta k_1^2+\gamma k_1+\delta}{(k_1-k_2)(k_1-k_3)(k_1-k_4)} = \frac{\alpha k_1^3+\beta k_1^2+\gamma k_1+\delta}{4k_1^3-3\sigma_1 k_1^2+2\sigma_2 k_1-\sigma_3} \qquad -(A1.25)$$

or can be reduced to it by application of the quartic equation (A1.4) to any other powers appearing in the numerator. Now in summing terms of the form

$$\frac{k_1^n}{(k_1-k_2)(k_1-k_3)(k_1-k_4)} + \cdots$$

expansion to

$$k_1^n(k_2-k_3)(k_2-k_4)(k_3-k_4) + \cdots$$

$$(k_1-k_2)(k_1-k_3)(k_1-k_4)(k_2-k_3)(k_2-k_4)(k_3-k_4)$$

easily shows that the sum is zero if n = 0, 1 or 2. Thus in summing the coefficients B_i in the form (A1.25) only the αk_1^3 term contributes. B_1 may be rewritten

$$B_1 = \frac{\alpha}{4} + \frac{(\text{terms in } k_1^0, k_1^1, k_1^2)}{4k_1^3-3\sigma_1 k_1^2+2\sigma_2 k_1-\sigma_3} \qquad -(A1.25)$$

and $B_1 + B_2 + B_3 + B_4 = I_1(0) = \alpha$. —(A1.26)

Now $k_1 B_1 = \dfrac{\alpha k_1^4 + \beta k_1^3 + \gamma k_1^2 + \delta k_1}{4k_1^3 - 3\sigma_1 k_1^2 + 2\sigma_2 k_1 - \sigma_3}$.

The term in k_1^4 can be reduced to terms in k_1^3 down to k_1^0 via the quartic equation (A1.4). Only the term in k_1^3 is relevant and is clearly $\sigma_1 k_1^3$. Thus

$$k_1 B_1 = \frac{(\alpha\sigma_1 + \beta)k_1^3 + (\text{terms in } k_1^0, k_1^1, k_1^2)}{4k_1^3 - 3\sigma_1 k_1^2 + 2\sigma_2 k_1 - \sigma_3} = \frac{1}{4}(\alpha\sigma_1 + \beta) + \text{other terms} \qquad (A1.27)$$

and $\sum_{i=1}^{4} k_i B_i = \dot{I}_1(0) = \alpha\sigma_1 + \beta = \sigma_1 I_1(0) + \beta$

or $\beta = \dot{I}_1(0) - \sigma_1 I_1(0)$. —(A1.28)

A similar treatment, successively reducing terms in k_1^4, k_1^5 and k_1^6 to terms in $k_1^3, k_1^2, k_1^1, k_1^0$ via equation (A1.4) yields

$$\gamma = \ddot{I}_1(0) - \sigma_1 \dot{I}_1(0) + \sigma_2 I_1(0) \qquad —(A1.29)$$

$$\delta = \dddot{I}_1(0) - \sigma_1 \ddot{I}_1(0) + \sigma_2 \dot{I}_1(0) - \sigma_3 I_1(0) = -\sigma_4 Q_1(0) \; . \qquad —(A1.30)$$

The last step in (A1.30) is an application of the differential equation obeyed by I_1, namely

$$\dddot{I}_1 - \sigma_1 \ddot{I}_1 + \sigma_2 \dot{I}_1 - \sigma_3 I_1 + \sigma_4 Q_1 = 0 \qquad —(A1.31)$$

and illustrates the marked similarity between the form of this and the form of α, β, γ and δ.

The solution for B_1 is then

$$B_1 = \frac{I_1(0)k_1^3 + [\dot{I}_1(0) - \sigma_1 I_1(0)]k_1^2 + [\ddot{I}_1(0) - \sigma_1 \dot{I}_1(0) + \sigma_2 I_1(0)]k_1 - \sigma_4 Q_1(0)}{4k_1^3 - 3\sigma_1 k_1^2 + 2\sigma_2 k_1 - \sigma_3} . \qquad (A1.32)$$

$\dot{I}_1(0)$ and $\ddot{I}_1(0)$ may be derived explicitly from the second order differential equations (A1.1) given $Q_1(0), Q_2(0), I_1(0)$ and $I_2(0)$.

Further coefficients are simply deduced. B_2 is a similar function of k_2; Y_1 is a similar function of $Q_2(0)$ and its derivatives. The charge coefficients may either be interpreted or more simply deduced via relations (A1.8).

APPENDIX 2

A Computer Program for the Solution of the LC-Inversion Circuit with Time-Varying Parameters

A Computer Program for the Solution of the LC-Inversion Circuit with Time-Varying Circuit Parameters

A2.1 Introduction

It was shown in Appendix 1 that the solution to the LC-inversion circuit of figure A1.1 can be written in terms of four parameters k_i for any region in which the circuit parameters are constant, given initial boundary conditions of capacitor voltages (or charges) and two loop currents. This appendix reports upon a computer program designed to evaluate these parameters and thereby to solve a given LC-inversion circuit of the form shown in figure 4.1.

By approximating a time-varying parameter such as discharge resistance to a series of sufficiently small steps the program can generate a numerical solution to a more complicated problem while being capable of providing a mathematical expression for the circuit behaviour near to any particular point.

A2.2 The Program Method

The program evaluates the parameters k_i and the charge and current coefficients A_i, X_i, B_i, Y_i in successive time intervals whose length is specified by the user. During one time interval the coefficients are evaluated from the initial charges and currents; the final charges and currents are then estimated by equations (A1.6) and (A1.7). These values are subsequently used as initial boundary conditions for the next interval. By further evaluating the circuit parameters such as resistance at the start of every interval, a time-varying

quantity is modelled as a series of steps. Clearly the accuracy of this approximation will depend directly upon the time interval chosen.

Specifically, the program allows time-varying terms of the form ae^{-Bt} to be defined for both R_1 and R_2. An initial constant (usually high) region for R_2 allows the program to begin cavity breakdown after a specified time or cavity voltage is reached.

A2.3 Evaluating the k_i

The subroutine KFIND takes an estimate of one k_i and returns a value to within one part in 10^{15} using double-precision complex arithmetic. The parameters k_i are evaluated numerically by the Newton-Raephson method from initial approximations. If k_e is an estimate of a root k of $f(k) = 0$ then a simple Taylor expansion

$f(k) = f(k_e + (k - k_e)) = 0 \cong f(k_e) + (k - k_e) f'(k_e)$ shows that

$$k \cong k_e - \frac{f(k_e)}{f'(k_e)}. \qquad \text{—(A2.1)}$$

The process is repeated until a specified accuracy is reached. The function f(k) is here the quartic equation (A1.4).

The estimates for k_3 and k_4 are based upon one of the uncoupled loops mentioned in section (A1.1) and equation (A1.5). The theory of equations predicts that any complex solutions to equation (A1.4) will appear in complex conjugate pairs and this is reflected in the approximation.

The subroutine KFIND is called (twice) to determine accurately k_3 and k_4. By combining equations (A1.13) and (A1.14) it is then possible to deduce k_1 and k_2:

$$k_{1,2} = (\sigma_1 - k_3 - k_4) \pm \sqrt{(\sigma_1 - k_3 - k_4) - \frac{4\sigma_4}{k_3 k_4}} \,. \qquad -(A2.2)$$

To maintain accuracy, k_1 and k_2 are then also processed by KFIND.

To ensure that the four k_i are four different k_i the subroutine CHECK compares sums defined by equations (A1.13) with the sums predicted by equations (A1.14). Clearly equation (A2.2) assumes two of these, leaving the remaining two as valid checks. Should the sums be incorrect, the program returns to use the remaining uncoupled loop as a source of an estimate for k_3 and k_4, and this was found to be adequate in the cases studied.

The theory developed for the LC-Inversion circuit implicitly assumes that the four k_i are indeed different. Should the circuit parameters in one time interval cause two of the k_i to be equal (or very close) the theory is not adequate since it then allows only three independent arbitrary constants. The form $(A_1 t + A_2) \exp(k_1 t)$ would in fact be appropriate should, for example, k_1 and k_2 coincide. The subroutine CHECK causes the circuit parameters to return to their values of the previous time interval should such a coincidence occur to within 10^{-10}.

A2.4 Generating the Coefficients and Solutions

The alternative formulation of section (A1.4) is used to generate the four coefficients for each variable Q_1, Q_2, I_1 and I_2. To this end it is necessary to know four other derivatives $\dot{I}_1$, $\ddot{I}_1$, $\dot{I}_2$ and $\ddot{I}_2$. These are evaluated from Q_1, Q_2, I_1 and I_2 via equations (A1.1) and/or their derivative equations.

Actually some flexibility is allowed by equation (A1.31) and the program uses $\int Q\,dt$ rather than $\ddot{I}$. [It should be noted that only Q_1, Q_2, I_1 and I_2 are continuous over the boundaries between time intervals.] Each coefficient is evaluated via an equation of the type (A1.32). A check ensures that the coefficients sum to their correct initial values.

The subroutine SOLVE takes any set of four coefficients, say A_i, and performs a sum of the form $\Sigma\, A_i \exp(k_i t_{inc.})$ for a time increment $t_{inc.}$. This then provides the charge Q_1, say, at the end of an interval $t_{inc.}$ long. The subroutine is called once for each variable Q_1, Q_2, I_1 and I_2. A check is performed in the subroutine to ensure that each result is real.

From these four "main" variables other circuit variables such as voltage and power are derived. [For the voltage across an inductance it is first necessary to calculate one or two of the $\dot{I}$.] The power is integrated step by step by the trapezoidal rule to yield the energy deposited into a resistance.

The results are output at predetermined intervals and may be plotted graphically.

A2.5 The Computer Program List

A listing of the computer program is given on the following pages.

```
EDIT: DRA1:[PHRDWJLC]FULL.FOR;6
*P2/1:*/2
00100            INTEGER N,M,J,DIAFLAG,SUMFLAG,HILOFLAG,NUM
00200            COMPLEX*16 A(4),X(4),AI(4),XI(4),SOL,K(4),KU,CHK(4),DUM,DUM2
00300            COMPLEX*16 AID(4),XID(4),AOUP(4),XOUP(4)
00400            COMMON C1,C2,L1,L2,R1,R2,L,R/KBLK/KU/BLK/K,SOL/DIABLK/DIAFLAG
00500           *  /SBLK/S
00600            DOUBLE PRECISION Q(2),I(2),TIME,TLIM,TINC,C1,C2,L1,L2,R1,R2
00700            DOUBLE PRECISION RDUM,VO(2),R20,AA,BB,POWER(3),LASTP(3)
00800            DOUBLE PRECISION R10,AA1,BB1,AMAX,XMAX,AIMAX,XIMAX,ENERGY(3),
00900           *  V(2),ID(2),PLOT1(0:100),PLOT2(0:100),PLOT3(0:100),TSPACE
01000            DOUBLE PRECISION PLOT4(0:100),L2LASER,L2NOTL,R2BEGIN
01100            DOUBLE PRECISION STEP,TBRK,R2NOTL,R20LASER,VL,DENOM,R,L,S(4),
01200           *  QUP(2),PLOT5(0:100),PLOT6(0:100),R1LAST,R2LAST,VLBRK,VLMAX,P2MX
01300     C-----------------------------------------------------------------------
01400     C                  input original boundary conditions
01500     1        TIME=0
01600              ENERGY(1)=0
01700              ENERGY(2)=0
01800              ENERGY(3)=0
01900              POWER(1)=0
02000              POWER(2)=0
02100              POWER(3)=0
02200              M=0
02300              NUM=1
02400              PLOT1(0)=0
02500              PLOT2(0)=0
02600              PLOT3(0)=0
02700              PLOT4(0)=0
02800              PLOT5(0)=0
02900              PLOT6(0)=0
03000              WRITE(6,4999)
03100     4999     FORMAT(' DO YOU REQUIRE DIAGNOSTICS? 1:YES 0:NO ')
03200              READ(6,*)DIAFLAG
03300              WRITE(6,4970)
03400     4970     FORMAT(' DO YOU WANT HIGH OR LOW STEPS? 1:HIGH 0:LOW ')
03500              READ(6,*)HILOFLAG
03600              WRITE(6,5000)
03700     5000     FORMAT(' ENTER TIME LIMIT ',$)
03800              READ(6,*)TLIM
03900              WRITE(6,5001)
04000     5001     FORMAT(' ENTER TIME INCREMENT ',$)
04100              READ(6,*)STEP
04200              WRITE(6,5101)
04300     5101     FORMAT(' HOW MANY NSECS. BETWEEN LISTINGS OF CURRENTS ETC.? ',$)
04400              READ(6,*)TSPACE
04500              WRITE(6,5002)
04600     5002     FORMAT(' ENTER C1 ',$)
```

```
04700           READ(6,*)C1
04800           WRITE(6,5003)
04900    5003   FORMAT(' ENTER C2 ',$)
05000           READ(6,*)C2
05100           WRITE(6,50031)
05200    50031  FORMAT(' ENTER L ',$)
05300           READ(6,*)L
05400           WRITE(6,50032)
05500    50032  FORMAT(' ENTER R ',$)
05600           READ(6,*)R
05700           WRITE(6,5004)
05800    5004   FORMAT(' ENTER L1 ',$)
05900           READ(6,*)L1
06000           WRITE(6,5005)
06100    5005   FORMAT(' ENTER L2 NON-LASER COMPONENT ',$)
06200           READ(6,*)L2NOTL
06300           WRITE(6,50051)
06400    50051  FORMAT(' ENTER L2 LASER COMPONENT ',$)
06500           READ(6,*)L2LASER
06600           L2=L2NOTL+L2LASER
06700           WRITE(6,5007)
06800    5007   FORMAT(' ENTER V0(1) ',$)
06900           READ(6,*)V0(1)
07000           WRITE(6,50071)
07100    50071  FORMAT(' ENTER V0(2) ',$)
07200           READ(6,*)V0(2)
07300           Q(1)=V0(1)*C1-V0(2)*C2
07400           Q(2)=C2*V0(2)
07500           V(1)=V0(1)
07600           V(2)=V0(2)
07700           I(1)=0
07800           I(2)=0
07900    C-------------------------------------------------------------------------
08000    C               insert changing parameters
08100           WRITE(6,50079)
08200    50079  FORMAT(' THE RESISTANCE OF THE LASER LOOP HAS TWO DOMAINS')
08300           WRITE(6,50080)
08400    50080  FORMAT(' FOR THE FIRST CONSTANT DOMAIN ENTER R2 '$)
08500           READ(6,*)R2BEGIN
08600           WRITE(6,50082)
08700    50082  FORMAT(' THIS DOMAIN FINISHES WHEN? ',$)
08800           READ(6,*)TBRK
08900           IF(TBRK.LT.0)THEN
09000           TBRK=1.D6
09100           WRITE(6,50084)
09200    50084  FORMAT(' AT WHAT VOLTAGE DOES CAVITY BREAKDOWN BEGIN? ',$)
09300           READ(6,*)VLBRK
09400           ELSE
```

```
09500           VLBRK=-1
09600           END IF
09700           WRITE(6,5112)
09800   5112    FORMAT(' ENTER R2 NON-LASER COMPONENT ',$)
09900           READ(6,*)R2NOTL
10000           WRITE(6,5008)
10100           WRITE(6,5080)
10200           WRITE(6,5009)
10300           READ(6,*)R20LASER
10400           WRITE(6,5010)
10500           READ(6,*)AA
10600           WRITE(6,5011)
10700           READ(6,*)BB
10800   5008    FORMAT(' The resistance of the laser decays as')
10900   5080    FORMAT('                R2(t)=R20LASER+AA*exp(-BB*t)')
11000   5009    FORMAT(' ENTER R20LASER ',$)
11100   5010    FORMAT(' ENTER AA ',$)
11200   5011    FORMAT(' ENTER BB ',$)
11300           WRITE(6,5012)
11400           WRITE(6,5013)
11500           WRITE(6,5014)
11600   5012    FORMAT(' The resistance of the rinsing arm decays as')
11700   5013    FORMAT('                  R1(t)=R10+AA1*EXP(-BB1*t)')
11800   5014    FORMAT(' ENTER R10 ',$)
11900           READ(6,*)R10
12000           WRITE(6,5015)
12100   5015    FORMAT(' ENTER AA1 ',$)
12200           READ(6,*)AA1
12300           WRITE(6,5016)
12400   5016    FORMAT(' ENTER BB1 ',$)
12500           READ(6,*)BB1
12600           R20=R2NOTL+R20LASER
12700   99      TINC=STEP
12800           IF((TIME+TINC.GT.TBRK).AND.(TIME.LT.TBRK))TINC=TBRK-TIME
12900           RDUR=NUM*TSPACE
13000           IF((TIME+TINC.GT.RDUR).AND.(TIME.LT.RDUR))TINC=RDUR-TIME

 Page 2.
00100           R1=R10
00200           IF(HILOFLAG.EQ.0)TIME=TIME+TINC
00300           IF(-BB1*TIME.GT.-30)R1=R10+AA1*EXP(-BB1*TIME)
00400           IF(HILOFLAG.EQ.0)TIME=TIME-TINC
00500           IF(TIME.LT.TBRK)R2=R2BEGIN+R2NOTL
00600           IF(TIME.GE.TBRK)THEN
00700           TIME=TIME-TBRK
00800           IF(HILOFLAG.EQ.0)TIME=TIME+TINC
00900           R2=R20
01000           IF(BB*TIME.LT.30.)R2=R20+AA*EXP(-BB*TIME)
```

```
01100           IF(HILOFLAG.EQ.0)TIME=TIME-TINC
01200           TIME=TIME+TBRK
01300           END IF
01400   C-------------------------------------------------------------------
01500   54      DENOM=L*(L1+L2)+L1*L2
01600           S(1)=-((L+L1)*R2+(L+L2)*R1+R*(L1+L2))/DENOM
01700           S(2)=-(L2/C1+L/C2+L1*(1/C1+1/C2)+R*(R1+R2)+R1*R2)/DENOM
01800           S(3)=-(R1*(1/C1+1/C2)+R/C2+R2/C1)/DENOM
01900           S(4)=1/(C1*C2*DENOM)
02000           ID(1)=(R1*(L+L2)+R*L2)*I(1)+(R*L2-R2*L)*I(2)
02100           ID(1)=-(ID(1)+L2*Q(1)/C1+(L2/C1-L/C2)*Q(2))/DENOM
02200           ID(2)=(R2*(L+L1)+R*L1)*I(2)+(R*L1-L*R1)*I(1)
02300           ID(2)=-(ID(2)+(L1*(1/C1+1/C2)+L/C2)*Q(2)+L1*Q(1)/C1)/DENOM
02400           QUP(2)=C2*(L1*I(1)+R1*Q(1)-L2*I(2)-R2*Q(2))
02500           QUP(1)=-C1*(L1*I(1)+R1*Q(1)+L*(I(1)+I(2))+R*(Q(1)+Q(2)))-QUP(2)
02600   C-------------------------------------------------------------------
02700   C               find k values by newton-raephson method
02800           IF(TIME.GT.0) THEN
02900           DO 22 J=1,4
03000           CALL KFIND(K(J),0)
03100           IF(ABS(KU).LE.0) GOTO 33
03200   22      CONTINUE
03300           GOTO 554
03400           END IF
03500   33      DUM=SQRT(DCMPLX((R+R2)**2-4*(L+L2)*(1/C1+1/C2)))
03600           K(3)=(-(R+R2)+DUM)/(2*(L+L2))
03700           K(4)=(-(R+R2)-DUM)/(2*(L+L2))
03800   771     DO 60 J=3,4
03900           CALL KFIND(K(J),1)
04000   60      K(J)=KU
04100           DUM2=S(1)-K(3)-K(4)
04200           DUM=S(4)/(K(3)*K(4))
04300           K(1)=(DUM2+SQRT(DUM2**2-4*DUM))/2
04400           K(2)=(DUM2-SQRT(DUM2**2-4*DUM))/2
04500           DO 123 J=1,2
04600           CALL KFIND(K(J),1)
04700   123     K(J)=KU
04800   554     DO 555 N=1,4
04900           IF(TIME.LE.0) THEN
05000           WRITE(6,8888)TIME,N,K(N)
05100           GOTO 555
05200           END IF
05300           IF(DIAFLAG.EQ.1)WRITE(6,8888)TIME,N,K(N)
05400   555     CONTINUE
05500   8888    FORMAT(6H TIME=,F6.2,1H+,3H K(,I1,2H)=,D20.12,2H +,D20.12,2H i)
05600           CALL CHECK
05700           IF(ABS(K(1)).LE.0) THEN
05800           WRITE(6,1999)TIME
```

```
05900   1999    FORMAT(' A RE-ESTIMATE HAS BEEN MADE FOR TIME= ',F6.2,'+')
06000           GOTO 771
06100           END IF
06200           IF(ABS(K(2)).LE.0)THEN
06300           WRITE(6,1998)TIME
06400   1998    FORMAT(' R1 & R2 HAVE BEEN RESET FOR TIME= ',F6.2,'+')
06500           R1=R1LAST
06600           R2=R2LAST
06700           GOTO 54
06800           END IF
06900   C-----------------------------------------------------------------
07000   C                 set main constants with checks
07100           DO 400 N=1,4
07200   400     CHK(N)=0
07300           AMAX=0
07400           XMAX=0
07500           AIMAX=0
07600           XIMAX=0
07700           DO 10 N=1,4
07800           DUM2=4*K(N)**3-3*S(1)*K(N)**2+2*S(2)*K(N)-S(3)
07900           A(N)=Q(1)*K(N)**3+(I(1)-S(1)*Q(1))*K(N)**2
08000           X(N)=Q(2)*K(N)**3+(I(2)-S(1)*Q(2))*K(N)**2
08100           A(N)=A(N)+(ID(1)-S(1)*I(1)+S(2)*Q(1))*K(N)
08200           X(N)=X(N)+(ID(2)-S(1)*I(2)+S(2)*Q(2))*K(N)
08300           A(N)=(A(N)-S(4)*QUP(1))/DUM2
08400           X(N)=(X(N)-S(4)*QUP(2))/DUM2
08500           AI(N)=I(1)*K(N)**3+(ID(1)-S(1)*I(1))*K(N)**2
08600           XI(N)=I(2)*K(N)**3+(ID(2)-S(1)*I(2))*K(N)**2
08700           AI(N)=AI(N)+(S(3)*Q(1)-S(4)*QUP(1))*K(N)
08800           XI(N)=XI(N)+(S(3)*Q(2)-S(4)*QUP(2))*K(N)
08900           AI(N)=(AI(N)-S(4)*Q(1))/DUM2
09000           XI(N)=(XI(N)-S(4)*Q(2))/DUM2
09100           AID(N)=ID(1)*K(N)**3
09200           XID(N)=ID(2)*K(N)**3
09300           AID(N)=AID(N)+(-S(2)*I(1)+S(3)*Q(1)-S(4)*QUP(1))*K(N)**2
09400           XID(N)=XID(N)+(-S(2)*I(2)+S(3)*Q(2)-S(4)*QUP(2))*K(N)**2
09500           AID(N)=(AID(N)+(S(3)*I(1)-S(4)*Q(1))*K(N)-S(4)*I(1))/DUM2
09600           XID(N)=(XID(N)+(S(3)*I(2)-S(4)*Q(2))*K(N)-S(4)*I(2))/DUM2
09700           AQUP(N)=QUP(1)*K(N)**3+(Q(1)-S(1)*QUP(1))*K(N)**2
09800           XQUP(N)=QUP(2)*K(N)**3+(Q(2)-S(1)*QUP(2))*K(N)**2
09900           AQUP(N)=AQUP(N)+(I(1)-S(1)*Q(1)+S(2)*QUP(1))*K(N)
10000           XQUP(N)=XQUP(N)+(I(2)-S(1)*Q(2)+S(2)*QUP(2))*K(N)
10100           AQUP(N)=AQUP(N)+ID(1)-S(1)*I(1)+S(2)*Q(1)-S(3)*QUP(1)
10200           XQUP(N)=XQUP(N)+ID(2)-S(1)*I(2)+S(2)*Q(2)-S(3)*QUP(2)
10300           AQUP(N)=AQUP(N)/DUM2
10400           XQUP(N)=XQUP(N)/DUM2
10500           CHK(1)=CHK(1)+A(N)
10600           CHK(2)=CHK(2)+X(N)
```

```
10700           CHK(3)=CHK(3)+AI(N)
10800           CHK(4)=CHK(4)+XI(N)
10900           IF(ABS(A(N)).GT.AMAX)AMAX=ABS(A(N))
11000           IF(ABS(X(N)).GT.XMAX)XMAX=ABS(X(N))
11100           IF(ABS(AI(N)).GT.AIMAX)AIMAX=ABS(AI(N))
11200           IF(ABS(XI(N)).GT.XIMAX)XIMAX=ABS(XI(N))
11300   10      CONTINUE
11400           CHK(1)=(CHK(1)-Q(1))/AMAX
11500           CHK(2)=(CHK(2)-Q(2))/XMAX
11600           CHK(3)=(CHK(3)-I(1))/AIMAX
11700           IF(AIMAX.LT.1.D-6) CHK(3)=0
11800           CHK(4)=(CHK(4)-I(2))/XIMAX
11900           IF(I(2).LT.1.D-6)CHK(4)=0
12000           DO 600 N=1,4
12100           IF(ABS(CHK(N)).GT.1.D-6)THEN
12200           WRITE(6,2200)N,CHK(N)
12300   2200    FORMAT(1H ,'CHECK FAULT:CHK(',I1,')=',D12.4,'+',D12.4,'i')
12400           END IF
12500   600     CONTINUE
12600   C-----------------------------------------------------------------------
12700   C               solve for q1,q2,i1,i2
12800           IF(TIME.LE.0.) THEN
12900           WRITE(6,5555)
13000   5555    FORMAT(7H   TIME,5X,'R1',10X,'R2',10X,'I1',10X,'I2',10X,'V1',
13100        *10X,'V2',10X,'VL',10X,'E1',10X,'E2',10X,'E3')
13200           WRITE(6,9999)TIME,R1,R2,I,V,VL,ENERGY
13300           END IF
13400           TIME=TIME+TINC
13500           CALL SOLVE(A,TINC)
13600           Q(1)=DREAL(SOL)
13700           CALL SOLVE(X,TINC)
13800           Q(2)=DREAL(SOL)
13900           CALL SOLVE(AI,TINC)
14000           I(1)=DREAL(SOL)
14100           CALL SOLVE(XI,TINC)
14200           I(2)=DREAL(SOL)
14300   C       CALL SOLVE(AID,TINC)
14400   C       ID(1)=DREAL(SOL)
14500   C       CALL SOLVE(XID,TINC)
14600   C       ID(2)=DREAL(SOL)
14700   C       CALL SOLVE(AQUP,TINC)
14800   C       QUP(1)=DREAL(SOL)
14900   C       CALL SOLVE(XQUP,TINC)
15000   C       QUP(2)=DREAL(SOL)
15100   C
15200   C               set power and energy
15300   C
15400           POWER(1)=I(1)**2*R1
```

```
15500           POWER(2)=I(2)**2*(R2-R2NOTL)
15600           POWER(3)=(I(1)+I(2))**2*R
15700           ENERGY(1)=ENERGY(1)+(POWER(1)+LASTP(1))*TINC/2
15800           ENERGY(2)=ENERGY(2)+(POWER(2)+LASTP(2))*TINC/2.
15900           ENERGY(3)=ENERGY(3)+(POWER(3)+LASTP(3))*TINC/2
16000           LASTP(1)=POWER(1)
16100           LASTP(2)=POWER(2)
16200           LASTP(3)=POWER(3)
16300           R1LAST=R1
16400           R2LAST=R2
16500           ID(1)=(R1*(L+L2)+R*L2)*I(1)+(R*L2-R2*L)*I(2)
16600           ID(1)=-(ID(1)+L2*Q(1)/C1+(L2/C1-L/C2)*Q(2))/DENOM
16700           ID(2)=(R2*(L+L1)+R*L1)*I(2)+(R*L1-L*R1)*I(1)
16800           ID(2)=-(ID(2)+(L1*(1/C1+1/C2)+L/C2)*Q(2)+L1*Q(1)/C1)/DENOM
16900           V(1)=(Q(1)+Q(2))/C1
17000           V(2)=Q(2)/C2
17100           VL=-((R2-R2NOTL)*I(2)+L2LASER*ID(2))
17200           IF(VL.LT.VLMAX)VLMAX=VL
17300           IF(POWER(2).GT.P2MX)P2MX=POWER(2)
17400           IF((VLBRK.GT.0).AND.(-VL.GE.VLBRK).AND.(TBRK.GE.1.D6))TBRK=TIME
17500   C
17600           RNUM=ABS(TIME-NUM*TSPACE)
17700           IF(RNUM.LT.1.D-6)THEN
17800           WRITE(6,9999)TIME,R1,R2,I,V,VL,ENERGY
17900           PLOT1(NUM)=I(1)
18000           PLOT2(NUM)=I(2)
18100           PLOT3(NUM)=POWER(2)
18200           PLOT4(NUM)=-I(2)*VL
18300           PLOT5(NUM)=VL
18400           PLOT6(NUM)=V(1)+V(2)+L*(ID(1)+ID(2))+R*(I(1)+I(2))
18500           NUM=NUM+1
18600           END IF
18700   9999    FORMAT(1H ,F6.2,10D12.4)
18800   C-----------------------------------------------------------------
18900   C               set constants for ???????????
19000   C-----------------------------------------------------------------
19100   C               reset times and return if necessary
19200           IF((TIME-TLIM).GE.0) GOTO 100
19300           GOTO 99
19400   100     WRITE(6,60005)VLMAX,P2MAX
19500   60005   FORMAT(' VLMAX= ',D12.4,' P2MAX= ',D12.4)
19600           CALL GRAPH(PLOT1,PLOT2,NUM)
19700           CALL GRAPH(PLOT3,PLOT4,NUM)
19800           CALL GRAPH(PLOT5,PLOT6,NUM)
19900           WRITE(6,3434)
20000   3434    FORMAT(1H ,'DO YOU REQUIRE ANOTHER RUN? 1:YES 0:NO ')
20100           READ(6,*)J
20200           IF(J.EQ.1)GOTO 1
```

```
20300           STOP
20400           END
20500   C-------------------------------------------------------------------
20600   C                          ***************
20700   C                          * END OF MAIN *
20800   C                          ***************
20900   C-------------------------------------------------------------------
21000   C
21100           SUBROUTINE SOLVE(B,T)
21200           COMMON /BLK/K,SOL
21300           COMPLEX*16 K(4),B(4),SOL
21400           DOUBLE PRECISION T
21500           SOL=0
21600           DO 50 J=1,4
21700   C       IF(DREAL(K(J))*T.LT.-50.)GOTO 50
21800           SOL=SOL+B(J)*EXP(K(J)*T)
21900   50      CONTINUE
22000           IF(ABS(DIMAG(SOL)).GT.ABS(DREAL(SOL))*(1.D-13))WRITE(6,1111)SOL
22100   1111    FORMAT(1H ,'BEWARE:SOL=',D12.4,'+',D12.4,'i')
22200           RETURN
22300           END
22400   C-------------------------------------------------------------------
22500   C
22600           SUBROUTINE KFIND(B,FLAG)
22700           INTEGER J,FLAG,DIAFLAG
22800           COMPLEX*16 G,H,B,COR,F,FD,KU
22900           DOUBLE PRECISION C1,C2,L1,L2,R1,R2,ERR,S(4),L,R
23000           COMMON C1,C2,L1,L2,R1,R2,L,R/KBLK/KU/DIABLK/DIAFLAG/SBLK/S
23100           ERR=1.D-15
23200           J=0
23300   40      F=B**2*(B**2+S(2))-B*(S(1)*B**2+S(3))+S(4)
23400           FD=B**2*(4*B-3*S(1))+2*S(2)*B-S(3)
23500           COR=F/FD
23600           IF(ABS(COR).LT.ABS(B*ERR)) THEN
23700           IF(DIAFLAG.EQ.1)GOTO 75
23800           GOTO 70
23900           END IF
24000           IF(FLAG.EQ.0) THEN
24100           KU=0
24200           GOTO 80
24300           END IF
24400           B=B-COR
24500           J=J+1
24600           IF(J.EQ.99)GOTO 75
24700           GOTO 40
24800   75      WRITE(6,99)J,COR
24900   99      FORMAT(6H AFTER,I2,'LOOPS COR=',D12.4,'+',D12.4,'i')
25000   70      KU=B
```

```
25100    80      RETURN
25200            END
25300    C-------------------------------------------------------------------
25400    C
25500            SUBROUTINE CHECK
25600            INTEGER SUMFLAG,N,J,JJ
25700            COMMON C1,C2,L1,L2,R1,R2,L,R/BLK/K/SELBLK/SUMFLAG/SBLK/S
25800            COMPLEX*16 KSUM(4),K(4),DUMMY
25900            DOUBLE PRECISION C1,C2,L1,L2,R1,R2,S(4),L,R
26000            KSUM(1)=K(1)+K(2)+K(3)+K(4)
26100            KSUM(2)=K(1)*K(2)+K(1)*K(3)+K(1)*K(4)
26200            KSUM(2)=KSUM(2)+K(2)*K(3)+K(2)*K(4)+K(3)*K(4)
26300            KSUM(3)=K(1)*K(2)*K(3)+K(1)*K(2)*K(4)
26400            KSUM(3)=KSUM(3)+K(2)*K(3)*K(4)+K(1)*K(3)*K(4)
26500            KSUM(4)=K(1)*K(2)*K(3)*K(4)
26600    C
26700            DO 200 N=1,4
26800            KSUM(N)=KSUM(N)-S(N)
26900            IF(ABS(KSUM(N)/S(N)).GT.1.D-13) THEN
27000            IF(SUMFLAG.EQ.0)THEN
27100            DUMMY=SQRT(DCMPLX((R+R1)**2-4*(L+L1)/C1))
27200            K(3)=(-(R+R1)+DUMMY)/(2*(L+L1))
27300            K(4)=(-(R+R1)-DUMMY)/(2*(L+L1))
27400            K(1)=0
27500            SUMFLAG=1
27600            GOTO 201
27700            END IF
27800            DO 247 J=1,4
27900            DO 247 JJ=J+1,4
28000            IF(ABS(K(J)-K(JJ)).LE.1D-10)THEN
28100            K(2)=0
28200            SUMFLAG=0
28300            GOTO 201
28400            END IF
28500    247     CONTINUE
28600            WRITE(6,2000)N,KSUM(N)
28700    2000    FORMAT(1H ,'CHECK FAULT:KSUM(',I1,')=',D12.4,'+',D12.4,'I')
28800            END IF
28900    200     CONTINUE
29000            SUMFLAG=0
29100    201     RETURN
29200            END
29300            SUBROUTINE GRAPH(AA,AS,NP)
29400            DOUBLE PRECISION AA,MAX,MIN,MULT,AS,MAXT,MINT,MULTT
29500            DIMENSION AA(NP),AS(NP),LINE(65)
29600            INTEGER BLANK
29700            DATA MAST,BLANK/'+','-'/
29800            DATA MIST/'0'/
```

```
29900           MAX=-1E20
30000           MIN=1E20
30100           MAXT=-1E20
30200           MINT=1E20
30300           DO 10 I=1,NP
30400           IF(AA(I).GT.MAX)MAX=AA(I)
30500           IF(AA(I).LT.MIN)MIN=AA(I)
30600           IF(AS(I).GT.MAXT)MAXT=AS(I)
30700           IF(AS(I).LT.MINT)MINT=AS(I)
30800   10      CONTINUE
30900           MULTT=60./(MAXT-MINT)
31000           MULT=60./(MAX-MIN)
31100           WRITE(6,7085)MIN,MAX
31200   7085    FORMAT(' MIN= ',D12.4,30X,' MAX= ',D12.4)
31300           WRITE(6,7086)MINT,MAXT
31400   7086    FORMAT(' MINT= ',D12.4,29X,' MAXT= ',D12.4)
31500           DO 20 I=1,65
31600   20      LINE(I)=BLANK
31700           DO 40 I=1,NP
31800           J=NINT((AA(I)-MIN)*MULT+3.)
31900           IF(J.GT.65)J=65
32000           JT=NINT((AS(I)-MINT)*MULTT+3.)
32100           IF(JT.GT.65)JT=65
32200           LINE(J)=NAST
32300           LINE(JT)=MIST
32400           WRITE(6,30)(I-1),LINE
32500   30      FORMAT(' ',I3,65A1)
32600           LINE(JT)=BLANK
32700   40      LINE(J)=BLANK
32800           RETURN
32900           END
```

APPENDIX 3

An Exact Solution to the Energy Deposited into the Resistances for Constant Circuit Parameters

An Exact Solution to the Energy Deposited into the Resistances for Constant Circuit Parameters

A3.1 Introduction

The results of Appendix 1 allow solutions to the LC-inversion circuit of Fig. (A1.1) to be written in terms of four unspecified but numerically soluble parameters k_1 , k_2 , k_3 and k_4 during any interval when circuit parameters of resistance, inductance and capacitance are constant. While a closed form solution is generally possible for these k_i it is possible, via the theory of equations [section (A1.2)], to sum exactly terms symmetrical in the k_i and by extension terms symmetrical in the four coefficients of either Q_1 , Q_2 or of their derivatives.

A useful example of such a sum is provided by $\int_o^\infty I^2\,dt$ for one of the currents I_1 or I_2. Multiplication of this integral by a constant resistance will yield the total energy deposited by the current I into this resistance after the time chosen as zero.

A3.2 The Solution

The following analysis will solve $\int_o^\infty I_1^{\,2}\,dt$ but the method is easily applied to I_2 . It is first necessary to expand $I_1^{\,2}$.

$$I_1^{\,2}(t) = [\, B_1 \exp(k_1 t) + B_2 \exp(k_2 t) + B_3 \exp(k_3 t) + B_4 \exp(k_4 t)\,]^2$$

$$= B_1^{\,2} \exp(2k_1 t) + B_2^{\,2} \exp(2k_2 t) + \cdots$$

$$+ 2B_1 B_2 \exp[\,(k_1 + k_2)t\,] + 2B_1 B_3 \exp[\,2(k_1 + k_3)t\,] + \cdots . \qquad \text{—(A3.1)}$$

For a physically reasonable solution the real part of each k_i must be negative. Integration therefore yields

$$-\int_0^\infty I_1^2\,dt = \frac{B_1^2}{2k_1} + \frac{B_2^2}{2k_2} + \cdots + 2\frac{B_1B_2}{(k_1+k_2)} + 2\frac{B_1B_3}{(k_1+k_3)} + \cdots \quad . \qquad \text{—(A3.2)}$$

It is convenient to define

$$\Psi = \frac{[\,(k_2+k_3)(k_2+k_4)(k_3+k_4)B_1 + (k_1+k_3)(k_1+k_4)(k_3+k_4)B_2 + \cdots\,]^2}{(k_1+k_2)(k_1+k_3)(k_1+k_4)(k_2+k_3)(k_2+k_4)(k_3+k_4)} \qquad \text{—(A3.3)}$$

$$= \frac{(k_2+k_3)(k_2+k_4)(k_3+k_4)}{(k_1+k_2)(k_1+k_3)(k_1+k_4)} B_1^2 + \cdots + 2\frac{(k_3+k_4)}{(k_1+k_2)} B_1B_2 + \cdots \quad .$$

Two results from the theory of equations are useful:

$$(k_2+k_3)(k_2+k_4)(k_3+k_4) = \sigma_1k_1^2 - \sigma_1^2k_1 + \sigma_1\sigma_2 - \sigma_3 \qquad \text{—(A3.4)}$$

$$(k_1+k_2)(k_1+k_3)(k_1+k_4) = \sigma_1k_1^2 + \sigma_3 \; . \qquad \text{—(A3.5)}$$

Their product is independent of k_1 and is

$$\sigma_1\sigma_2\sigma_3 - \sigma_1^2\sigma_4 - \sigma_3^2 \; . \qquad \text{—(A3.6)}$$

Further substituting for (k_3+k_4) via equation (A1.13), Ψ becomes

$$\Psi = \frac{(\sigma_1k_1^2 - \sigma_1^2k_1 + \sigma_1\sigma_2 - \sigma_3)}{(\sigma_1k_1^2+\sigma_3)} B_1^2 + \cdots + 2\frac{[\sigma_1 - (k_1+k_2)]}{(k_1+k_2)} B_1B_2 + \cdots$$

and manipulation of the two parts yields

$$\Psi = \left[\frac{(4k_1^3 - 3\sigma_1k_1^2 + 2\sigma_2k_1 - \sigma_3)}{(\sigma_1k_1^2+\sigma_3)} + 1\right]\frac{B_1^2\sigma_1}{2k_1} - B_1^2 + \cdots + 2\sigma_1\frac{B_1B_2}{(k_1+k_2)} - 2B_1B_2 + \cdots$$

$$= -\sigma_1\int_0^\infty I_1^2\,dt - I_1^2(0) + \frac{(4k_1^3 - 3\sigma_1k_1^2 + 2\sigma_2k_1 - \sigma_3)}{(\sigma_1k_1^2+\sigma_3)}\frac{B_1^2\sigma_1}{2k_1} + \cdots \quad . \qquad \text{—(A3.7)}$$

The B_1^2 term in equation (A3.7) will be labelled $\frac{1}{2}\sigma_1\Omega_1$ such that Ω_i is a function of k_i. The denominator of Ω_1 may be replaced via equation (A3.5). The numerator contains

$$4k_1^3 - 3\sigma_1k_1^2 + 2\sigma_2k_1 - \sigma_3 = (k_1 - k_2)(k_1 - k_3)(k_1 - k_4) \qquad \text{—(A3.8)}$$

as the derivative of the quartic equation (A1.4) evaluated at $k = k_1$. Then

$$\Omega_1 = \frac{(k_1 - k_2)(k_1 - k_3)(k_1 - k_4)}{(k_1+k_2)(k_1+k_3)(k_1+k_4)} \frac{B_1^2}{k_1} \qquad \text{—(A3.9)}$$

With the notation adopted in equation (A1.25) for B_1

$$\Omega_1 = \frac{[\,\alpha^2 k_1^5 + 2\alpha\beta k_1^4 + (\beta^2 + 2\alpha\gamma)k_1^3 + 2(\alpha\delta+\beta\gamma)k_1^2 + (\gamma^2 + 2\beta\delta)k_1 + 2\gamma\delta + \frac{\delta^2}{k_1}\,]}{(k_1^2 - k_2^2)(k_1^2 - k_3^2)(k_1^2 - k_4^2)} \quad \text{—(A3.10)}$$

In summing the Ω_i, expansion shows that terms in the numerator in k_i^0, k_i^2, k_i^4 sum to zero. An exactly analogous argument was given in section (A1.4) with single powers of k_i rather than squared terms. It is only necessary, therefore, to deal with an effective part of Ω_i ignoring these terms.

$$\Omega_{1(\text{eff.})} = \frac{[\,\alpha^2 k_1^5 + (\beta^2 + 2\alpha\gamma)k_1^3 + (\gamma^2 + 2\beta\delta)k_1 + \frac{\delta^2}{k_1}\,]}{(k_1^2 - k_2^2)(k_1^2 - k_3^2)(k_1^2 - k_4^2)} \quad \text{—(A3.11)}$$

Any power of k_i may be replaced by several smaller (or larger) powers by the use of the quartic equation (A1.4). $\Omega_{1(\text{eff.})}$ reduces to

$$\Omega_{1(\text{eff.})} = \frac{k_1 \frac{1}{\sigma_1}[\,\alpha^2(\sigma_2\sigma_3 - \sigma_1\sigma_4) - (\beta^2 + 2\alpha\gamma)\sigma_3 + (\gamma^2 + 2\beta\delta)\sigma_1 + \frac{\delta^2}{\sigma_4}(\sigma_3 - \sigma_1\sigma_2)\,]}{(k_1^2 - k_2^2)(k_1^2 - k_3^2)(k_1^2 - k_4^2)} \quad \text{—(A3.12)}$$

Disregarding for the moment the constant in the numerator, it is necessary to sum

$$\frac{k_1}{[\,4\sigma_1 k_1^5 - 3\sigma_1^2 k_1^4 + 2(\sigma_1\sigma_2 + 2\sigma_3)k_1^3 - 4\sigma_1\sigma_3 k_1^2 + 2\sigma_2\sigma_3 k_1 - \sigma_3^2\,]}$$

where the denominator has been expanded via equations (A3.5) and (A3.8). To achieve this summation, the process whereby equation (A3.11) was reduced to (A3.12) can be usefully reversed. The quartic equation (A1.4) shows that the following substitutions, can be made in the numerator of $\Omega_{1(\text{eff.})}$:

$$k_1^3 \rightarrow -\frac{\sigma_3}{\sigma_1}k_1 \quad \text{—(A3.13)}$$

$$k_1^5 \rightarrow -\sigma_2 k_1^3 - \sigma_4 k_1 \rightarrow (\frac{\sigma_2\sigma_3}{\sigma_1} - \sigma_4)k_1 \,. \quad \text{—(A3.14)}$$

Multiplication of equation (A3.12) by

$$4\sigma_1(\frac{\sigma_2\sigma_3}{\sigma_1} - \sigma_4) - 2(\sigma_1\sigma_2 + 2\sigma_3)\frac{\sigma_3}{\sigma_1} + 2\sigma_2\sigma_3 = \frac{4}{\sigma_1}(\sigma_1\sigma_2\sigma_3 - \sigma_1^2\sigma_4 - \sigma_3^2)$$

thus places $4\sigma_1 k_1^5 + 2(\sigma_1\sigma_2 + 2\sigma_3)k_1^3 + 2\sigma_2\sigma_3 k_1$ in the numerator.

Bearing in mind the ability to add k_1^4, k_1^2, k_1^0 arbitrarily to the numerator this is effectively equal to the denominator. Then

$$\Omega_{1\,(\text{eff.})} = \frac{[\,\alpha^2(\sigma_2\sigma_3 - \sigma_1\sigma_4) - (\beta^2 + 2\alpha\gamma)\sigma_3 + (\gamma^2 + 2\beta\delta)\sigma_1 + \frac{\delta^2}{\sigma_4}(\sigma_3 - \sigma_1\sigma_2)\,]}{4(\sigma_1\sigma_2\sigma_3 - \sigma_1^2\sigma_4 - \sigma_3^2)} \qquad \text{—(A3.15)}$$

and $\Omega_{1\,(\text{eff.})}$ is independent of k_1. The sum $(\Omega_1 + \Omega_2 + \Omega_3 + \Omega_4)$ will be simply four times this value.

Combining equations (A3.7) and (A3.15) yields an expanded form of Ψ in which $\int_0^\infty I_1^2\,dt$ appears as the only unknown.

$$\Psi = -\sigma_1 \int_0^\infty I_1^2\,dt - I_1^2(0) + \frac{\sigma_1[\alpha^2(\sigma_2\sigma_3 - \sigma_1\sigma_4) - (\beta^2 + 2\alpha\gamma)\sigma_3 + (\gamma^2 + 2\beta\delta)\sigma_1 + \frac{\delta^2}{\sigma_4}(\sigma_3 - \sigma_1\sigma_2)]}{2(\sigma_1\sigma_2\sigma_3 - \sigma_1^2\sigma_4 - \sigma_3^2)} \qquad \text{—(A3.16)}$$

It remains to evaluate Ψ as it was defined in equation (A3.3) to obtain the required solution. Using equation (A3.4) on the numerator and equation (A3.6) on the denominator,

$$\Psi = \frac{\{[\,\sigma_1 k_1^2 - \sigma_1^2 k_1 + (\sigma_1\sigma_2 - \sigma_3)\,]B_1 + \cdots\}^2}{(\sigma_1\sigma_2\sigma_3 - \sigma_1^2\sigma_4 - \sigma_3^2)}$$

$$\Psi = \frac{\{\sigma_1 \ddot{I}_1(0) - \sigma_1^2 \dot{I}_1(0) + (\sigma_1\sigma_2 - \sigma_3) I_1(0)\}^2}{(\sigma_1\sigma_2\sigma_3 - \sigma_1^2\sigma_4 - \sigma_3^2)}$$

$$\Psi = \frac{\{\sigma_1\gamma - \sigma_3\alpha\}^2}{(\sigma_1\sigma_2\sigma_3 - \sigma_1^2\sigma_4 - \sigma_3^2)} \qquad \text{—(A3.17)}$$

Combining equations (A3.16) and (A3.17), and taking $I_1^2(0) = \alpha^2$ into the numerator,

$$\int_0^\infty I_1^2\,dt = \frac{[\,\frac{\delta^2}{\sigma_4}(\sigma_3 - \sigma_1\sigma_2) + 2\beta\delta\sigma_1 - \beta^2\sigma_3 - \sigma_1\gamma^2 + 2\sigma_3\alpha\gamma + \alpha^2(\sigma_1\sigma_4 - \sigma_2\sigma_3)\,]}{2(\sigma_1\sigma_2\sigma_3 - \sigma_1^2\sigma_4 - \sigma_3^2)} . \qquad \text{—(A3.18)}$$

A3.3 Expansion of the Solution

The solution will be expanded for the case

$r = 0$, $l = 0$, $I_1(0) = 0$, $I_2(0) = 0$

Using equation (A1.1) and the results of section (A1.4):-

For I_1:

$$\alpha = I_1(0) = 0$$

$$\beta = \dot{I}_1(0) - \sigma_1 I_1(0) = \frac{-V_1}{L_1}$$

$$\gamma = \ddot{I}_1(0) - \sigma_1 \dot{I}_1(0) + \sigma_2 I_1(0) = -\frac{R_2}{L_1 L_2} V_1$$

$$\delta = -\sigma_4 Q_1 = -\frac{(C_1 V_1 - C_2 V_2)}{L_1 L_2 C_1 C_2} \qquad \text{—(A3.19)}$$

For I_2:

$$\alpha = 0$$

$$\beta = -\frac{1}{L_2}(V_1 + V_2)$$

$$\gamma = -\frac{R_1}{L_1 L_2}(V_1 + V_2)$$

$$\delta = -\frac{V_2}{L_1 L_2 C_1} \,. \qquad \text{—(A3.20)}$$

Potentials V_1 and V_2 across the capacitors C_1 and C_2 respectively have been defined by

$$C_1 V_1 = Q_1 + Q_2 \quad \text{and} \quad C_2 V_2 = Q_2 \,. \qquad \text{—(A3.21)}$$

The energies deposited into R_1 and R_2 are defined by

$$E_1 = R_1 \int_0^\infty I_1^2 \, dt \quad \text{and} \quad E_2 = R_2 \int_0^\infty I_2^2 \, dt \,. \qquad \text{—(A3.22)}$$

Then expanding the numerator and denominator of equation (A3.18) via equations (A1.14), (A3.19) and (A3.20)

$$E_1 = \tfrac{1}{2} C_1 V_1^2 - \epsilon \qquad E_2 = \tfrac{1}{2} C_2 V_2^2 + \epsilon \quad \text{where} \qquad \text{—(A3.23)}$$

$$\epsilon = \frac{\left\{ \begin{array}{l} \tfrac{1}{2} C_1 V_1^2 \left[\frac{R_1 R_2}{L_1 L_2} \left(\frac{R_1}{L_1} + \frac{R_2}{L_2} \right) \frac{R_1}{C_1} + \frac{R_1 R_2}{L_2^2} \left(\frac{1}{C_1^2} + \frac{1}{C_1 C_2} \right) + \frac{R_2^2}{L_2^2 C_1^2} \right] \\ - \tfrac{1}{2} C_2 V_2^2 \left[\frac{R_1 R_2}{L_1 L_2} \left(\frac{R_1}{L_1} + \frac{R_2}{L_2} \right) \frac{R_1}{C_1} + \frac{R_1 R_2}{L_2^2} \left(\frac{1}{C_1^2} + \frac{1}{C_1 C_2} \right) + \frac{R_1^2}{L_1^2 C_1^2} \right] \\ + C_1 V_1 V_2 \left[\frac{R_1 R_2}{L_1 L_2} \left(\frac{R_1}{L_1} + \frac{R_2}{L_2} \right) \frac{R_1}{C_1} + \frac{R_1 R_2}{L_2^2} \left(\frac{1}{C_1^2} + \frac{1}{C_1 C_2} \right) - \frac{R_1 R_2}{L_1 L_2 C_1^2} \right] \end{array} \right\}}{\left\{ \begin{array}{l} \frac{R_1 R_2}{L_1 L_2} \left(\frac{R_1}{L_1} + \frac{R_2}{L_2} \right) \left[R_1 \left(\frac{1}{C_1} + \frac{1}{C_2} \right) + R_2 \frac{1}{C_1} \right] + \frac{R_1 R_2}{L_2^2} \left(\frac{1}{C_1} + \frac{1}{C_2} \right)^2 \\ + \frac{R_1^2}{L_1^2 C_1^2} + \frac{R_2^2}{L_2^2 C_1^2} + \frac{R_1 R_2}{L_1 L_2 C_1^2} - \frac{2 R_1 R_2}{L_1 L_2 C_1 C_2} \end{array} \right\}} \,.$$

—(A3.24)

APPENDIX 4

WKB Solutions for Discharges in an LCR Circuit

WKB Solutions for Discharges in an LCR Circuit

A4.1 A Brief Review of the Method

The WKB method gives for the second order differential equation

$$\frac{d^2\Psi}{dx^2} + [\frac{q(x)}{\lambda}]^2 \Psi = 0 \qquad \text{—(A4.1)}$$

a solution of the form

$$\Psi(x) = \exp[\frac{1}{\lambda}\int_{x_0}^{x} dx \sum_{n=0}^{\infty} y_n(x)\lambda^n] \qquad \text{—(A4.2)}$$

in the hope that the first few terms of the series will suffice to give an approximate solution. Substituting the solution into the differential equation and equating coefficients of λ yields

$$y_0 = \pm iq \,.\; y_1 = -\frac{1}{2}\frac{d}{dx}(\log_e q)\,,\; y_2 = \pm\frac{1}{2} i\epsilon_0 q$$

$$\text{where } \epsilon_0 = q^{-\frac{3}{2}} \frac{d^2}{dt^2}(q^{-\frac{1}{2}}) \,. \qquad \text{—(A4.3)}$$

In general

$$\frac{dy_{n-1}}{dx} = -\sum_{m=0}^{n} y_m \; y_{n-m} \quad n = 1, 2, 3\ldots \quad . \qquad \text{—(A4.4)}$$

Since λ has acted simply as a mathematical tool, it may be set conveniently to one.

The appropriate level of approximation will depend upon the relative values

$$|y_2| : |y_1| : |y_0| \quad \text{or} \quad |\tfrac{1}{2}\epsilon_0| : |\tfrac{1}{2}\frac{d}{dt}(\frac{1}{q})| : 1 \quad . \qquad \text{—(A4.5)}$$

A4.2 The Appropriate Form of the Differential Equation

The equation for the current I is

$$\frac{Ld^2I}{dt^2} + R(t)\frac{dI}{dt} + [\frac{1}{C} + \dot{R}(t)]\, I = 0 . \qquad -(A4.6)$$

Putting $I(t) = u(t) \exp[-\tfrac{1}{2}\int \frac{Rdt}{L}]$ $\qquad -(A4.7)$

then $\frac{d^2u}{dt^2} + \frac{u}{L}[\frac{1}{C} + \frac{\dot{R}}{2} - \frac{R^2}{4L}] = 0 .$ $\qquad -(A4.8)$

and if $\lambda = 1$

$$q(t) = \sqrt{\frac{1}{LC} + \frac{\dot{R}}{2L} - \frac{R^2}{4L^2}} \ . \qquad -(A4.9)$$

A4.3 Regions of Validity of the WKB Approximation

The resistance R(t) is a rapidly decaying function of time. In the low t region q is dominated by R such that $q \sim R$ and

$$\frac{d^2}{dt^2}(q^{-\frac{1}{2}}) \sim R^{-\frac{1}{2}}, \quad \frac{d}{dt}(\frac{1}{q}) \sim R^{-1} . \qquad -(A4.10)$$

The ratios (A4.5) are then

$R^2 : R^{-1} : 1$

and a first order approximation ignoring y_2 is appropriate.

In the high t region, R(t) is approximately constant. Then q is also practically constant and the WKB solution reduces to the exact solution to the LCR circuit for a constant resistance.

The WKB solution is exponential or oscillatory depending as q^2 is negative or positive. Since R(t) is a decreasing function of time, the solution will involve an exponential region followed by an oscillatory one and separated from it by a turning point where q passes through zero. Near to this point q varies rapidly in relation to its own size and the

first order solution fails, becoming infinite at the turning point. The differential equation here is approximated by the Stokes differential equation and its analysis provides a suitable connection formula between the two solutions.

A4.4 The WKB Solutions

Using only y_0 and y_1 equation (A4.2) becomes

$$\Psi(x) = \frac{1}{\sqrt{q}} \exp[\pm i \int_{x_0}^{x} q \, dx]$$

where $q(x_0) = 0$. Specifically

$$u(t) \sim \frac{\exp[\pm i \int_{t_0}^{t} \sqrt{\frac{1}{LC} + \frac{\dot{R}}{2L} - \frac{R^2}{4L^2}} \, dt}{[\frac{1}{LC} + \frac{\dot{R}}{2L} - \frac{R^2}{4L^2}]^{1/4}} \qquad \text{—(A4.11)}$$

With boundary conditions given at $t = 0$ the exponential region will be considered first.

A4.5 The Region $t < t_0$

The two solutions are

$$u(t) \sim \frac{\exp[\pm \int_{t_0}^{t} \sqrt{\frac{R^2}{4L^2} - \frac{\dot{R}}{2L} - \frac{1}{LC}} \, dt}{[\frac{R^2}{4L^2} + \frac{\dot{R}}{2L} - \frac{1}{LC}]^{1/4}} \qquad \text{—(A4.12)}$$

For very small t this reduces to yield

$$I(t) \sim \frac{1}{\sqrt{R}} \exp[-\tfrac{1}{2} \int_{0}^{t} \frac{R}{L} dt] \exp[\pm \int_{0}^{t} (\frac{R}{2L} - \frac{\dot{R}}{2R}) dt]$$

where the lower limit has been replaced by zero since this maintains consistency with the low t stipulation and only introduces a constant factor. Then I(t) becomes

$$I(t) \sim \frac{1}{R} + \text{constant} \times \exp[-\int_{0}^{t} \frac{R}{L} dt] \qquad \text{—(A4.13)}$$

since $\int_0^t \frac{\dot{R}}{2R}\,dt = [\log_e \sqrt{R}\,]_0^t = \log_e \sqrt{\frac{R(t)}{R(0)}}$.

The second term in equation (A4.13) is a rapidly decaying function and serves only to satisfy the boundary condition $I(0) = 0$. For small $t \neq 0$

$$I(t) \sim \frac{1}{R(t)} \,. \qquad \text{—(A4.14)}$$

This approximation will be valid while $R(t)$ greatly dominates q. Nearer to t_0 the full expression (A4.12) is required and this will be expanded for the particular case of an exponentially decaying resistance of the form

$$R(t) = R_0 + ae^{-Bt} \,. \qquad \text{—(A4.15)}$$

It has been shown that one of the WKB solutions is a rapidly decaying one whose extremely small coefficient is only overcome near to $t = 0$. The relevant solution therefore consists of an exponentially increasing term

$$u(t) \sim \frac{\exp\left[\int_{t_0}^{t} \sqrt{\frac{a^2}{4L^2}e^{-2Bt} + \frac{a}{2L}\left(B + \frac{R_0}{L}\right)e^{-Bt} - \left(\frac{1}{LC} - \frac{R_0^2}{4L^2}\right)}\,dt\right]}{\left[\frac{a^2}{4L^2}e^{-Bt} + \frac{a}{2L}\left(B + \frac{R_0}{L}\right)e^{-Bt} - \left(\frac{1}{LC} - \frac{R_0^2}{4L^2}\right)\right]^{1/4}} \,. \qquad \text{—(A4.16)}$$

The integral in the exponent may be solved numerically, but is soluble analytically. The substitution

$$x = e^{-Bt}, \quad dx = -Bx\,dt \qquad \text{—(A4.17)}$$

reduces the integral to a form which may be found in tables of indefinite integrals. Defining

$$p = \frac{2L}{a}\left(B + \frac{R_0}{L}\right), \quad r = \frac{4L^2}{a^2}\left(\frac{1}{LC} - \frac{R_0^2}{4L^2}\right)$$

and $\phi = x^2 + px - r$, $\phi(x_0) = 0$, $\qquad$ —(A4.18)

$$u(t) \sim \frac{\exp \frac{a}{2LB}\left[-\sqrt{\phi} + \tfrac{1}{2}p \log_e \left(\frac{p + 2x_0}{p + 2x + 2\sqrt{\phi}} \right) + \tfrac{1}{2}\pi\sqrt{r} + \sqrt{r} \tan^{-1} \left(\frac{px - 2r}{2\sqrt{r\phi}} \right) \right]}{\phi^{1/4}} \qquad \text{—(A4.19)}$$

$$\text{and} \quad I(t) \sim u(t) \exp\left[\frac{1}{2L} \left(\frac{a}{B} e^{-Bt} - R_0 t \right) \right] \qquad \text{—(A4.20)}$$

with reference to equation (A4.7). Terms concerned with the lower limits of integration have been ignored in equation (A4.20) as constant factors. These factors are taken up in the boundary condition at t = 0

$$I(0) = \frac{V_0}{a + R_0} \cong \frac{V_0}{a} \qquad \text{—(A4.21)}$$

appropriate to this analysis where the true value I(0) = 0 is satisfied by a rapidly decaying term and where all the initial potential V_0 is taken across R such that $I \sim \frac{1}{R}$ while $R^2 \gg \frac{L}{C}$. In calculating the necessary coefficient for I(t) it must be remembered that I(0) as derived from equations (A4.19) and (A4.20) involves two large exponents of roughly equal magnitude but opposite sign. These have a non-negligible but simply calculated sum.

A4.6 The Region $t > t_0$

The solution to u(t) connecting to a single decaying (away from t_0) exponential for $t < t_0$ is

$$u(t) \sim \frac{2 \cos\left[\int_{t_0}^{t} \sqrt{\frac{1}{LC} - \frac{aBe^{-Bt}}{2L} - \frac{(R_0 + ae^{-Bt})^2}{4L^2}} \, dt - \frac{\pi}{4} \right]}{\left[\frac{1}{LC} - \frac{aBe^{-Bt}}{2L} - \frac{(R_0 + ae^{-Bt})^2}{4L^2} \right]^{1/4}} \qquad \text{—(A4.22)}$$

To evaluate this integral, ϕ is redefined as

$$\phi = r - px - x^2 \qquad \text{—(A4.23)}$$

to keep it positive. For $t \gg t_0$, ϕ becomes constant and the

integral becomes a linear function of t as expected.

Performing the integration generally

$$u(t) \sim \frac{2\cos\left\{\frac{a}{2LB}\left[-\sqrt{\phi}+\sqrt{r}\log_e\left[\frac{(2r-px+2\sqrt{r\phi})\,x_0}{(2r-px_0)\,x}\right]-\frac{1}{4}p\pi+\frac{1}{2}p\tan^{-1}\left(\frac{2x+p}{2\sqrt{\phi}}\right)\right]-\frac{\pi}{4}\right\}}{\phi^{\frac{1}{4}}} \qquad \text{—(A4.24)}$$

and as previously

$$I(t) \sim u(t)\exp\left[\frac{1}{2L}\left(\frac{a}{B}e^{-Bt}-R_0t\right)\right] \qquad \text{—(A4.20)}$$

requiring the same coefficient as derived from the boundary conditions in $t < t_0$.

REFERENCES

ALI A.W., "A study of the nitrogen laser power density and some design considerations", Applied Optics, Vol. 8, No. 5, Pages 993 - 996 (May 1969).

ANDREWS A.J., KEARSLEY A.J., WEBB C.E., HAYDON S.C., "A KrF fast discharge laser in mixtures containing NF_3, N_2F_4 or SF_6", Optics Communications, Vol. 20, No. 2, Pages 265 - 268 (Feb. 1977).

BUDDEN K.G., "Radio Waves in the Ionosphere", C.U.P. (1961).

BURNHAM R., POWELL F.X., DJEU N., "Efficient electric discharge lasers in XeF and KrF", Applied Physics Letters, Vol. 29, No. 1, Pages 30 - 32 (July 1976).

CARY W.K., MAZZIE J.A., "Time-resolved resistance during spark gap breakdown", IEEE Transactions on Electron Devices, Vol 26, No. 10, Pages 1422 - 1427 (Oct. 1979).

CHUBB D.L., MICHELS C.J., "Study of a rare-gas transverse fast discharge", Journal of Applied Physics, Vol. 50, No. 10, Pages 6230 - 6240 (Oct. 1979).

DICKEY F.R., "Contribution to the theory of impulse breakdown", Journal of Applied Physics, Vol. 23, No. 12, Pages 1336 - 1339 (Dec. 1952)

FELSENTHAL P., PROUD J.M., "Nanosecond-pulse breakdown in gases", Physics Review, Vol.139, No. 6A, Pages 1796 - 1804 (Sept. 1965).

FISHER C.H., CENTER R.E., MULLANEY G.J., Mc DANIEL J.P., "A 490nm XeF electric discharge laser", Applied Physics Letters, Vol. 35, No. 1, Pages 26 - 28 (July 1979).

FITZSIMMONS W.A., ANDERSON L.W., RIEDHAUSER C.E., VRTILEK J.M., "Experimental and theoretical investigation of the nitrogen laser", IEEE Journal of Quantum Electronics,

Vol. 12, No. 10, Pages 624 - 633 (Oct. 1976)

FLETCHER R.C., "Impulse breakdown in the 10^{-9}- secs. range of air at atmospheric pressure" Physics Review, Vol. 76, No. 10, Pages 1501 - 1511 (Nov. 1949).

GEAR C.W., "Numerical Initial Value Problems in Ordinary Differential Equations", Englewood Cliffs, N.J., Prentice-Hall (1971).

GERRY E.T., "Pulsed-molecular-nitrogen laser theory", Applied Physics Letters, Vol. 7, No. 1. Pages 6 - 8 (July 1965).

GOULD L., ROBERTS L.W., Journal of Applied Physics, Vol. 27, No. 10, Pages 1162 - 1170 (Oct. 1956).

GREENE A.E., BRAU C.A., "Theoretical studies of UV-pre-ionized transverse discharge KrF and ArF lasers", IEEE Journal of Quantum Electronics, Vol. 14, No. 12, Pages 951-957 (Dec. 1978).

HASSON V., von BERGMANN H.M., "Spatial control of pulsed high-pressure preionization stabilized glow discharges", Journal of Physics E:Sci. Instrum., Vol. 13, Pages 632 - 638 (1980).

HSIA J., "A model for U.V. preionization in electric-discharge-pumped XeF and KrF lasers", Applied Physics Letters, Vol. 30, No. 12, Pages 101 - 103 (Jan. 1977).

JAVAN, LEVINE, "The feasibility of producing laser plasmas via photoionization", IEEE Journal of Quantum Electronics, Vol. 8, No. 11. Pages 827 - 832 (1972).

JOHNSON T.H., PALUMBO L.J., HUNTER A.M., "Kinetics simulation of high power gas lasers", IEEE Journal of Quantum Electronics, Vol. 15, No. 5, Pages 289 - 301 (May

1979).

KARNYSHIN V.N. , MALOV A.N., SOLOUKHIN R.I., "Influence of preionization conditions on the development of a homogeneous discharge in gases", Soviet Journal of Quantum Electronics, Vol. 8, No. 3, Pages 319 - 323 (March 1978).

KLINE L.E., SIAMBIS J.G., "Computer simulation of electrical breakdown in gases; avalanche and streamer formation", Physics Review A, Vol. 5, No. 2, Pages 794 - 805 (Feb. 1972).

LIN S.C., LEVATTER J.I., "X-ray preionization of electric discharge lasers", Applied Physics Letters, Vol. 34, No. 8, Pages 505 - 508 (April 1979).

MARTIN J.C., "Duration of the resistive phase and inductance of spark channels," A.W.R.E. report SSWA/JCM/ /1065/25 (1965).

MATHEWS J., WALKER R.L., "Mathematical Methods of Physics", second edition, Addison-Wesley (1973).

MATSUMOTO K., SUEOKA K., OBARA M., FUJIOKA T., YAMAMOTO H., "Properties of pulsed gas lasers pumped by LC inversion circuit made of $BaTiO_3$ and $SrTiO_3$ series ceramic capacitors", Review of Scientific Instruments, Vol. 51, No. 8, Pages 1046 - 1048 (Aug. 1980).

MAUREL J., SEGUR P., BLANC D., Comptes Rendus de l'Académie des Sciences, B266, Pages 1390 - 1393 (May 1968).

MERSON - see HALL G. and WATT J.M. (eds.), "Modern Numerical Methods for Ordinary Differential Equations", O.U.P. (1976).

MESYATS G.A., BYCHKOV Y. I., ISKOL'DSKII A.I., "Nanosecond formation time of discharges in short air gaps", Soviet Physics Technical Physics, Vol. 13, No. 8, Pages 1051 - 1055 (Feb. 1969).

MESYATS G.A., BYCHKOV Y. I., KREMNER V.V., "Pulsed nano-second electric discharges in gases", Soviet Physics USPEKHI, Vol. 15, No. 3, Pages 282 - 297 (Nov. 1972).

NEWTON-RAEPHSON method - see for example the book by MATHEWS and WALKER, Page 360.

PALMER A.J., "A physical model on the initiation of atmospheric - pressure glow discharges", Applied Physics Letters Volume 25, No. 3, Pages 138 - 140 (Aug. 1974).

RAETHER H., "Electron Avalanches and Breakdown in Gases", Butterworths (1964).

ROTHE D.E., GIBSON R.A., "Analysis of a spark-preionized large-volume XeF and KrF discharge laser",Optics Communications, Vol. 22, No. 3, Pages 265 - 268 (Sept. 1977).

SCHWAB A.J., HOLLINGER F.W., "Compact high power N_2 laser; circuit theory and design", IEEE Journal of Quantum Electronics, Vol. 12, No. 3, Pages 183 - 188 (March 1976).

SORENSON T.P., RISTIC V.M., "Rise time and time-dependent spark-gap resistance in nitrogen and helium", Journal of Applied Physics, Vol. 48, No. 1, Pages 114 - 117 (Jan. 1977).

STRIGEL R., Wiss. Veroff. Siemens-Konzern, Vol. 11, No. 2, Page 52 (1932).

SZE R.C., LOREE T.R., "Experimental studies of a KrF and ArF discharge laser", IEEE Journal of Quantum Electronics, Vol. 14, No. 12, Pages 944 - 950 (Dec. 1978).

SZE R.C., SCOTT P.B., "¼J discharge pumped KrF laser", Review of Scientific Instruments, Vol. 49, No. 6, Pages 772 - 774 (June 1978).

TAYLOR R.S., SARJEANT W.J., ALCOCK A.J., LEOPOLD K.E., "Glow-discharge characteristics of a 0·8J multi-atmosphere

rare-gas halide laser", Optics Communications, Vol. 25, No. 2, Pages 231 - 234 (May 1978).

WATANABE S., SATO T., KASHIWAGI H., "Amplification characteristics of an efficient discharge-pumped KrF laser", IEEE Journal of Quantum Electronics, Vol. 15, No. 5, Pages 322 - 327 (May 1979).

*SZE R.C., "Rare-gas halide avalanche discharge lasers", IEEE Journal of Quantum Electronics, Vol. 15, No. 12, Pages 1338 - 1347 (Dec. 1979).